

Interactions between Cellulose Nanocrystals and Polymer Chains in Aqueous Solutions

by

Hale Oguzlu

A thesis submitted in partial fulfillment of the requirements for the degree of

Doctor of Philosophy

in

CIVIL CROSS DISCIPLINARY

Department of Civil and Environmental Engineering
University of Alberta

© Hale Oguzlu, 2016

ABSTRACT

Cellulose nanocrystal (CNC), a new breathtaking nanomaterial, is of scientific and commercial interest because of its low density, renewability, biodegradability, non-toxicity and wide range of application potential such as personal care, paints, pharmaceuticals, coatings, drilling fluids, etc. ¹. Besides the non-isotropic orientation or percolation, rod-like CNC particles in suspensions result in self-assembly, elasticity, thixotropy and birefringence at low concentrations. In the presence of electrolytes, polymer solutions, micelles, foams and other colloidal particles, the degree of ordering of CNC particles can be controlled in mesoscopic level, leading to certain macroscopic properties useful for a wide range of products. Therefore, in this research, interactions between CNCs particles with neutral (polyethylene oxide) and anionic polymer (carboxymethyl cellulose) chains in aqueous solutions were investigated in terms of rheological measurements, structure formation, stability of particles, turbidity and Nuclear Magnetic Resonance (NMR) measurements.

The steady-state shear flow and dynamic oscillation measurements were carried out to investigate the rheological properties of CNC suspensions in carboxymethyl cellulose (CMC) and polyethylene oxide (PEO) solutions. CNC particles due to their short length ($L < 250$ nm) does not cause any significant viscosity increase in water at dilute and semi-dilute concentration ($< 4\%$). By contrast, adding both dilute (0.5%) and semi-dilute entangled (1.00%, 2.00% and 3.00%) CMC solutions in CNC suspensions, within the concentration range of 0.33-2.00 vol%, increased the viscosity drastically. When linear viscoelastic properties was measured, it was found that the structure formation in CNC-CMC mixtures led to $G' > G''$ and gel-like behavior. Adding polyethylene oxide (PEO) in CNC suspensions showed a different shear viscosity trend

than CMC solutions and didn't cause any significant change in the steady-shear viscosity and viscoelasticity. The presence of anionic CMC and non-ionic PEO in CNC suspensions led to different phase behaviors due to different interaction mechanisms.

The structures of CNC in the presence of polymer solutions were investigated by Scanning Transmission Electron Microscopy (STEM) and Polarized Optical Microscopy (POM). Ordered CNC structures, as nematic flocs, were observed in STEM images of dilute CMC-CNC solutions. POM images of CNC-CMC solutions showed phase transitions from the isotropic state to nematic and chiral nematic phases, indicating depletion interactions. In the case of dilute PEO-CNC solutions, there were no specific alignments of CNC particles in PEO matrix. However, birefringence structures, which are a sign of the nematic order of CNC particles, were observed in the case of 2.00 vol% CNC suspensions in 5.0 wt% PEO solutions.

Stability of particles was studied in terms of dynamic light scattering and zeta potential and turbidity measurements. The diffusion coefficient of CNC decreased in the presence of CMC chains since the depletion flocculation was more probable. Moreover, the values of electrophoretic mobility didn't change in the presence of CMC chains. The adsorption of PEO chains onto the surface of CNCs increased the zeta potential values from -56 mV to the range between -29 and -22 mV.

^1H spin-lattice relaxation NMR data direct techniques for understanding interactions of CMC and PEO chains with CNC particles. The minima of the specific relaxation rate, (R_2), constants with respect polymer concentration showed depleted CNC nanoparticles in CMC and PEO solutions. In the case of CNC-PEO solutions, obtaining two different spin-spin relaxation time (T_2) values indicates the adsorption of PEO chains onto CNC.

Consequently, the depletion flocculation was identified as the main interaction mechanism between CMC chains and CNC particles in an aqueous medium. This mechanism created nematic flocs of CNC particles. The presence of blob structures from nematic flocs in CNC-CMC solutions resulted in a dramatic increase in the steady-state viscosity and gel-like behavior. The PEO adsorption onto CNC surfaces weakened depletion interactions so viscosity and viscoelasticity of CNC suspensions didn't change significantly in the presence of PEO chains. This study explained that the different interaction mechanisms between polymers and CNC nanoparticles can generate different structure and rheological behaviors.

PREFACE

Preliminary experiments were conducted on CNC in aqueous polymer solution at Alberta Innovates Technology Futures. Unique results in these preliminary experiments made me and my supervisor to focus on interactions between CNC and CMC chains.

Following the introduction on colloidal suspensions, polymer solutions, objectives of this study in Chapter 1, Chapter 2 describes non-Newtonian flow behavior of dilute and semi-dilute CMC solutions in the presence CNC. All experiments were conducted by Hale Oguzlu with an exception of Figure 2.3. Dr. Damunah took images in Figure 2.3. Experiments, results interpretation and manuscript writing were performed under the supervision and guidance from Dr. Boluk. The manuscript was accepted by Canadian Journal of Chemical Engineering.

Chapter 3 describes the flow dynamics and mesoscopic structures of CNC suspensions in CMC polymer solutions. All experiments were conducted by Hale Oguzlu with few exceptions: viscosity measurements of 2-Hydroxyethyl cellulose (HEC) and hydrophobically modified 2-Hydroxyethyl cellulose (hmHEC) solutions. Viscosity measurements of HEC and hmHEC solutions were conducted in Alberta Innovates Technology Futures under the supervision of Dr. Boluk. Experiments, results interpretation and manuscript writing were performed under the supervision and guidance from Dr. Boluk. The manuscript was submitted to Journal of Rheology.

Chapter 4 describes the non-Newtonian flow behavior, flow dynamics and mesoscopic structures of CNC suspensions in nonionic PEO polymer solutions. All experiments were conducted by Hale Oguzlu. Experiments, results interpretation and manuscript writing were

performed by the author with inspiration and guidance from Dr. Boluk. This work will be submitted as a manuscript to Journal of Rheology.

Chapter 5 describes interactions between CNCs suspended in aqueous solutions of CMC and PEO. All experiments were conducted by Hale Oguzlu with an exception of NMR measurements. These measurements were conducted by Mr. Mark Miskolize in NMR Laboratory, Department of Chemistry of University of Alberta. Experiments, results interpretation and manuscript writing were performed by the author with inspiration and guidance from Dr. Boluk. The manuscript was submitted to Cellulose.

Chapter 6 describes self-assembly of CNC particles in the presence of CMC and PEO chains. All experiments were conducted by Hale Oguzlu. Experiments, results interpretation and manuscript writing were performed by the author with inspiration and guidance from Dr. Boluk. This work will be submitted as a manuscript to Nanoscale Royal Society of Chemistry.

Appendix A describes dimension determination method of CNC particles. This method was developed by Dr. Boluk and Dr. Damunah. Corresponding method was published: Boluk, Y.; Danumah, C. Journal of Nanoparticle Research **2014**, 16, 1-7.

Appendix B is a supplementary document for Chapter 4.

Alberta Innovates Biosolutions and ArboraNano, Canadian Forest Nanoproducts Network of Natural Sciences and Engineering Research Council of Canada (NSERC) financially supported this research. The CNC samples were kindly provided by Alberta Innovates Technology Futures and Celluforce under the ArboraNano research program “Investigating Nanocrystalline Cellulose as Loss Circulation Materials in Drilling Fluids”. The following conference presentations and journal papers have been published from the research are listed below.

CONFERENCES

Y.Boluk*, **H. Oguzlu**, Z. Khalili, *Structure and Rheological Properties of Rod-Shaped Cellulose Nanocrystal Suspensions in Aqueous Dilute Polymer Solutions* The Society of Rheology 87th Annual Meeting, Baltimore, Maryland, USA, 11 - 15, 2015.

H. Oguzlu*, Z. Khalili, Y.Boluk, *Interactions between Rod-Shaped Nanoparticles and Polymer Chains in Aqueous Solutions*, 249th ACS National Meeting, Denver, Colorado, USA, 22-26 March, 2015.

H. Oguzlu*, Y.Boluk,, *Stability and Rheology of Cellulose Nanocrystal Solutions in Adsorbing Non-Adsorbing Polymers Solutions*, 2014 TAPPI International Conference on Nanotechnology for Renewable Materials, Vancouver, British Columbia, Canada, 23-26 June, 2014.

H. Oguzlu, Y.Boluk*, *Unusual Effects of Rod Shaped Nanocrystalline Cellulose Particles on the Flow Behaviour of Polyethylene Oxide Solutions*, 245th ACS National Meeting, New Orleans, Louisiana,USA, 7-11 April, 2013.

* represents the presenter of published study in the conference

JOURNALS

H. Oguzlu and Y. Boluk *Depletion induced gelling in cellulose nanocrystals (CNC) colloid carboxymethyl cellulose (CMC) polymer mixtures*, submitted to Journal of Rheology, June 20, 2016

H. Oguzlu and Y. Boluk, *Interactions between Cellulose Nanocrystals and Anionic and Neutral Polymers Suspended in Aqueous Solutions of Anionic and Neutral Polymers*, submitted to Cellulose, May 25, 2016

H. Oguzlu, C. Danumah, Y. Boluk, *The Role of Dilute and Semi-dilute Cellulose Nanocrystal (CNC) Suspensions on the Rheology of Carboxymethyl Cellulose (CMC) Solutions*, submitted to Canadian Journal of Chemical Engineering, 94, 1841–1847, 2016.

To my beloved family

ACKNOWLEDGMENTS

I would like to express my sincere gratitude to my supervisor Prof. Dr. Yaman Boluk for the continuous support of my doctoral study and research, for his patience, motivation, enthusiasm, and immense knowledge. I have been extremely lucky to have a supervisor who cared so much about my work, and who supported me in every step.

I am also especially indebted to my thesis committee members Prof. Dr. Philip Choi and Assoc. Prof. Dr. Mark McDermott, who, by discussing my ideas, have provided suggestions and advice. I would also thank to Prof. Dr. Muhsin Ciftcioglu and Prof. Dr. Funda Tihminlioglu who supported me and helped me to find a doctoral position in the University of Alberta.

I would like to thank to my former colleagues Dr. Christophe Danumah, Dr. Usha Hemraz and Dr. Vanessa Incani for sharing basic knowledge about laboratory and research group when I became part of our research group. I owe thank to National Institute for Nanotechnology (NINT) researcher, Dr. Jae-Young Cho for his guidance to Atomic Force Microscopy measurements. For Nuclear Magnetic Resonance experiments and discussions, I would like to thank Mark Miskolzie. I also would like to thank to NINT researchers, Dr. Steve Launspach, Dr. Mike Xia and Dr. Kai Cui for their training instruments and discussions.

I deeply thank to my husband Alberto Baldelli, who was always with me no matter how stressful I was. He always gives me warm encouragement and love in every situation. I owe deepest thanks to my parents Sengul and Nasip who have supported me since I was born. I would like to thank to my lovely sister Gizem who made my life cheerful. Similarly, I would like to thank my parents-in-law Luisa and Sergio for their encouragement. I strongly thank to my close friends, Irmak Kocabas Arkilic, Shadi Nayeri, Vianey Landeros, Ergem Karakamisoglu, Jingsi Chen, Hui Wang, and Onur Ozcalik who helped me to release my stress with little chats.

Table of Contents

<i>Table of Contents</i>	<i>xi</i>
<i>List of Figures</i>	<i>xiv</i>
<i>List of Tables</i>	<i>xix</i>
<i>Nomenclature</i>	<i>xx</i>
Chapter 1. Introduction	1
1.1 Rod-Like Colloidal Suspensions	3
1.1.1 Dilute Suspensions	3
1.1.2 Concentration Effect	4
1.1.3 Brownian Motion	4
1.1.4 Shape Factor	5
1.1.5 Electroviscous Effect	7
1.1.6 CNC Suspensions	8
1.2 Polymer Solutions	8
1.2.1 Molecular Weight and Length of Polymers	9
1.2.2 Single Chain Conformations	10
1.2.3 Polymer Solutions and Flory Huggins Theory	12
1.2.4 Stability and Phase Diagrams	15
1.2.5 Concentration Regime	16
1.2.6 Viscosities of Polymer Solutions	18
1.2.7 PEO and CMC Solutions	22
1.3 Nanoparticle Suspensions in Polymer Solutions	23
1.3.1 Adsorbing Polymers	24
1.3.2 Flocculation by Bridging	25
1.3.3 Steric Stabilization	27
1.3.4 Non-absorbing Polymers	28
1.3.5 Phase Diagrams	29
1.4 Objectives and Experimental Design	30
1.4.1 Scope of Study	31
1.4.2 Experimental Approach	31
Chapter 2. The Role of Dilute and Semi-Dilute Cellulose Nanocrystal (CNC) Suspensions on the Rheology of Carboxymethyl Cellulose (CMC) Solutions	42
2.1 Abstract	42
2.2 Introduction	42
2.3 Experimental	44

2.3.1	Materials	44
2.3.2	Methods.....	44
2.4	Results	45
2.5	Discussions	54
2.6	Conclusion.....	57
<i>Chapter 3. Depletion induced gelling in cellulose nanocrystals (CNC) colloid carboxymethyl cellulose (CMC) polymer mixtures</i>		59
3.1	Abstract.....	59
3.2	Introduction	59
3.3	Experimental.....	61
3.3.1	Materials	61
3.3.2	Methods.....	62
3.4	Results and Discussion.....	62
3.4.1	CNC Suspensions in Aqueous Polymer Solutions.....	62
3.4.2	CNC Suspensions in CMC Solutions.....	66
3.5	Conclusions	78
<i>Chapter 4. Rheological Properties of CNC Suspensions in Polyethylene Oxides Solutions</i>		80
4.1	Abstract.....	80
4.2	Introduction	80
4.3	Experimental.....	81
4.3	Results and Discussion	82
4.3.1	Shear Viscosity and Structure Relation.....	82
4.3.2	Linear Viscoelastic Behavior	86
4.3.3	Comparison of Steady and Dynamic Viscosities	90
4.4	Conclusion.....	92
<i>Chapter 5. Interactions between Cellulose Nanocrystals Suspended in Aqueous Solutions of Anionic and Neutral Polymers</i>		94
5.1	Abstract.....	94
5.2	Introduction	95
5.3	Experimental.....	97
5.3.1	Materials	97
5.3.2	Polarized Filter Plates	98

5.3.3	Polarized Optical Microscopy (POM)	98
5.3.4	Scanning Transmission Electron Microscopy (STEM)	99
5.3.5	Dynamic Light Scattering (DLS).....	99
5.3.6	Nuclear Magnetic Resonance (NMR).....	99
5.4	Results and Discussion.....	100
5.4.1	Structure Formation	100
5.4.2	DLS and Zeta Potential Measurements.....	107
5.4.3	¹ H Solvent Relaxation NMR.....	111
5.5	Conclusion.....	117
<i>Chapter 6. Atomic Force Microscopy (AFM) Studies on Self-Assembly of CNC Films from Aqueous Polymer Solutions</i>		<i>118</i>
6.1	Abstract.....	118
6.2	Introduction	118
6.3	Experimental.....	119
6.3.1	AFM Measurements.....	119
6.3.2	X-ray Diffraction Analyses.....	119
6.4	Results	119
6.5	Conclusion.....	127
<i>Chapter 7. Conclusion</i>		<i>128</i>
7.1	Contribution to Knowledge.....	129
7.2	Future Recommendations	130
<i>References.....</i>		<i>132</i>
<i>Appendix A. Supplementary for NMR Results in Chapter 4</i>		<i>146</i>

List of Figures

Figure 1.1 Relative viscosity as a function of the Peclet number for a monolayer of hard sphere: (-o-) total relative viscosity; (--Δ--) Brownian contribution; (-□-) hydrodynamic contribution without the self-part.	5
Figure 1.2 Illustration of random coil with the end-to-end distance, R_{e-e}	10
Figure 1.3 The conformation of neutral and nonionic polymer chains with respect to solvent quality.	14
Figure 1.4 Phase diagram of polymer solution.	15
Figure 1.5 Upper critical temperature (a) and lower critical temperature of polymer solution in phase diagrams	16
Figure 1.6 Concentration regime of polymer solution with the respect to molecular weight and concentration.	17
Figure 1.7. A blob of size ζ has monomers of size b from the same chain	17
Figure 1.8 Zero-shear viscosity as function of molecular weight and concentration	21
Figure 1.9 Viscosity vs. shear rate plots of a cellulose ether polymer at various polymer concentrations	22
Figure 1.10 Schematic representation of a) adsorbed polymer layer and b) possible structure of adsorbed layers	25
Figure 1.11 Schematic representation of bridging mechanism; a) two particles by one polymer molecule and b) two particles by two separately adsorbed polymer molecules.	27
Figure 1.12 Illustration of depletion interaction between polymer chains and hard spheres.	29
Figure 1.13 Interaction potential W_{dep} versus distance between between two spherical particles ⁵	29
Figure 1.14 State diagram of a colloid–polymer mixture	30
Figure 1.15 The schematic diagram of main components of STEM	35
Figure 1.16. The schematic diagram of main components of DLS	36
Figure 1.17. Schematic representation of the ionic concentration as a function of distance from the charged particles in suspensions	37
Figure 1.18. Schematic representation of cone-and-plate rheometer.	38
Figure 1.19. Behavior of T_1 and T_2 as a function of correlation time (τ_c).	39

Figure 1.20 Schematic of typical AFM system.	40
Figure 1.21 Schematic representation of stability behaviors of CNC suspensions.	41
Figure 2.1 Shear viscosities of CNC suspensions measured at 25°C	46
Figure 2.2 Shear viscosities of CMC polymer solutions measured at 25°C.	47
Figure 2.3 Photographs of 0.33 vol% CNC suspension in CMC (700 kDa) solutions. Cuvettes are in (a) upward position; (b) 180° rotated position.....	48
Figure 2.4. Shear viscosities of (a) 0.5 wt%, (b) 1.0 wt% and (c) 2.0 wt% CMC polymer solution with various CNC concentrations measured at 25°C.....	49
Figure 2.5 Maximum shear dependent viscosity versus CMC polymer concentration at various CNC additions.	50
Figure 2.6 Flow curve ingredient of CMC solutions at various CNC additions.	51
Figure 2.7. Nonisotropic structures of (a) 0.67 vol% and (b) 1.34 vol% CNC in CMC polymer solutions placed between crossed polarizers showing birefringent domains	52
Figure 2.8 Nonisotropic structures of CNC in CMC polymer solutions as shown under POM...	53
Figure 2.9 Light transmission of 1.0 wt.% CMC solution along the sample cell height with various CNC concentrations.....	54
Figure 2.10 The solution states of CMC polymer as a function of CMC molecular weight and concentration and the role of CNC addition to shift from one state to another (a); Schematic representations of CMC polymer solution in semi-dilute entangled state (b); and CMC polymer solution in concentrated network solution state due to the CNC presence (c).....	57
Figure 3.1 Steady shear rate viscosity as a function of shear rate of: (a) 1.0% CMC 700 kDa with and without 0.67% CNC; (b) 1.0% HEC 250 kDa with and without 0.67% CNC; (c) 1.0% hmHEC 250 kDa with and without 0.67% CNC and 0.25% SDS; (d) 1.0% PEO 600 kDa with and without 0.67% CNC.....	65
Figure 3.2 Steady state shear viscosities of (a) CMC solutions with and without 1.34 vol.% CNC addition; (b) Various 1.0 wt.% CMC solutions with various CNC concentrations.	67
Figure 3.3 Low shear rate viscosities of CNC suspensions in CMC solutions: (a) before scaling; (b) after scaling with inner box shows scaling factor at each CNC concentrations.	69
Figure 3.4 Dynamic storage and loss moduli versus oscillatory frequency of CNC suspensions in: (a) 0.5 wt.% CMC solution; (b) 1.0 wt.% CMC solution; (c) 2.0 wt.% CMC solution.	71

Figure 3.5 Storage (G') and loss (G'') modulus values of (a) 0.5 wt.% CMC, (b) 1.0 wt.% CMC, (c) 2.0 wt.% CMC and (d) 3.0 wt.% CMC with respect to CNC concentration at 1 rad/s....	73
Figure 3.6 The steady-shear (filled) and complex (hallow) viscosity for (a) aqueous CMC (700 kDa) solutions with different concentrations, CNC suspensions with aqueous (b) 0.5 wt.% CMC (c) 1.0 wt.% CMC (d) 2.0 wt.% CMC and (e) 3.0 wt.% CMC solutions at 25°C.....	75
Figure 3.7 (a) STEM image of dilute CNC particles in CMC (700 kDa) solutions and (b) POM image of 2.00 vol.% CNC suspensions in 1.0wt.% CMC solution.	76
Figure 3.8 Schematic representation of depletion flocculation CNC and increasing the apparent CMC solution concentration.....	77
Figure 4.1 Shear viscosity change with shear rate for (a) PEO solutions without and with 1.34 vol.% CNC suspensions and (b) CNC suspensions without and with 1.0 wt.% PEO solutions.....	84
Figure 4.2 Schematic representation of 1.0 wt.% PEO solutions with (a) 0.00 vol.% , (b) 0.33 vol.% (c) 0.67 vol.% and (d) 1.34 vol.% CNC suspensions and (e) STEM image of CNC-PEO solution.....	85
Figure 4.3 (a) STEM image of dilute CNC particles in PEO (600 kDa) solutions and (b) POM image of 2.00vol.% CNC suspensions in 5.0wt.% PEO solution.	85
Figure 4.4. Viscosity versus the $\phi^{1.3}M$ product for PEO solutions ($M_w=300$ and 600 kDa) in CNC suspensions at 25°C.	86
Figure 4.5 Dynamic storage and loss moduli versus oscillatory frequency of (a-b) 1.0 wt.% PEO solutions and (c-d) 5.0 wt.% PEO solutions in CNC suspensions.	87
Figure 4.6 Storage (G') and loss (G'') modulus values of (a) 1.0 wt.% PEO, (b) 2.0 wt.% PEO and (c) 5.0 wt.% PEO with respect to CNC concentration at 1 rad/s.....	89
Figure 4.7 The steady-shear (filled) and complex (hallow) viscosity for (a) aqueous PEO (600 kDa) solutions with different concentration, CNC suspension with aqueous (b) 1.0 wt.% PEO (c) 2.0 wt.% PEO and (d) 5.0 wt.% PEO solutions at 25°C.....	92
Figure 5.1 POM images of 1.67 vol.% of CNC suspensions in 0.0 wt.%, 0.5 wt.%, 3.0 wt.% of CMC polymer solutions.....	95
Figure 5.2 STEM picture of CNC.....	101
Figure 5.3 Photographs of 0.67 vol.% CNC suspensions in CMC (700 kDa) solutions. Vials are in (a) upward position; (b) 180° rotated position.....	102

Figure 5.4 Crossed-polarized images of vials of 0.33 vol.% CNC suspensions in CMC polymer solutions showing birefringent domains.....	103
Figure 5.5 (a) POM images of 0.33 vol.% of CNC suspensions in (a) 0.0 wt.%, (b) 0.5 wt.%, (c) 1.0wt.%, (d) upper part of 2.0wt.%, (e) upper part of 3.0wt.%, (f) lower part of 2.0wt.% and (g) lower part of 3.0wt.% of CMC polymer solutions.....	104
Figure 5.6 Phase diagram for CNC suspensions in CMC solutions.	106
Figure 5.7 POM images, digital photographs and crossed-polarized images of (a) 0.67 vol.% CNC suspensions in 5.0wt.% PEO solution, (b) 1.34 vol.% CNC suspensions in 5.0wt.% PEO solution, (c) 2.02 vol.% CNC suspensions in 1.0wt.% PEO solution, (d) 2.02 vol.% CNC suspensions in 5.0wt.% PEO solution.	107
Figure 5.8. Schematic of (a) CMC polyelectrolytes leading to osmotic depletion of CNC particles strengthen with electrostatic repulsion, (b) the zoomed-in view of the depletion zone of the CNC-CMC system, and (c) the presence of salt leading to the kinetic adsorption mechanism of PEO on sulfate groups of CNC (dashline refers to e).	110
Figure 5.9 Change in relaxation rate constant (R_{2sp}) with respect to polymer concentration of 1.0 wt.% of CNC suspensions in aqueous CMC and PEO solutions	115
Figure 5.10 Illustration of 1.0 wt.% CNC suspensions with various CMC concentration.....	115
Figure 6.1 Illustration of sample preparation for AFM measurements	119
Figure 6.2 AFM Height images of surface of film cast from droplet of 0.50 wt% CNC suspension with the scan size of (a) 100 μm x 100 μm and (b) 50 μm x 50 μm , and 1.00 wt% CNC suspension with the scan size of (c) 100 μm x100 μm , (d) 50 μm x 50 μm , (e) 10 μm x10 μm and (f) 5 μm x 5 μm	121
Figure 6.3 AFM Height images of surface of film cast from droplet of 2.00 wt% CMC solution with the scan size of (a) 100 μm x 100 μm and (b) 50 μm x 50 μm and 1.00 wt% PEO solution with the scan size of (c) 100 μm x 100 μm and (d) 50 μm x 50 μm	122
Figure 6.4 AFM Height images of surface of film cast from droplet of (a) 0.50 wt% CMC-0.50 wt% CNC mixture (50 μm x 50 μm), (b) 0.50 wt% CMC-2.00 wt% CNC mixture (50 μm x 50 μm) and 0.05 wt CMC-1.00 wt% CNC mixture with the scan size of (c) 100 μm x 100 μm and (d) 5.00 μm x 5.00 μm	122

Figure 6.5 AFM Height images of surface of film cast from droplet of 0.05 wt% PEO-1.0wt% CNC mixture (a) (50 μm x 50 μm), (b) (10 μm x 10 μm), (c) (5 μm x 5 μm), and (d) 1.0wt% PEO-1.0wt% CNC mixture (50 μm x 50 μm). 123

Figure 6.6. X-ray diffractogram of 1.00 wt% CNC, 1.00 wt% PEO and 1.00 wt% CNC+1.00 wt% PEO. 124

Figure 6.7 AFM results of surface of film cast from droplet of 0.01 wt% CNC suspensions (a) 2D height image (5 μm x 5 μm), (b) 3D height image (5 μm x 5 μm) obtained by tapping mode, (c) roughness profile along a line chosen in arbitrary direction on the surface and is shown by the diagonal line in (a)..... 125

Figure 6.8 AFM results of surface of film cast from droplet of 0.01 wt% CNC- 0.01 wt% CMC mixtures: (a) 2D height image (5 μm x 5 μm), (b) 3D height image (5 μm x 5 μm) obtained by tapping mode, (c) roughness profile along a line chosen in arbitrary direction on the surface and is shown by the diagonal line in (a). 126

Figure 6.9 AFM results of surface of film cast from droplet of 1.00 wt% CNC- 1.00 wt% PEO solution: (a) 2D height image (5 μm x 5 μm), (b) 3D height image (5 μm x 5 μm) obtained by tapping mode, (c) roughness profile along a line chosen in arbitrary direction on the surface and is shown by the diagonal line in (a). 127

List of Tables

Table 1.1 Studies on phase behaviors of CNC suspensions	8
Table 1.2 Solvent quality change with respect to χ parameter for neutral polymers.....	14
Table 1.3 Correlation length and end-to-end distance with respect to polymer and solvent types	18
Table 1.4. Properties and concentration regimes of CNC	33
Table 1.5. Properties of polymers	34
Table 3.1 Polymers used for solution preparations in experiments	61
Table 4.1 Terminal slopes of G' and G'' for PEO solutions with CNC suspensions at 25°C.	90
Table 5.1 Properties of polymers	98
Table 5.2 Dimensions and surface charge analysis of CNC with different polymer solutions ..	109
Table 5.3 Spin-spin relaxation times and relaxation rate constants of samples with respect to molecular weight, CNC concentration and salt concentration.	113
Table A.1. Spin-lattice relaxation times of samples with respect to molecular weight, CNC concentration and salt concentration.	146

Nomenclature

a	Mark–Houwink–Sakurada Equation constant
a_s	Spherical particle radius
b	Monomer size
B	External applied magnetic field
B_0	Initial applied field
c	Concentration
c_n	Number density of monomers
c_2, c_3	Quadratic terms
C_∞	Characteristic ratio
c^*	Overlap concentration
c^{**}	Critical concentration
d	Diameter of rod
D_r	Rotational diffusion coefficient
D_0	Diffusion coefficient
ΔE	Energy difference between the spin states
f	Stokes friction coefficient
$f(K_a)$	Henry function
g	Number of monomers per correlation blob
G'	Storage modulus
G''	Loss modulus
$G(t)$	Linear relaxation modulus
G_e	Equilibrium relaxation modulus
G_i	Relaxation strength
ΔG_{mix}	Gibbs free energy of mixing
ΔH_{mix}	Enthalpy of mixing
h	Planck's constant
K	Flow consistency index
k_B	Boltzmann constant
K_H	Huggins coefficient

K_{η}	Mark–Houwink–Sakurada Equation constant
L	Length of rod
l	Length of bonds
l_k	Kuhn length
M_i	Molecular weight of chain “ i ”
M_n	Number average molecular weight
M_v	Viscosity average molecular weight
M_w	Weight average molecular weight
M_w^*	Critical molar mass
$M_z(0)$	Equilibrium value of longitudinal component of the magnetization vector
$M_z(t)$	Longitudinal component of the magnetization vector
$M_{xy}(0)$	Equilibrium value of transverse magnetization vector
$M_{xy}(t)$	transverse magnetization vector
N_i	Number of chains
N	Number of segments
n	Number of monomers
p	Probability
Pe	Peclet number
Pe_r	Rotational Peclet number
R	Spherical particle radius
R_{e-e}	End-to-end distance
R_o	Chain dimension
R_h	Hydrodynamic radius
R_F	Flory end to end distance
R_r	Radius of cone
R_2	Relaxation rate constant
R_2^0	Relaxation rate constant of solvent
R_{2sp}	Specific relaxation rate
r	Aspect ratio
$\langle r \rangle_f$	Extended chain length

ΔS_{mix}	Entropy of mixing
t	Time
T	Temperature
T_c	Critical temperature
T_1	Spin-lattice relaxation time
T_2	Spin-spin relaxation time
T_{2f}	Relaxation times of free solvent molecules
T_{2b}	Relaxation times of bound solvent molecules
T_r	Torque
u_E	Electrophoretic mobility
u_1^a	Adsorption energy of solvent molecule
u_2^a	Adsorption energy of polymer segment
v	Flory exponent
v_f	Free volume
v_p	Number density
v_{per}	Pervaded volume
z	Zeta potential
Z	Number of neighbors of monomer site
Z_o	Friction coefficient
γ	Gyromagnetic ratio
$\dot{\gamma}$	Shear rate
δ	Depletion layer thickness
ε	Dielectric constant
ε_{ij}	Interaction energy between two molecules
ε_{SM}	Interaction energy between solvent monomer molecules
ε_{MM}	Interaction energy between monomer molecules
ε_{SS}	Interaction energy between solvent molecules
ζ	Blob of size
η	Viscosity
$[\eta]$	Intrinsic viscosity

$[\eta]_0$	Intrinsic viscosity
$[\eta]_{ev}$	Viscosity of electro-viscous effect
η_0	Viscosity of the suspension
η_m	Viscosity of the medium
η_r	Reduced viscosity
θ_c	Angle between the cone and the plate
σ	Shear stress
λ_1	Lattice parameter
$\Delta\mu_p$	Change of chemical potential
τ_i	Relaxation time
χ	Chi parameter
χ_s	Adsorption energy
χ_{sc}	Critical adsorption energy
ω	Frequency of strain oscillation
Ω	Angular velocity

Chapter 1. Introduction

Since the early 1800's, scientists have studied on colloids, even definitions in colloidal research area were not as clear as today. In 1861, Thomas Graham introduced the term of "colloid" that was derived from Greek meaning "glue-like." Colloids received little attention until the discovery of modern physical chemistry by van't Hoff, Oswald and Nernst. In the beginning of the 20th century, colloids gained importance, as they were involved in industrial processes. Colloidal science became a fundamental part of everyday products such as polymers, agrochemicals, pharmaceuticals and food products, and technologies such as nucleation, chromatography and flotation ^{2,3}. With the discovery of nanoscience, colloids were clearly defined as dispersed-phase particles with at least one direction with a dimension between 1 nm and 0.1 μm . Moreover, colloidal science became a bridge to nanoscience in the last few decades. Addition to dimension range, colloidal systems can distinguish six major aspects ⁴:

- 1) Brownian motions
- 2) Near absence of inertial effects
- 3) Negligibility of gravity
- 4) Intermolecular interaction
- 5) Size effect on intensive thermodynamic properties
- 6) Interaction with electromagnetic radiation

In the 1940s, Derjaguin and Landau, Verwey and Overbeek introduced colloidal interaction studies to literature with the experiments of dispersion of charged particles in an electrolyte solution with the focus on Van der Waals attraction and electrical double layers ^{5,6}. This foundation for the stability of colloids is known as the DLVO theory and has been remarkably successful in explaining the results of a vast number and broad range of experiments. It was discovered that forces between colloidal particles affects physical properties of suspensions and colloidal suspensions. Therefore, colloidal suspensions became a promising research area in the last decades ^{5,6}.

Mixing colloids with polymers or other colloids results in phase transition or aggregation; these cause gelation, crystallization, glass transition, flocculation, or fluid–fluid demixing of the

dispersion. When a polymer coil in a solution approaches the colloidal surface, coils are either depleted from or adsorbed or anchored to colloidal surfaces that leads to strongly influence colloidal interactions. With that influence, phase behaviors, stability, rheological properties of polymer solutions can be manipulated ⁶.

In the literature, several researchers were interested in interactions of colloidal spheres between polymer chains with the focus on interaction forces, colloidal stability, phase behaviors, and rheological properties. For instance, McConnel and Howard (1966) worked with silica suspensions in polyethylene oxide (PEO) solutions to observe adsorption of spherical silica particles on PEO chains ⁷. De Gennes and coworkers (1979) studied colloidal stability and interaction of semi-dilute polymer solutions with spherical colloidal suspensions, theoretically ⁸. Senff and Richtering (1999) investigated phase behaviors and rheology of soft sphere particles in poly(N-isopropylacrylamide) solutions ⁹. In addition to spherical colloids, some researchers started working with other geometries of colloidal particles such as platelets and rod-shaped particles. Nabzar and coworkers' study (1984) on kalonite with polyacrylamide is an example of platelets like particles ¹⁰.

Among spherical particles, theoretical calculation shows that depletion interactions between rod-like colloidal particles and polymer chains are more effective due to the aspect ratio of rod-like particles ⁵. Carbon nanotubes (CNTs) became the most prevalent rod-like colloidal particles after Iijima brought carbon nanotubes (CNTs) to the awareness of the scientific community with his report in 1991, even though Radushkevich and Lukyanovich first discovered CNTs in 1952 ¹¹. However, studies of CNTs suspensions with polymer solutions are limited due to dispersion of CNTs. Thus, natural based cellulose nanocrystals (CNCs) attract attention because of its dispersion properties, sustainability and functional groups. CNC is natural based rod-like nanoparticles with a width of 5-10 nm and a length up to 300 nm and is produced by isolation of crystalline chains of cellulose by applying acid hydrolysis techniques ¹². Moreover, physical properties, stability and phase behaviors of polymers solutions can be manipulated by introducing CNC into a polymer matrix due to molecular interaction such as depletion or bridging effect. Therefore, this PhD study will investigate interactions between CNC suspensions with polymer solutions considering molecular forces, rheological properties, and phase behaviors.

1.1 Rod-Like Colloidal Suspensions

CNC suspensions will be studied by itself to interpret interactions between CNC and polymer in aqueous systems. Understanding of interactions between CNC and a polymer chain is essential with the examination of the flow behavior to investigate the mesoscopic structure of CNC suspensions. The flow behavior of CNC suspensions changes with volume fraction (Φ), particle shape, and the presence of electrical charges in the system.

1.1.1 Dilute Suspensions

Excluded volume interactions, interparticle forces, hydrodynamic forces, and Brownian motion affect the flow of colloidal suspensions. These interactions lead to an increase in the energy dissipation and in viscosity. With the absence of interparticle forces in dilute regime suspensions; the flow behavior of dilute suspensions was defined with Einstein relation in Equation 1.1:

$$\eta_r = \frac{\eta}{\eta_0} = 1 + [\eta]\phi \quad \text{Equation 1.1}$$

where η_r is reduced viscosity, η_0 is the viscosity of the suspension, η is the viscosity of the suspending medium, $[\eta]$ is the intrinsic viscosity of the particles and ϕ is the volume fraction of particles in suspension¹³. Theoretically, intrinsic viscosity $[\eta]$ (Equation 1.2) depends on particle shape, being 2.5 for rigid spheres suspension^{13,14}.

$$[\eta] = \lim_{c \rightarrow 0} \left(\frac{\eta_{sp}}{c} \right) \quad \text{Equation 1.2}$$

where η_{sp} is specific viscosity, which can be calculated with the flowing equation:

$$\eta_{sp} = (\eta - \eta_0)/\eta_0 = \eta_r - 1 \quad \text{Equation 1.3}$$

1.1.2 Concentration Effect

Colloidal suspensions exist in the semi-dilute phase when the relative motion between particles affects the flow behavior of suspensions with hydrodynamic interactions. In semi-dilute case, the reduced viscosity was expressed with the introduction of higher-order terms to Einstein relation by Batchelor and Green^{13,15}:

$$\eta_r = 1 + [\eta]\phi + c_2\phi^2 + c_3\phi^3 + \dots \quad \text{Equation 1.4}$$

In Equation 1.2, the higher-order terms are hard to calculate and also interpretation of these terms are complicated due to multibody interactions; therefore, the coefficient of the quadratic term c_2 is used to explain interparticle forces and microstructure of suspensions¹³. For dilute suspensions of hard spheres, c_2 term is derived as 6.2 by Batchelor in 1977.

1.1.3 Brownian Motion

Brownian motion becomes an effective force that acts to keep particles well distributed when the size of particles are in the order of $1\mu\text{m}$ or smaller. Brownian motions lead to a diffusive particle motion due to thermal energy ($k_B T$) that affects the flow behavior of colloidal suspensions. Brownian motion's contribution to suspension can be determined by using Peclet number (Pe); this parameter represents the dimensionless ratio of hydrodynamic shear to thermal motions, Equation 1.5¹³:

$$Pe = \frac{\dot{\gamma}a_s^2}{D_0} = \frac{6\pi\eta_m\dot{\gamma}a_s^3}{k_B T} \quad \text{Equation 1.5}$$

where $\dot{\gamma}$ is the magnitude of the shear rate and a_s is the spherical particle radius. When shear forces are effective, Pe number will go infinite whereas, Pe will be smaller than 1 when Brownian motion dominates the flow behavior of suspensions. It can be simply summarized that Pe goes infinite at higher shear rates and at lower shear rates the Pe will be smaller than 1. Therefore, Brownian motion will dominate the flow behavior of suspensions at lower shear rates (Pe)¹⁶.

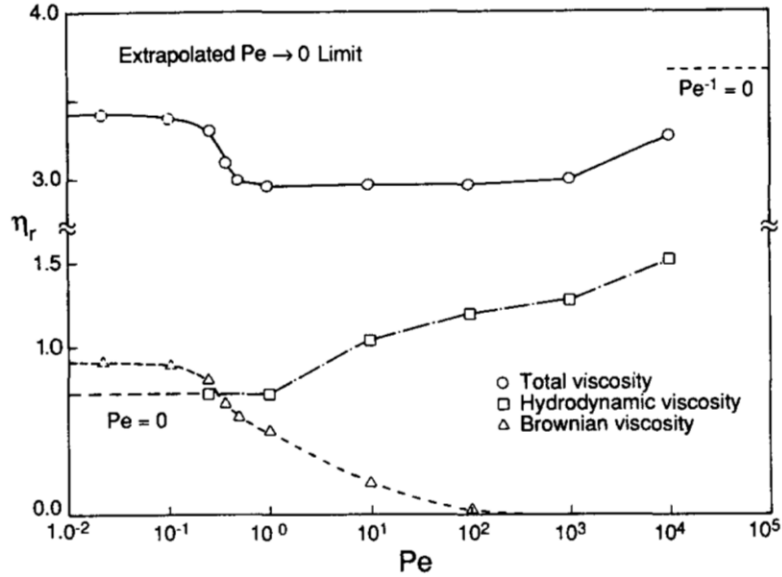


Figure 1.1 Relative viscosity as a function of the Peclet number for a monolayer of hard sphere: (-o-) total relative viscosity; (--Δ--) Brownian contribution; (-□-) hydrodynamic contribution without the self-part ¹⁷. Reprinted from: Bossis, G.; Brady, J. F. The rheology of Brownian suspensions. Journal of Chemical Physics 1989, 91, 1866-1873.

1.1.4 Shape Factor

Particle shape is another factor that affects the flow behavior of suspensions. Non-spherical particles can be found in different geometries such as spheroid, rod or disk. The flow behavior of rod-like particles will be focus of this paper as CNCs are rod-like nanoparticles. Rod-like particles can be characterized by an aspect ratio (r), defined as the ratio of the dimension of symmetry axis (length, L) to the dimension of the cross direction (diameter, d). Therefore, to consider rod-like particle shape effect on the flow behavior, the Einstein relation can be rewritten as ¹⁵:

$$\eta_r = 1 + [\eta]v_pL^3 + c_2(v_pL^3)^2 + c_3(v_pL^3)^3 + \dots \quad \text{Equation 1.6}$$

where v_p is the number density of the rods. Brownian motion does not affect the flow behavior of very dilute hard sphere suspensions, however; for non-spherical particles, translational Brownian motion affects the particles' position and rotary Brownian motion (rotational diffusion) randomizes the orientation distribution. In dilute rod-like suspensions ($vL^3 < 1$), translational diffusion motion is negligible compared to rotational Brownian motion to

investigate the change in flow behavior; thus, the ratio of shear forces to Brownian motion is defined with the rotational Peclet number (Pe_r)^{13,15}:

$$Pe_r = \frac{\dot{\gamma}}{D_r} \quad \text{Equation 1.7}$$

where D_r is rotational diffusion coefficient which is defined in Equation 1.8 for rod-like particles.

$$D_r = 3k_B T \frac{\ln(L/d)-0.8}{\pi\eta_m L^3} \quad \text{Equation 1.8}$$

Brownian motion and hydrodynamic interactions contribute the flow behavior of rod-like particle suspension. Brownian rotations lead to an additional friction in the fluid; therefore, this direct contribution was considered in intrinsic viscosity calculation for prolate spheroids by Onsager¹⁵:

$$[\eta] = \frac{4}{15} \frac{r^2}{\ln r} \quad \text{Equation 1.9}$$

for $r \gg 1$ and $Pe_{rot} \ll 1$. For prolate spheroids with finite dimensions ($r > 15$ and $Pe_{rot} < 1$) low shear intrinsic viscosity is derived as¹⁵:

$$[\eta] = \frac{r^2}{5} \left(\frac{1}{3(\ln 2r - 1.5)} + \frac{1}{(\ln 2r - 0.5)} \right) + 1.6 \quad \text{Equation 1.10}$$

Mansfield and Douglas (2008) calculated intrinsic viscosity of rigid rod-like particles suspensions at low shear rates (low Pe_{rot}) as^{18,19}:

$$[\eta] = \frac{8}{45} \frac{r^2}{\ln r} \quad \text{Equation 1.11}$$

At higher shear conditions, intrinsic viscosity of rigid rod-like particles suspensions became as¹⁵:

$$[\eta] = 0.315 \frac{r}{\ln r} \quad \text{Equation 1.12}$$

for $r \gg 1$ $Pe_{rot} \ll r^3$. With the direct and indirect contribution of Brownian motions, the intrinsic viscosity in high-shear limit is smaller than in the low-shear limit ¹⁵.

In the semi-dilute region ($l/L^3 \ll \nu \ll 1/(L^2d)$), particles cannot rotate freely because of entanglements and log-jamming. The entanglement of rod-like particles restricts the perpendicular translation diffusion and log-jamming hinders the longitudinal translation diffusion. Therefore, particle shape, aspect ratio and microstructure of rod-like particle suspensions will affect the flow behavior of CNC suspension in dilute and semi-dilute phases ¹⁵.

1.1.5 Electroviscous Effect

CNC nanoparticles are negatively charged particles, and an electric double layer surrounding CNC also contributes to the flow behavior that is called an electro-viscous effect. For rigid colloids, two electro-viscous effects can be marked: 1) Primary electro-viscous effect and 2) Secondary electro-viscous effect. The primary electro-viscous effect contributes to the intrinsic viscosity due to shear-distortion of the double layers. As an electrical body forces are affected by ions in the double layer that changes the flow and increase the viscous dissipation ¹⁵. Increase in viscosity can be calculated by introducing primary electro-viscous effect ¹⁸:

$$\frac{\eta}{\eta_0} = 1 + ([\eta]_0 + [\eta]_{ev})\phi \quad \phi \rightarrow 0 \quad \text{Equation 1.13}$$

Viscosity of electro-viscous effect is calculated (Equation 1.14) with the strong Brownian rotation of the particle in the low-shear limit by Sherwood ²⁰.

$$[\eta]_{ev} = l\kappa(\log d\kappa)^2/4(\log d/l)^2 \quad (l \gg \kappa^{-1} \gg a) \quad \text{Equation 1.14}$$

Moreover, the intrinsic viscosity of colloidal suspensions can be manipulated with the addition of the electrolyte that leads to a decrease in intrinsic viscosity because of compression of the double layer thickness (κ^{-1}) ¹⁵.

The secondary electro-viscous effect modifies the bulk stress because of the interactions between overlapping double layers. Large repulsion between overlapping double layers causes yield stress as the dispersion does not flow before the application of a certain minimum shear stress ¹⁵.

1.1.6 CNC Suspensions

In the literature, the flow behavior of CNC is generally studied to understand the phase behaviors and microstructure of CNC suspensions (Table 1.1). Isotropic-nematic phase range changes with dimensions and aspect ratio of CNC suspension. In other words, phase change starts in lower concentrated suspensions with higher aspect ratio due to excluded volume interactions of CNC nanoparticles and electro-viscous forces. In addition to phase behavior change, Boluk and coworkers (2011) measured the intrinsic viscosity of dilute CNC suspension to calculate the shape factor of CNC rods by considering electro-viscous effect ²¹. Interestingly, dilute and semi-dilute rheological behavior of CNC suspensions was not investigated in detail in the literature.

Table 1.1 Studies on phase behaviors of CNC suspensions

Article	Length (nm)	Width (nm)	(L/D)	Isotropic Concentration Range
Liu and coworkers (2010) ²²	90	10	9	0.91%-3.17%
Shafiei-Sabet et al. (2012) ²³	N/A	N/A	13-20	3.00 wt%-7.00 wt%
Urena-Benavides et al. (2012) ²⁴	100	20	5	3.07 vol%-10.40 vol%

1.2 Polymer Solutions

In our study, water soluble polymers are incorporated into CNC suspensions to generate CNC suspension in dilute and semi-dilute polymer solutions. In the last section, we reviewed the flow behavior of colloidal suspensions without the presence of polymer. Here we will review conformations and the flow behavior of water-based polymer solutions in dilute and semi-dilute concentration regime without the presence of colloidal particles. These two sections will help in an investigation of the flow behavior CNC suspension in polymer solutions. Since we are going to work with CNC suspension in non-ionic (polyethylene oxide, PEO) and anionic (carboxymethyl cellulose, CMC) linear flexible polymer solutions in dilute and semi-dilute states, discussions in this section focus on conformations, dilute and semi-dilute states and the flow behavior of such polymer solutions.

1.2.1 Molecular Weight and Length of Polymers

Polymers are organic macromolecular chains that consist of “*n*” number of repeating units, formed by polymerization of monomers. The number of repeating units, *n*, is also defined as the degree of polymerization. It is generally in the range of 10^3 and 10^6 . Molecular weight of polymers cannot be a single value as polymers are polydisperse, containing unequal length of polymer chains. Therefore, the molecular weight is defined as the distribution of chain lengths²⁵. The different approach of defining the contributions of distributions of long chains allows different expressions of molecular weight. The number average molecular weight (M_n) is statistical molecular weight of polymer chains²⁵:

$$M_n = \frac{\sum N_i M_i}{\sum N_i} \quad \text{Equation 1.15}$$

where M_i is the molecular weight of chain “*i*” and N_i is the number of chains with the molecular weight, M_i . Equation 1.16 is the average of the molecular weights of the individual polymer chains. M_n values are determined with colligative measurements methods such as ebulliometry, cryometry, osmometry and end group determination²⁶. The second approach to determine the molecular weight is the weight average molecular weight (M_w) and it is defined as²⁵:

$$M_w = \frac{\sum N_i M_i^2}{\sum N_i M_i} \quad \text{Equation 1.16}$$

Larger macromolecules will have larger contributions to M_w . M_w is experimentally measured by using static light scattering and ultracentrifuge methods. Gel permeation chromatography is the best method not only to determine M_n and M_w but also obtain the whole chain length distribution²⁶. Furthermore, the molecular weight distribution is practically expressed by the ratio of M_w to M_n which is called as polydispersity index (PDI) or heterogeneity index (HI). PDI explains how polydisperse is the polymer sample. PDI is equal to 1 when the polymer is monodisperse, and PDI is larger than 1 when the polymer is polydisperse.²⁵

1.2.2 Single Chain Conformations

A molecular structure of polymer chains and interactions between solvent molecules and polymer molecules result in different chain conformations. Dimensions of polymer chains in solutions depend on number of monomer repeating units, chain length, and their chemical bonding structure and polymer solvent interactions. Conformations of dilute polymer solutions in good solvents can be modelled based on dimension of a single chain. A single coil conformation can be defined for the calculation of the end-to-end distance, R_{e-e} based on random walk model (Figure 1.2).

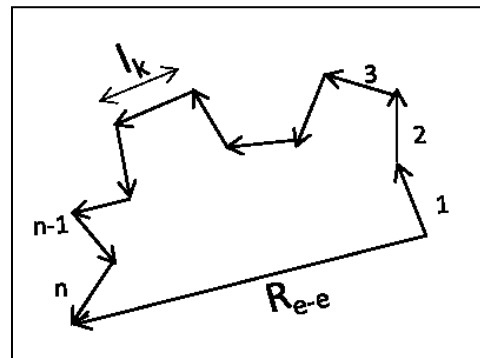


Figure 1.2 Illustration of random coil with the end-to-end distance, R_{e-e} .

When all bond lengths are the same, there is no correlation between the directions of bond angles, and there is no treatment of torsional angles, the polymer chain is considered as an ideal flexible chain. The end-to-end distance, R of flexible chain is calculated with the Equation 1.17 which is based on one dimensional random walk ²⁷:

$$\langle R^2 \rangle^{1/2} = ln^{1/2} \quad \text{Equation 1.17}$$

where l is the length of bonds between repeating unit monomers, and n is the number of monomers. In a real polymer chain, the valance between angles and between bonds is fixed, and also rotations of the bonds are not totally free. Therefore, the limitations to the flexibility of chains are defined by characteristic ratio (C_∞) in Equation 1.18 ²⁷.

$$\langle R^2 \rangle^{1/2} = C_\infty ln^{1/2} = l_k N^{1/2} \quad \text{Equation 1.18}$$

where l_k is Kuhn length and N is the number of segments. For freely jointed chains, the Kuhn length (l_k) and the number of segments (N) are equal to $C_\infty l$ and n/C_∞ , respectively. The larger values C_∞ correspond to the larger the spatial distance between intermolecular interference with free movement. Furthermore, l_k describes the minimum length between two points on a polymer and (Figure 1.2) where the orientation of each segment is independent of all others²⁷.

There is no direct experimental method to measure the R_{c-e} . Therefore, the radius of gyration, R_g is used to define the dimensions of the chain. R_g is the distance from the axis, where all mass can be concentrated to obtain the same mass moment of inertia; it is an experimentally measured property. For an ideal chain, linear and uniform flexible chain with a sufficient long random walk, R_g is²⁷:

$$\langle R_g^2 \rangle^{1/2} = C_\infty^{1/2} l \left(\frac{n}{6} \right)^{1/2} = l_k \left(\frac{N}{6} \right)^{1/2} \quad n \gg 1 \quad \text{Equation 1.19}$$

1.2.2.1 Excluded volume interaction

When two polymer segments on a single chain are far apart from each other, the long-range interactions between monomers affect the chain dimension. In real chains, excluded volume interaction restricts the random walk of chains that affects the distance along the chain. In other words, chains repel each other and that results in an expansion of the chain size. Coil expansion of polymer is expressed with a relation between R and N ²⁷.

$$\langle R^2 \rangle^{1/2} \cong l_k N^{3/5} \quad \text{Equation 1.20}$$

1.2.2.2 Hydrodynamic interaction

In the presence of solvent, the hydrodynamic interactions due to the solvent presence influence the chain conformation. Hydrodynamic interaction is caused by molecular friction coefficient (Z_o) which is the proportional constant in Stokes' law. In Stokes' law, the frictional force has an effect on polymer molecules, and drag solvent molecules along the same direction. In dilute suspensions of hard sphere, the friction coefficient is calculated as²⁷:

$$Z_o = 6\pi\eta_s R \quad \text{Equation 1.21}$$

In strong interactions, the polymer chain act as the hard sphere with a radius R_h as the chain interior is shielded from the flow. For the long chains, the hydrodynamic radius, R_h is predicted with ²⁷ :

$$R_h = \frac{kT}{6\pi\eta_s D_o} \quad \text{Equation 1.22}$$

where D_o is the diffusion coefficient of the chain.

1.2.2.3 Extension of polymeric chains by external forces

Stretching of chains is observed due to external forces and the extended chain length, $\langle r \rangle_f$ is expressed with ²⁷. The dimension of a chain due to stretching can be expressed as:

$$\langle r \rangle_f = \frac{f}{3kT} R_o^2 \quad \text{Equation 1.23}$$

where R_o is the chain dimension. Configurational entropy decreases due to external forces such as thermal, shear and extensional deformation that always stretch the chain and extend the end to end distance ²⁷.

1.2.3 Polymer Solutions and Flory Huggins Theory

The molecular structure of polymer chains and interactions between solvent molecules and polymer molecules result in different chain conformations. Solvent addition results in polymer dissolution as solvent molecules surround the polymer chain. Miscibility of the polymer in a given solvent is well explained by the Flory-Huggins lattice theory. The change in interactions such as hydrogen bonding, van der Waals interactions and dipole-dipole interaction affects enthalpy of mixing which governs the miscibility. These interactions are defined clearly with the change of the free energy of the system changes upon mixing ^{25,27}.

$$\Delta G_{mix} = \Delta H_{mix} - T\Delta S_{mix} \quad \text{Equation 1.24}$$

Based on thermodynamic response, solutions can be categorized into four kinds: (1) ideal, (2) athermal, (3) regular and (4) irregular (real) solutions. In ideal solutions, the enthalpy of mixing (ΔH_{mix}) equals to zero ,thus; the entropy of mixing (ΔS_{mix}) affects the Gibbs free energy change

(ΔG_{mix}). In athermal solutions, the enthalpy of mixing is zero but entropy of mixing known as excess entropy is different than ideal solutions. In regular solutions, entropy of mixing is the same as ideal solution but enthalpy of mixing is not zero. In real solutions, the enthalpy of mixing and the excess entropy have to be taken into account, and the enthalpy decreases by dissolution. According to Flory-Huggins theory, ΔS_{mix} is defined with the comparison of the number of possible arrangement of polymer chains on available sites with the number of possible arrangement of polymer chains before mixing give ΔS_{mix} ^{25,27}:

$$\Delta S_{mix} = -k_B n_{site} \left[\frac{\phi}{N} \ln \phi + (1 - \phi) \ln(1 - \phi) \right] \quad \text{Equation 1.25}$$

where ϕ is the volume fraction n_{site} is the number of available sites, and N is the number of monomers. However, the value of ΔS_{mix} is much lower in polymer-solvent systems especially in dilute state. Therefore, the change in enthalpy affects solubility of polymer. ΔH_{mix} is related to Flory interaction (χ) parameter (χ) that determines the miscibility trend²⁵.

$$\Delta H_{mix} = Z N_0 \left[\epsilon_{SM} - \frac{1}{2} (\epsilon_{MM} + \epsilon_{SS}) \right] \phi (1 - \phi) \quad \text{Equation 1.26}$$

$$\chi = Z [\epsilon_{SM} - (\epsilon_{MM} + \epsilon_{SS})/2] / k_B T \quad \text{Equation 1.27}$$

where Z is the number of neighbors of monomer site. χ is positive when the monomer-solvent contacts are less favored compared with the monomer-monomer and solvent-solvent contacts. A negative χ donates monomer-solvent contacts are preferred, promoting solvation of the polymer. According to relation, with the increase temperature, the magnitude of χ decreases. Moreover, the pair interactions also depend on the temperature and χ usually changes from negative to positive with the increase of temperature. Therefore, the quality of the solvent for a given polymer can be changed either by changing the temperature or by changing the mixing ratio of a good solvent to a poor solvent; the value of the χ parameter also defines the solvent quality (Table 1.2). Solvent quality is defined as athermal solution when ΔH is zero. In athermal solutions, the chain sizes have same dimensions as in good solvent. The solvent quality depends mainly on the specific chemistry determining the interaction between the solvent molecules and monomers. It can be changed by varying the temperature.

Table 1.2 Solvent quality change with respect to χ parameter for neutral polymers^{25,27,28}.

Solvent Quality	χ parameter	Chain Size (R)
Athermal Solution	=0	$=l_k N^{3/5}$
Good Solvent	<1/2	$=l_k N^{3/5}$
Theta Solvent	=1/2	$=l_k N^{1/2}$
Poor Solvent	>1/2	$\approx l_k N^{1/3}$

The conformation of polymer chain is changing constantly with the presence of solvent (Table 1.2 and Figure 1.3). In a poor solvent and dilute concentration range, neutral polymers at shrink into globule with the size $R \approx l_k N^{1/3}$ due to attractive interactions between monomers²⁸. On the other side, neutral polymers in dilute concentration range in theta solvent exhibit monomer-solvent interactions and monomer-monomer interactions are similar, leading to random walks with ideal end-to-end distance $R = l_k N^{1/2}$ ²⁸. This is also valid for polymer melts and concentrated polymer solution systems. In good solvent or in the extreme limit of athermal solution, chains of neutral polymers extend due to excluded volume and favorable interaction between monomers and solvent molecules. The size of neutral polymers in good solvent is described with self-avoiding walks, and defined with the Flory end-to end distance, $R_F = l_k N^{3/5}$ ²⁸. In polyelectrolyte solutions with no salt, charge repulsion controls the chain conformation so chains stay apart from each other and have the extended directed random walk conformation with length L proportional to N ²⁸.

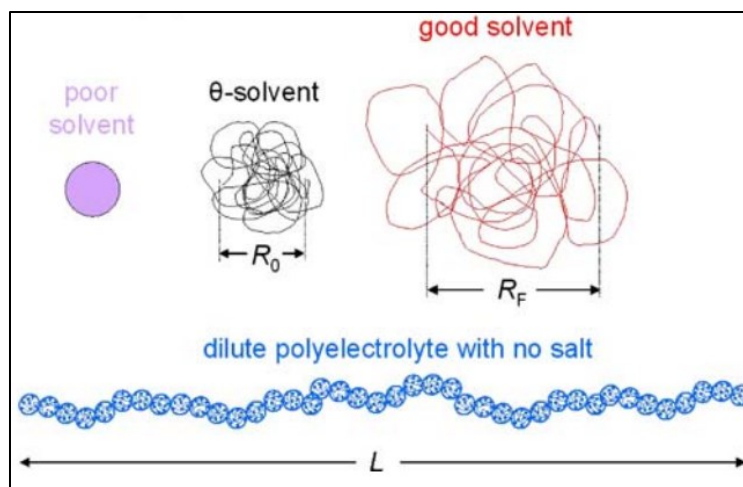


Figure 1.3 The conformation of neutral and nonionic polymer chains with respect to solvent quality²⁸
 Reprinted from: Colby, R. H. Structure and linear viscoelasticity of flexible polymer solutions: comparison of polyelectrolyte and neutral polymer solutions. Rheologica Acta 2010, 425-442.

1.2.4 Stability and Phase Diagrams

Stability and phase diagram (Figure 1.4) of polymer solution can be determined theoretically by using chemical potential relation with chi parameter²⁵.

$$\Delta\mu_p/k_B T = \ln\phi + N[\chi - 1 + (1 - 2\chi)\phi + \chi\phi^2] \quad \text{Equation 1.28}$$

The boundaries to the instability can be found from $\partial\Delta\mu_p/\partial\phi$. In phase diagrams (Figure 1.4), the coexistence curve and the spinodal line divide the diagram into three main regions: 1) Unstable region, 2) Metastable region, and 3) Stable region. Above the spinodal line, the system is unstable and the solution is separated into two phases spontaneously. The solution between two lines is metastable.

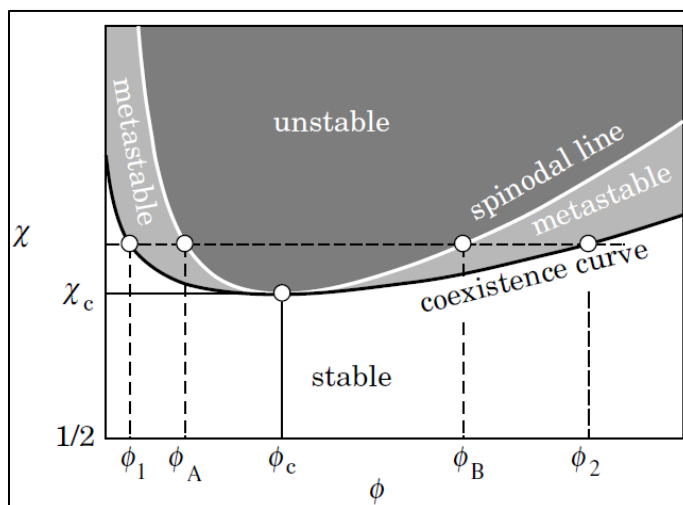


Figure 1.4 Phase diagram of polymer solution²⁵ Reprinted from: Teraoka, I. *Polymer solution: an introduction to physical properties*; Wiley: New York, 2002.

Interactions between solvent molecules and polymer chains determine the miscibility of polymer in certain solutions. However, not only polymer chain solvent interaction but also temperature is an effective parameter for phase separation as it influences entropy and enthalpy change. Phase separation is observed at elevated temperature unless enthalpy and entropy change decrease too rapidly from their initial values. Moreover, the mixing ratio of solvent or composition of solution is another effective parameter. In polymer solutions, upper critical

temperature and lower critical temperature shows higher and lower temperatures on the coexistence curve, and between these temperatures phase separation can be seen in Figure 1.5.

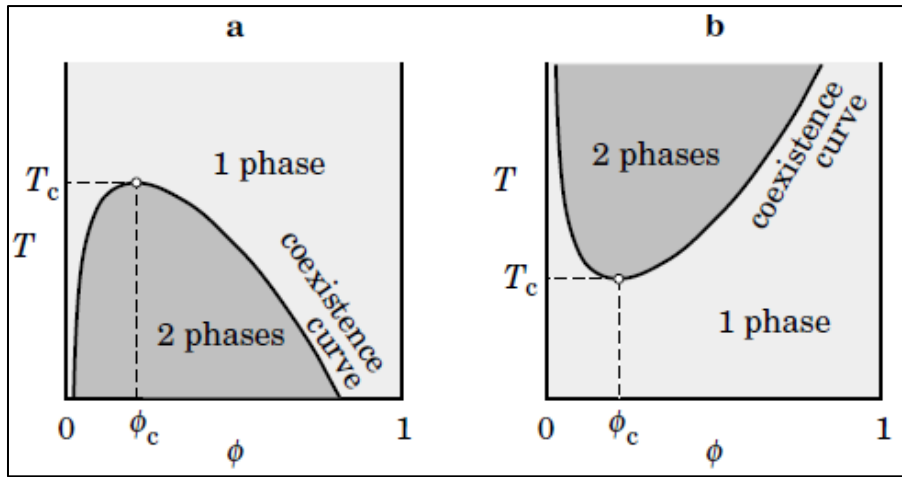


Figure 1.5 Upper critical temperature (a) and lower critical temperature of polymer solution in phase diagrams²⁵. Reprinted from: Teraoka, I. *Polymer solution: an introduction to physical properties*; Wiley: New York, 2002.

1.2.5 Concentration Regime

Concentration regime is a fundamental concept of interactions in polymer solutions. So far we discussed the properties of dilute and concentrated polymer solutions. The transition from dilute to semi-dilute concentration leads to different conformations of polymer chains in solutions. The concentration regime of polymer solutions varies with the change of molecular weight and concentration (Figure 1.6). With an increase in concentration, the individual chains start to overlap each other at a certain point which is called overlap concentration. The overlap concentration is the transition point from dilute to the semi-dilute concentration regimes. In the dilute regime, the polymer chain interacts primarily with the solvent molecules. The solution is close to an ideal solution. In the dilute regime, concentration is below overlap concentration (c^*)

^{28,29}.

$$c^* \approx \frac{N}{R_{dilute}^3} \approx N^{1-3\nu} \quad \text{Equation 1.29}$$

where R_{dilute} is directly proportional to N^ν and ν is equal to 1/2 for θ -solvent, 3/5 for good solvent, and 1 for polyelectrolytes without salt.

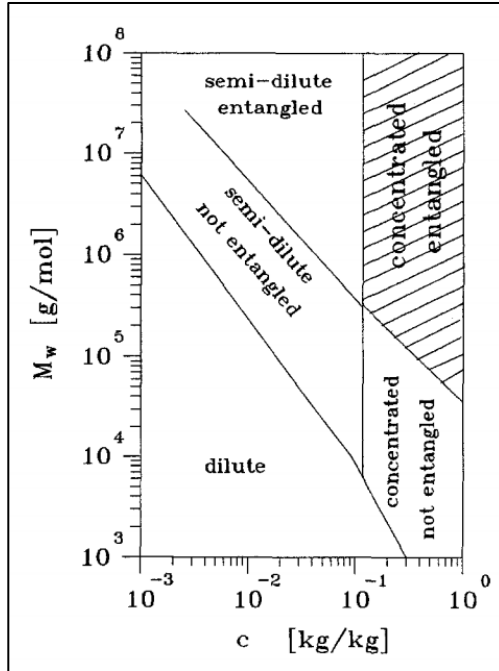


Figure 1.6 Concentration regime of polymer solution with the respect to molecular weight and concentration ²⁹ Reprinted from: Baumgärtel, M.; Willenbacher, N. The relaxation of concentrated polymer solutions. *Rheologica Acta* 1996, 35, 168-185.

When the concentration is above c^* , the polymer solution is in the semi-dilute regime, and the excluded volume interaction involves other interactions. The blob model is introduced to explain the structure of solution with respect to concentration in a semi-dilute state. In the model, the blob size is equal to correlation length; ζ is used to understand the structure of solution (Figure 1.7) ^{25,28}.

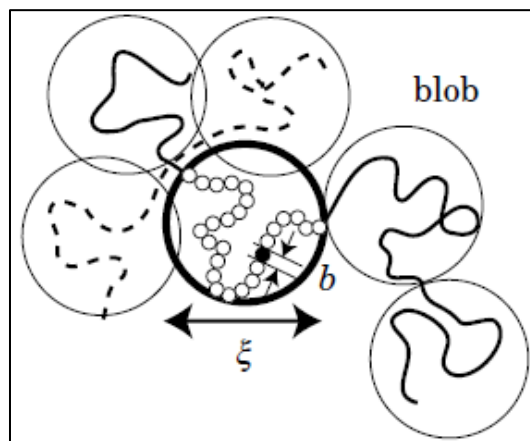


Figure 1.7. A blob of size ζ has monomers of size b from the same chain ²⁵ Reprinted from: Teraoka, I. *Polymer solution: an introduction to physical properties*; Wiley: New York, 2002.

When the chain length is smaller than ξ , the blob size polymer chains have conformations similar to dilute solution conformations (except for poor solvent). When the length is larger than ξ , the chain conformations have a random walk of correlation blobs of size ξ . In this case, a monomer on a given polymer chain will interact with other monomers in different blobs. Furthermore, an increase in concentration leads to a decrease in blob size. In polyelectrolyte solutions, repulsion interactions also become part of other interactions and the correlation length is termed as screening length. In 1979 de Gennes determined the dependency of the correlation length ²⁸:

$$\xi \approx R_{dilute}(c/c^*) \approx c^{-\nu/(3\nu-1)} \quad \text{Equation 1.30}$$

where ξ is independent of N . The random walk of correlation blobs gives the end-to-end distance of the chain in the semi-dilute solution ²⁸:

$$R \approx \xi(N/g)^{1/2} \sim N^{1/2} c^{-(\nu-1/2)/(3\nu-1)} \quad \text{Equation 1.31}$$

where g is the number of monomers per correlation blob. Moreover, g is equal to $c_n \xi^3$ and c_n is the number density of monomers. The correlation length can be listed in Table 1.3 with respect to solvent type and polymer type.

Table 1.3 Correlation length and end-to-end distance with respect to polymer and solvent types ^{25,28,30}.

Polymer Type	Solvent Types	ν	ξ	R
Neutral Polymer	Theta Solvent	1/2	$\sim c^{-1}$	$\sim N^{1/2} c^0$
Neutral Polymer	Good Solvent	3/5	$\sim c^{-0.76}$	$\sim N^{1/2} c^{-0.12}$
Polyelectrolytes	Solvent with no salt	1	$\sim c^{-1/2}$	$\sim N^{1/2} c^{-1/4}$

1.2.6 Viscosities of Polymer Solutions

Conformational changes of polymer in dilute and semi-dilute solutions are described above; however, polymer solutions are not in a static state. Position and shapes (structure) of polymer chains and solvent molecules change constantly due to thermal energy. Rheological measurement is a method to understand polymer dynamics as viscosity and viscoelasticity of polymer solutions, which give information of the structure of polymer solutions.

The intrinsic viscosity, $[\eta]$ which is already defined in Equation 1.2 and 1.3 can be used as a measure of polymer coil in solutions. A simple intrinsic viscosity measurement method developed by the extrapolation of $\frac{\eta_{sp}}{c}$ in Equation 1.2 ³⁰.

$$\frac{\eta_{sp}}{c} = [\eta] + K_H[\eta]^2 c \quad \text{Equation 1.32}$$

where K_H is the Huggins constant. Molecular weight and the intrinsic viscosity relation are determined with the Mark–Houwink–Sakurada Equation. This equation is applicable to many polymers and is extensively used to determine molecular weight ³⁰ :

$$[\eta] = K_\eta M_v^a \quad \text{Equation 1.33}$$

where M_v is the viscosity average molecular weight, and K_η and a both are constants. The M_v is a property that is empirically determined with rheological measurements. The order of magnitude of M_v is between M_n and M_w . K_η and a vary with polymer and solvents. The exponent a determines the polymer chain's three-dimensional configuration in the solvent environment and varies from 0.5 to 2.0. When a values are from 0.0–0.5, the polymer chain reflects as a rigid sphere in an ideal solvent. " a " values from 0.5–0.8 correspond to a random coil in a good solvent. " a " values between 0.8 and 2.0 refer to a rigid or rod-like configuration (stiff chain). When a exponent is close to 0.75 or higher, the solvent quality of polymer solutions called “good solvent”. In poor solvents, a exponent is close to 0.5 ³⁰.

The intrinsic viscosity also shows a relationship between molecular weight and chain dimension. When we assume polymer chains as hard spheres, we can merge Equation 1.32 with Equation 1.4. The definitions of η and K_H derived as $\frac{5}{2}(\phi/c)$ and 0.99, respectively. The volume fraction, ϕ of polymer chains in the solution is the product of molecular number density, ν and pervaded volume, $\nu_{per} = 4\pi R_g^3/3$. The mass concentration is the product of molecular number density per molecule, $c = \nu M/N_a$. Therefore, M- R_G relation is expressed as ²⁷:

$$[\eta] \sim \frac{10\pi N_a R_g^3}{3 M} \quad \text{Equation 1.34}$$

Additionally, $[\eta]$ measurement is used to define overlap concentration defining in previous section. The overlap concentration is directly proportional to the chain dimension (Equation

1.28). In good solvent, c^* can be approximately related to the intrinsic viscosity $[\eta]$ (Equation 1.34):

$$c^* \sim \frac{1}{[\eta]} \quad \text{Equation 1.35}$$

Equation 1.35 is consistent with Equation 1.31 when we can neglect the higher power-terms of concentration. Polymer solutions exhibit in non-Newtonian range. The measurement of zero shear viscosity, η_0 of polymer solutions can be used for the concentration range determination as η_0 is the viscosity of polymer solutions that exist in the Newtonian range. The change in concentration and molecular weight are directly proportional to η_0 (Figure 1.8). For instance, an increase in concentration and molecular weight (M_w) results in an increase in η_0 because of an increase in polymer molecule interactions. After a certain critical point, entanglement formation occurs and concentration regime changes from semi-dilute unentangled state to semi-dilute entangled state, leading to a drastic increase in η_0 . This critical point is defined as critical molar mass (M_w^*) when the change in molecular weight is considered. Below M_w^* , η_0 increases linearly with respect to M_w . Above M_w^* , η_0 is proportional to M_w^{*4} . Consideration of the change in concentration, “critical concentration, c^{**} ” term is used to define concentration transition point. Moreover, the crossover point (c^{**}) in Figure 1.9 corresponds to transition concentration from semi-dilute unentangled to semi-dilute entangled solution ³⁰. Also, Equation 1.35 is used to determine the transition concentration between semi-dilute unentangled and semi-dilute entangled ^{31,32}.

$$c^{**} \approx 8c^* \quad \text{Equation 1.36}$$

In addition, the viscosity dependency of polymer concentration in a good solvent in the semi-dilute regime can be summarized as ³²:

$$\eta \sim \begin{cases} a c^{1.25} & \text{Semi-dilute unentangled} \\ a c^{4.25-4.5} & \text{Semi-dilute entangled} \end{cases} \quad \text{Equation 1.37}$$

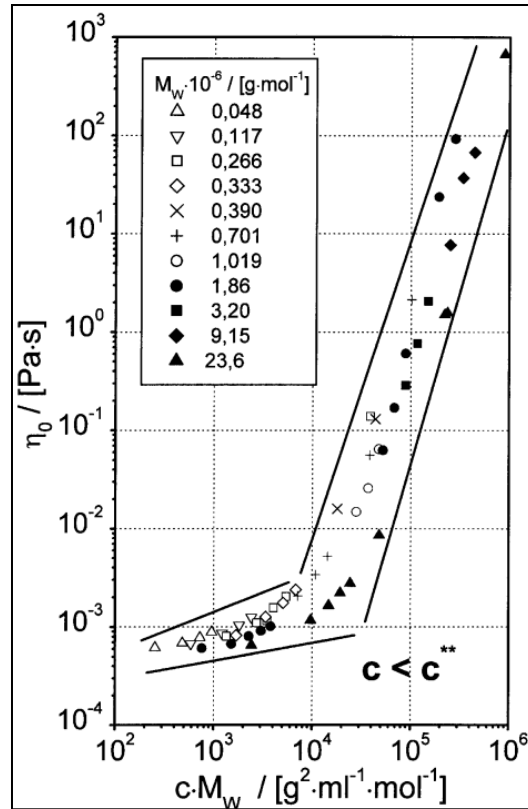


Figure 1.8 Zero-shear viscosity as function of molecular weight and concentration ³⁰ Reprinted from: Clasen, C.; Kulicke, W. -. *Progress in Polymer Science* 2001, 26, 1839-1919.

Polymer solutions even at diluted concentrations, display Newtonian (shear independent) viscosity only at very low shear rates, (dy/dt). Viscosities of polymer solutions decrease as shear rate increases after reaching to a critical shear rate. Figure 1.9 shows a general picture of shear thinning polymer solutions. This linearly on a log-log scale plots (Shear thinning fluids). Therefore viscosity becomes a function of not only molecular weight and polymer concentration but also rate of shear deformation. It is necessary to know: 1) at which critical shear rate the shear thinning behavior of viscosity starts; 2) The slope of viscosity versus shear rate on the log-log plot during the shear rate dependent region.

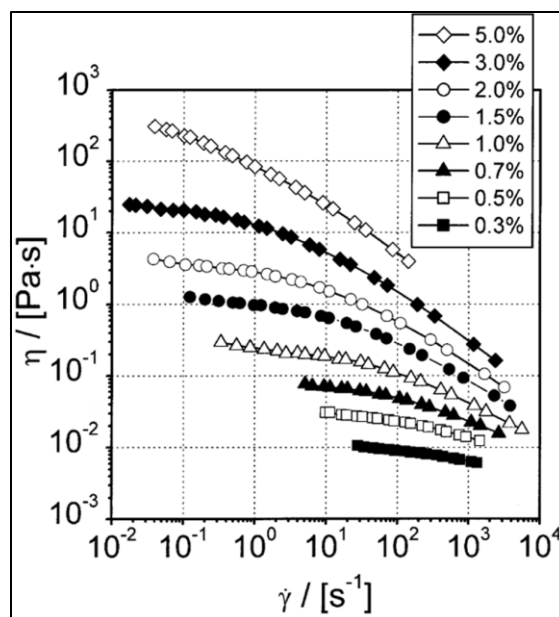


Figure 1.9 Viscosity vs. shear rate plots of a cellulose ether polymer at various polymer concentrations ³⁰
 Reprinted from: Clasen, C.; Kulicke, W. Determination of viscoelastic and rheo-optical material functions of water-soluble cellulose derivatives. *Progress in Polymer Science* 2001, 26, 1839-1919.

The characteristics time behavior of polymer solutions at dilute and semi-dilute concentrations have to be considered for the analysis of non-Newtonian behavior of polymer solutions.

1.2.7 PEO and CMC Solutions

In this thesis, we are working with polyethylene oxide (PEO) and sodium carboxymethyl cellulose (Na-CMC); thus, the previous studies with PEO and Na-CMC are the focus in this part. Kjellander and Florin (1981) studied phase behaviors of aqueous solutions of polyethylene oxide (PEO) ³³. They found negative values of enthalpy and entropy change due to the overlap between hydration shells of neighboring chains. This property of PEO shows that PEO with a certain a MW has the upper critical and the lower critical temperature values. To determine the phase separation experimentally, the cloud point method is commonly used. In this method, cloud point temperature, in which the solution becomes turbid, is determined with the use turbidity analyzer.

Devanand and Selser (1991) developed two relations between molecular weight and radius of gyration and second virial coefficient for different molecular weights of polyethylene oxide by using multi-angle light scattering experiments ³⁴.

$$R_g = 0.215 M_w^{0.583 \pm 0.031} \quad \text{Equation 1.38}$$

Daga and Wagner (2006) determined the c^* and the c^{**} of aqueous polyethylene oxide solution with the combination of Equation 1.33 and 1.34, Mark-Houwink-Sakurada relation (Equation 1.31) and the rheological measurements³¹. They theoretically calculated the c^* and the c^{**} values as 0.23 wt% and 1.83 wt%, respectively. They empirically found the c^{**} about 3.2 wt% with the determination of the change in slope of η_0 versus concentration. They empathized large molecular weight polydispersity in the PEO caused the difference between experimental and theoretical values.

Kulicke and coworkers (1995) characterized CMC structure by varying molecular weight from 200000 to 2 000000 g mol^{-1} . The $[\eta]$ -M relationship, were determined with multi-angle laser light scattering and size exclusion chromatography (Equation 1.38). The influence of concentration and the influence of the molecular weight on zero-shear viscosity were found as $\eta_0 \propto c^{4.3}$ and $\eta_0 \propto M^{3.9}$, respectively³⁵.

$$[\eta] = 1.43 \times 10^{-2} M_w^{0.90} (\text{cm}^3 \text{g}^{-1}) \quad \text{Equation 1.39}$$

Chatterjee and Das (2013) determined radius of gyration of Na-CMC with different molecular weight with $[\eta]$ measurements. They used M- R_G relation (Equation 1.33) to calculate and they observed that the value of the radius of gyration is decreased with an increase in concentration, whereas the radius gyration's values increase with an increase in molecular weight³⁶.

Benchabane and Bekkour (2008) studied the rheological properties of Na-CMC with the M_v of 700 kDa and found the critical concentration c^{**} around 1% by plotting specific viscosity based on concentration change. The zero shear rate viscosity, η_0 is used as intrinsic viscosity to calculate specific viscosity (Equation 1.3)³⁷.

1.3 Nanoparticle Suspensions in Polymer Solutions

When colloidal particles are incorporated into polymer solution, polymer chains can either be adsorbed onto particles or deplete particles. Adsorption and depletion can be defined with respect to change in polymer chain composition near the particle interface.

1.3.1 Adsorbing Polymers

Adsorption can be considered when the concentration of the polymer chains increase in the interfacial region which can results in both bridging and aggregation of particles or steric stabilization of polymer chains. Thermodynamically, adsorption depends on the net adsorption energy of polymer chain. The net adsorption energy of polymer chain is the difference between the free energy of chain-surface contacts and that of solvent- surface contacts. If difference is negative, adsorption will be observed ³⁸.

Adsorption of polymer chains on the surface can be distinguished as two types. When the formation of chemical bonds between chain and surface occurs, this is defined as chemisorption. Otherwise, physisorption term is used when physical interactions such as van der Waals interactions, dipolar couplings and hydrogen bonds exist between polymer chain and surface. In physisorption case, the adsorbed chain may be displaced by another chain from the bulk solution but there is no possibility such displacement for grafted (chemisorbed) chain. In chemisorption, polymer molecules are attached to surface. In the case of adsorption, there are various systems: physisorbed homopolymers, polyelectrolytes, block copolymers and terminally attached chains³⁹. Homopolymer adsorption case, chain length, chain length distribution, solvency and adsorbent properties are effective parameter. The adsorbed amount at fixed concentration varies with molecular weight depends on solvent type. In good solvents, the adsorbed amount of polymer chain on the surface increase with the increase of chain length in low molecular weight range. On the other hand, adsorbed amount does not depend on chain length in theta solvents especially in high molecular range. High molecular range refers to the high-affinity character of adsorption isotherm. Copolymers consist of more than one type of structural unit, therefore; primary structure of copolymer is a dominant parameter to determine the adsorbed amount. Random copolymers are similar to homopolymers whereas block copolymers are rather different. In that case, only one type of block tends to adsorbed onto surface and other block extends away from the surface. In polyelectrolytes, electrostatic interaction play important role, thus; charge densities of polymer and surface, salt concentration are significant variables ³⁹.

Adsorption causes conformational change of polymer chains. Adsorption of polymer chain onto surface can be seen schematically in Figure 1.10.a, which consists of three types of sub-chains: trains, loops and tails. Trains are the segments of polymer chain contact with surface and

loops are non-contacted segments of polymer chains and tails are non-adsorbed chain ends. High amount of trains refers to strong adsorption, whereas in weak adsorption tail and loop amount is higher than train amount. As seen in Figure 1.10.b, polymers can be attached to as mushrooms, brushes or as adsorbed chains (pancake structures) depending on adsorption energy (χ_s):

$$\chi_s = (u_1^a - u_2^a)/kT \quad \text{Equation 1.40}$$

where u_1^a and u_2^a are adsorption energy of solvent molecule and polymer segment, respectively. Polymer adsorbs onto surface when χ_s is positive, besides conformational change occurs with the magnitude of χ_s compared to critical adsorption energy (χ_{sc}):

$$\chi_{sc} = -\ln(1 - \lambda_1) \quad \text{Equation 1.41}$$

where λ_1 is lattice parameter which is $1/4$ for a hexagonal or tetrahedral lattice. When χ_s is less than χ_{sc} , chain is entropically repelled from the surface and mushroom structure occurs. Whereas, pancake structure can be seen when χ_s is greater than χ_{sc} as polymer segment revisits the surface. In brush regime, structure is independent of χ_s except in the region close to surface. In that case, solvent quality plays role to determine structure. In a good solvent, brushes tend to extend and find parabolic shape, polymer segments become more compressed and collapse when the solvency becomes worse³⁹.

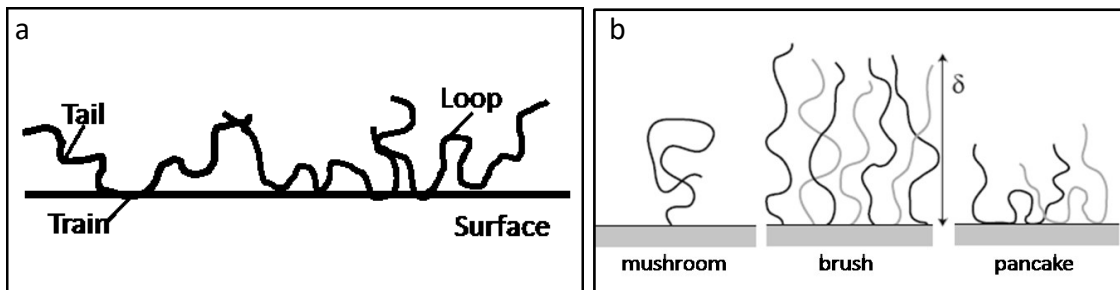


Figure 1.10 Schematic representation of a) adsorbed polymer layer and b) possible structure of adsorbed layers⁵ Reprinted from: Lekkerkerker, H. N. W.; Tuinier, R. Colloids and the depletion interaction; Springer: New York, 2011.

1.3.2 Flocculation by Bridging

A polymer chain adsorbs onto more than two particles to bind them together called polymer bridging. With the partial surface coverage, destabilization of particles occurs due to adsorbed polymers. Bridging mechanism leads to flocculation of colloidal suspensions when the polymer

chain is long enough to adsorb onto two particles and has a very strong affinity for the particle surface. When polymer length is too short, the layer thickness is generally too small for bridging. Furthermore, coverage and a certain minimum layer thickness are needed for effective bridging. Thermodynamically, flocculation is defined with the Gibbs free energy change, ΔG upon the interaction of the adsorbed layers. The flocculation occurs when ΔG of the overlap interaction of the adsorbed layers is negative (Equation 1.24) ⁴⁰.

There are two kinds of bridging mechanism leading to flocculation. The first bridging mechanism happens by the binding of two or more particles with one polymer molecule (Figure 1.11.a). For effective flocculation, the polymer molecule should have more than two adsorbable sites. Moreover, polymer chains should be long enough to adsorb onto more than one particle surface. The surface coverage, θ should be low enough for adsorption of polymer extending from one particle to another particle ⁴¹. The second bridging mechanism occurs when the polymer chains are long and surface coverage is higher compared to the first mechanism (Figure 1.11.b). Generally optimum bridging occurs when the half surface of nanoparticle is covered where the surface coverage, θ is 0.5 ⁴². In this case, polymer chains in different surfaces interact with attractive surface bridging forces and that overcomes repulsion forces. The attractive energy and force per binding molecule is determined when $h < L_c$ ⁶:

$$w(h) = -\varepsilon(L_c - h)/l_k \quad \text{Equation 1.42}$$

$$f(h) = -\varepsilon/l_k \quad \text{Equation 1.43}$$

where h is the distance between particle surface, L_c equals to nl_k and ε is the binding energy per segment. The interaction energy per unit area $W(h)$ is determined by merging tail density, $\Gamma = 1/s^2$ where s is the mean distance between adsorbing points⁶:

$$W(h) = 2\Gamma w(h) = -2\Gamma\varepsilon(L_c - h)/l_k \quad \text{Equation 1.44}$$

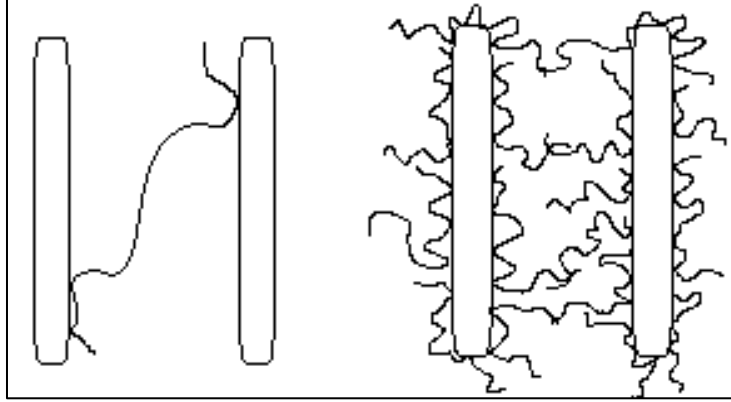


Figure 1.11 Schematic representation of bridging mechanism; a) two particles by one polymer molecule and b) two particles by two separately adsorbed polymer molecules.

1.3.3 Steric Stabilization

When two particles with adsorbed polymer layers approach each other at a distance below a few R_g , interaction of the two layers takes place (5). This interaction generally results in a repulsive osmotic force because of the unfavorable entropy. Thus, the adsorbed layer is compressed and the polymer segments present in the interaction region lose configurational entropy. In this case, this interaction named as steric repulsion or stabilization. The degree of stabilization can be defined thermodynamically in terms of ΔG occurring upon the interaction of the adsorbed layers (Equation 1.24). If ΔG is positive upon the overlap of the adsorbed layers, the steric stabilization will result ⁴⁰.

The steric interaction forces depend on the coverage of polymer on each surfaces, quality of the solvent and adsorption type of the polymer (physisorption or chemisorption). For chemisorbed polymer chains on flat surface with the low surface coverage in theta solvent, there is no entanglement or overlap of neighboring chain and each chain interacts opposite surface independently. For this case, repulsive energy per unit area can be defined when the distance regime is in between $2R_g$ and $8R_g$ as the chain conformation is like mushroom shape on the surface ⁶:

$$W(h) = 2\Gamma kT e^{-h^2/4R_g^2} + \dots + 36 k_B T e^{-h/R_g} \approx 36 k_B T e^{-h/R_g} \quad \text{Equation 1.45}$$

For the high coverage chemisorbed or physisorbed chains, the chain extends away from the surface more than R_g or R_F . This conformation is named brush conformation. For brushes in theta solvent, thickness of brushes, δ is directly proportional with M^ν where ν varies from 0.5 to 1 that

corresponds to from very low coverage to high coverage. In good solvent, the segments repel each other and they generally don't become entangled, the layer thickness can be defined as ⁶.

$$\delta = nl_k^{5/3}/s^{2/3} = \Gamma^{1/3}nl_k^{5/3} = R_F(R_F/s)^{2/3} \quad \text{Equation 1.46}$$

When two brushed covered surfaces are closer than $2L$ from each other, osmotic pressure leads to repulsive energy and repulsive energy can be calculated as ⁶:

$$W(h) = 32\Gamma^{3/2}\delta kT e^{-\pi h/L} \quad \text{Equation 1.47}$$

1.3.4 Non-absorbing Polymers

A decrease of solute concentration near interfacial area in polymer solutions is known as depletion. Depletion interaction colloidal polymer suspensions explained by Asakura and Oosawa in 1954. Their theory proves the increase in free volume of non-absorbing polymers when two hard spheres get close sufficiently (Figure 1.12). Depletion interaction can be determined with this theory. According to Asakura-Oosawa and Vrij model, depletants with a diameter $2R_g$ and bulk density n_p applied osmotic pressure of the polymer (Π) to hard spheres with a diameter $2R$ and surrounded by depletion layer with a thickness δ that resulted in overlap volume (V_{ov}). Interaction potential W_{dep} can be calculated with the relations below ⁶:

$$\Pi = n_b k_B T \quad \text{Equation 1.48}$$

$$V_{ov}(h) = \frac{\pi}{6}(2\delta - h)^2(3R + 2\delta + h/2) \quad \text{Equation 1.49}$$

$$W_{dep} = \infty \quad h < 0 \quad \text{Equation 1.50}$$

$$= -\Pi V_{ov}(h) \quad 0 \leq h \leq 2\delta \quad \text{Equation 1.51}$$

$$= 0 \quad h \geq 2\delta \quad \text{Equation 1.52}$$

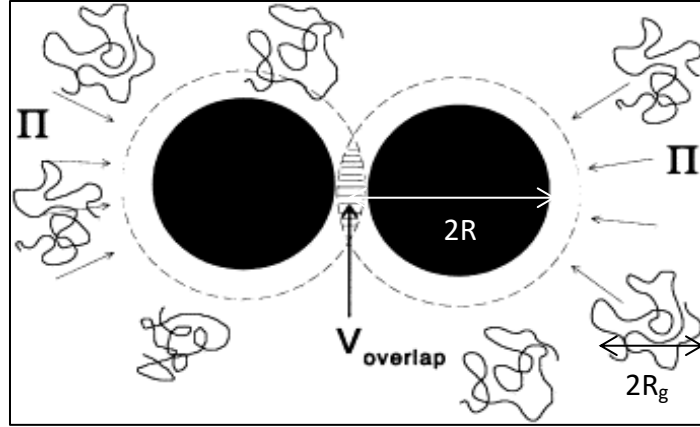


Figure 1.12 Illustration of depletion interaction between polymer chains and hard spheres ⁵ Reprinted from: Lekkerkerker, H. N. W.; Tuinier, R. Colloids and the depletion interaction; Springer: New York, 2011.

In Figure 1.13, the Asakura-Oosawa and Vrij interaction potential, W_{dep} between two hard spheres in a solution containing free polymers is plotted. W_{dep} is decreasing with a decrease in distance between two spherical particles. When the particles touch each other, interaction potential goes infinite.

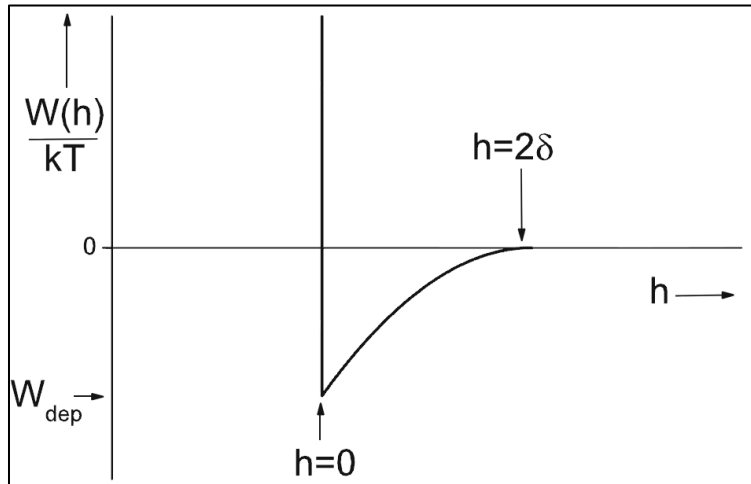


Figure 1.13 Interaction potential W_{dep} versus distance between two spherical particles ⁵ Reprinted from: Lekkerkerker, H. N. W.; Tuinier, R. Colloids and the depletion interaction; Springer: New York, 2011.

1.3.5 Phase Diagrams

In colloid polymer mixture, solution can be found in several states with the function of polymer concentration and particle concentration (Figure 1.14). Lekkerkerker pointed out that at high concentration of particles only crystalline, fluid and fluid crystals can be seen. However, at lower particle concentration, all phases in Figure 1.14 can be observed as depletion force controls the range and strength of attraction independently ⁵. For instance, Khalli (2013) worked

on phase diagrams of CNC suspensions with several polymer solutions. In addition, her study revealed that CNC concentration is one of the effective parameter to observe phase change ⁴³. Moreover, Doxastakis and coworkers (2004) investigated depletion and packing effect of polymer particle mixtures ⁴⁴. They pointed out that depletion interaction is dependent on particle size to chain length ratio and concentration regime of polymer. In the dilute regime, chains are strongly depleted in the vicinity of particle and chain length is effective parameter. In the concentrated regime, depletion interaction is independent of chain length.

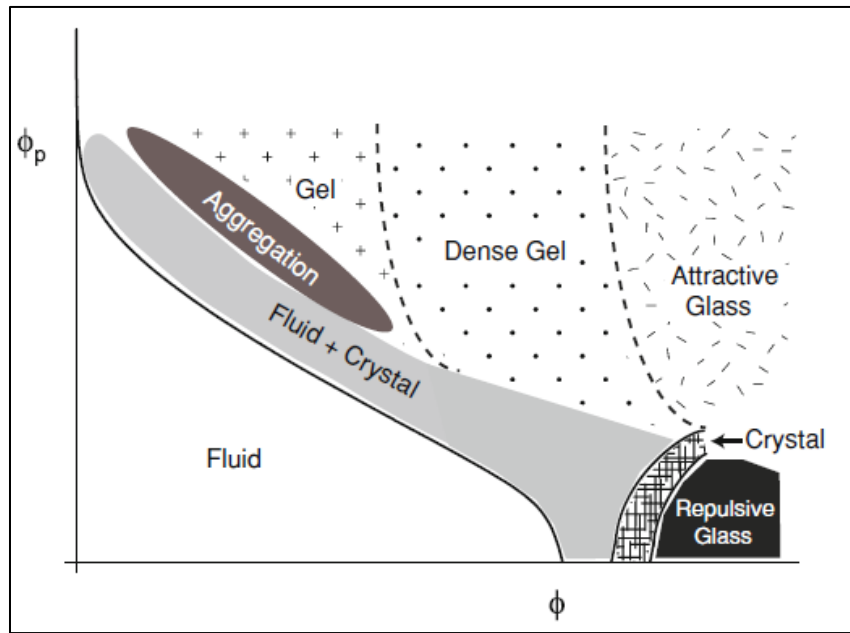


Figure 1.14 State diagram of a colloid–polymer mixture ⁵ Reprinted from: Lekkerkerker, H. N. W.; Tuinier, R. Colloids and the depletion interaction; Springer: New York, 2011.

Besides, Ramakrishnan and coworkers (2004) studied concentrated depletion gels that consisted of hard sphere octadecylsilica and polystyrene solution ⁴⁵. They mentioned that depletion interaction causes gelation in polymer solution and gel elastic modulus (G'), which depend on polymer to particle asymmetry size ratio, R_p/R and reduced polymer concentration (Equation 1.52).

$$G \sim (R_G^2/R)^{-2} (c_p/c^*)^{0.44} \quad \text{Equation 1.53}$$

1.4 Objectives and Experimental Design

In this section, the purpose of this study, selected materials, sample preparation procedures and experimental methods will be discussed.

1.4.1 Scope of Study

The overarching objective of this study is to investigate interaction of cellulose nanocrystals (CNC) suspensions in polymer solutions with the focus on stability, phase diagrams, mesoscopic structures and rheological properties. We would like to achieve following objectives:

- Determining bridging or depletion interaction between CNC and polymer chains.
- Investigating effect of polymer on interactions and bulk properties based on molecular weight, concentration of polymer, radius of gyration.
- Investigating effect of CNC on interactions and bulk properties based on aspect ratio, concentration of CNC.

1.4.2 Experimental Approach

1.4.2.1 Materials

1.4.2.1.1 Cellulose Nanocrystals

Cellulose nanocrystals (CNC) from Celluforce, Inc. (Quebec, Canada) and AITF (Alberta, Canada) were used as nanoparticles. CNC particles can be described by their shape and size which are also critical for their applications⁴⁶. To measure dimensions of rod-shaped CNC particles, microscopic (atomic force microscopy (AFM), transmission electron microscopy (TEM), scanning electron microscopy (SEM) and scattering techniques (depolarized dynamic light scattering (DDLS), small angle neutron scattering (SANS) are the most widely used methods in the literature (ref). Since the width of CNC particles only depend on cellulose feedstock but not on CNC preparation process conditions and also monodisperse by distribution, STEM micrographs is a reliable method to measure the width of CNC particles. However, the length of CNC particles is not uniform and also varies with process conditions. Therefore for a statistically meaningful length, measurements of at least 200 particles have to be measured on the micrographs.

Boluk and Danumah (2014) used STEM and DLS together as a practical way to determine the width and length of CNC particles ⁴⁷. They calculated length of CNC with the use translational self-diffusion coefficient (D_t) of particles and Broersma's correlations. The diameter of CNC is measured with scanning transmission electron microscopy (STEM). Hydrodynamic

diameter of spherical particles (R_h) is obtained by measuring translational diffusion coefficient in DLS measurements ⁴⁷.

$$D_t = \frac{kT}{3\pi\eta R_h} \quad \text{Equation 1.54}$$

where k is Boltzmann's constant, T is absolute temperature, and η is viscosity of suspension. Translational and rotational diffusional motions are observed ⁴⁷.

$$D_t = \frac{kT}{3\pi\eta L} (\ln p + v) \quad \text{Equation 1.55}$$

with the combination of Broersma's correlations (3-5) with translational diffusion coefficient equation 1.56; the length of CNC can be calculated by introducing the diameter (d) from SEM measurements ⁴⁷.

$$v = (\ln 2 - \frac{1}{2(\gamma_{\parallel} + \gamma_{\perp})}) \quad \text{Equation 1.56}$$

$$\gamma_{\parallel} = 0.807 + \frac{0.15}{\delta} + \frac{13.5}{\delta^2} + \frac{37}{\delta^3} + \frac{22}{\delta^4} \quad \text{Equation 1.57}$$

$$\gamma_{\perp} = -0.193 + \frac{0.15}{\delta} + \frac{8.1}{\delta^2} + \frac{18}{\delta^3} + \frac{9}{\delta^4} \quad \text{Equation 1.58}$$

where $\delta = \frac{2L}{d}$ and $p = \frac{L}{d}$.

After determining CNC dimensions, concentration regime of rod-like particles can be determined with Doi and Edwards' method. Doi and Edwards (1986) discussed concentration regime of rigid polymer chains that can apply on rod-like nanoparticles in solution. A thin rod-like particle with length, L and diameter, d allows tumbling of the molecule without colliding with other molecules ⁴⁸. Dilute regime of rod-like particles is defined with relation (Equation 1.59) where particles can freely rotate without interference by other particles.

$$v_p < 1/L^3 \quad \text{Equation 1.59}$$

where number density (v_p) is number of particles per unit volume. In semi-dilute regime, rod-shaped particles occupy space in another particle's excluded volume. Semi-dilute concentration regime is defined in the relation below:

$$1/L^3 \leq v_p \leq 1/dL^2 \quad \text{Equation 1.60}$$

The solution loses isotropy and turns into different phases in concentrated regime that is defined in relation 8.

$$1/dL^2 < v_p \quad \text{Equation 1.61}$$

According to dimension analyses, the width of CNC-1 and CNC-2 are measured 15 ± 2.0 nm and 8 ± 0.8 nm, respectively and length of CNC-1 and CNC-2 are calculated as 275 nm and 214 ± 0.4 nm, respectively. Concentration regimes of each CNCs were calculated by using Doi and Edwards' (1986) method. When weight fractions of CNC-1 and CNC-2 are smaller than 0.3%(w/w) and 0.2% (w/w) respectively, both CNC suspensions are in dilute regime and concentrated CNC suspensions can be obtained when more than 7.0% (w/w) CNC-1 and 2% (w/w) CNC-2 are used to prepare suspensions. Between these ranges, CNC suspensions are in semi-dilute regime.

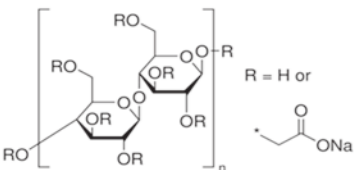
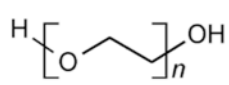
Table 1.4. Properties and concentration regimes of CNC

CNC type	CNC-1	CNC-2
Width (nm)	15.0±2.0	8.0±0.8
Length (nm)	275±2.5	214.0±0.4
Aspect ratio	18.33	26.75
Zeta potential (mV)	-55.3±2.5	-56.60±0.4
Dilute regime ($v_p < 1/L^3$)		
Number density (#ofpart./m³)	4.81x10 ⁺¹⁹	1.01x10 ⁺²⁰
Volume fraction (%)	0.002	0.001
Weight fraction (%)	0.003	0.002
Concentrated regime ($1/dL^2 < v_p$)		
Number density (#of part./m³)	8.81 x10 ⁺²⁰	2.11x10 ⁺²¹
Volume fraction (%)	0.043	0.02-0.03
Weight fraction (%)	0.07	0.02

1.4.2.1.2 Polymer

Carboxymethyl cellulose (CMC) and polyethylene oxide (PEO) were purchased from Sigma-Aldrich, Inc. (Missouri, US). The properties of polymers are summarized in Table 1.5. The characterization of polymer was defined in the section of 1.27 of Chapter 1.

Table 1.5. Properties of polymers

Polymer	Material Morphology	M _w (kDa)	D.S.	R _g (nm)	Molecular structure
Carboxymethyl cellulose (CMC)	Linear Chain	700	0.85-0.90	153	
	Anionic	250	0.70	99	
		90	0.70	40	
Polyethylene oxide (PEO)	Linear chain	600	-	50	
	Nonionic	300	-	34	
		100	-	18	

1.4.2.2 Methods

Various solutions with different concentration were prepared by mixing CNC suspensions in water soluble polymer solutions at room temperature. Procedure of preparing these solutions can be generalized in two steps. Initially, CNC are suspended in water by using mechanical stirring for an hour. Then suspensions were sonicated for 5 minutes. Secondly, polymer was dissolved in CNC suspension overnight. Prepared samples were used following experiments.

1.4.2.3 Scanning Transmission Electron Microscopy

The scanning transmission electron microscope (STEM) is used to characterize nanostructures such as morphology, elemental composition and structure of nanoparticles. The working principle of the STEM is similar to the scanning electron microscope (SEM). The main components of STEM can be seen in Figure 1.15⁴⁹. Electrons are generated from an electron gun with a tungsten filament cathode. Accelerated electrons are focused into a point on the sample by a set of condenser lenses and an objective lens. Spherical aberration corrector is used to obtain high resolution image, and scan coils limits the maximum angle of illumination and lead the beam to scan over a square area on the sample surface. The electron beam scatters from and transmits through sample, and the usual detectors are used to create a proper image. The bright

field (BF) detector detects the intensity in the transmitted beam from a point on the specimen. The annular dark field (ADF) detector form image from scattered electrons. Both detectors are used to form the contrast of an image. The high-angle annular dark field (HAADF) detector captures the high angle electrons to get Z-contrast of the image. Moreover, the secondary electron (SE) detector is used to obtain morphological information ⁴⁹.

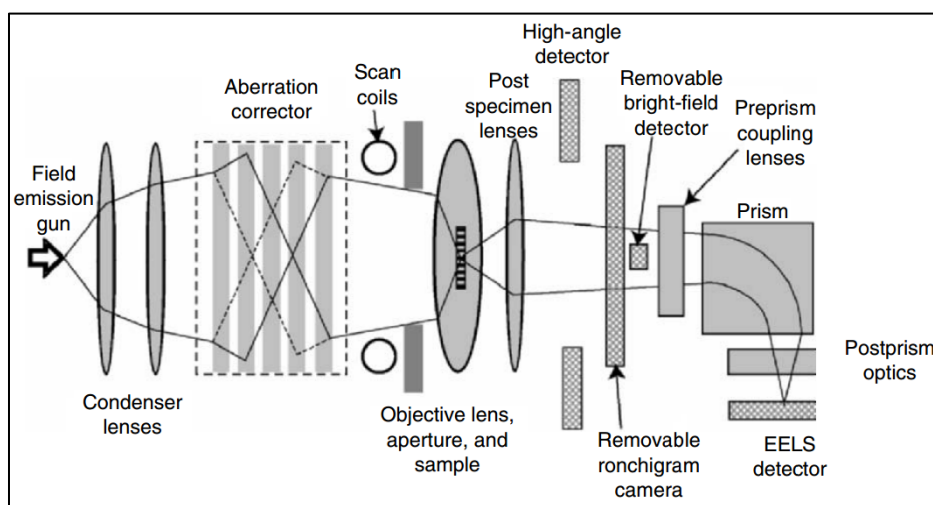


Figure 1.15 The schematic diagram of main components of STEM ⁴⁹ Reprinted from: Pennycook, S. J.; Lupini, A. R.; Varela, M.; Borisevich, A.; Peng, Y.; Oxley, M. P.; Van Benthem, K.; Chisholm, M. F. Scanning Transmission Electron Microscopy for Nanostructure Characterization. In ; Zhou, W., Wang, Z., Eds.; Springer New York: 2007; pp 152-191.

To get a high resolution image, the sample should be conductive or be coated with conductive material such as gold, tungsten, platinum. In solution sample preparation, a standard procedure is applied to form conductive sample for STEM measurements. Colloidal suspension with/without polymers drops on a carbon-coated TEM grid for three minutes. The excess of suspensions is absorbed with filter paper. The TEM grid is dried for three minutes. After, the sample is stained with a drop of uranyl acetate solution for five minutes. The excess liquid is absorbed with filter paper and is dried in the vacuum dryer before imaging. The structures of prepared samples are investigated with high-resolution SEM using a Hitachi model S-4800. The accelerating voltage of 30kV is applied in transmission mode.

1.4.2.4 Dynamic Light Scattering (DLS)

In theory, diffusion of hard sphere is related with the hydrodynamic radius. In dynamic light scattering measurements, diffusivity of particles with respect to time is measured. A typical DLS system consists of six main components (Figure 1.16). The first component is laser source that provides a laser beam. The laser beam passes through or is scattered from particles in sample

cell. Particles scatter beam in all direction and to measure scattered light a detector is placed in any position generally with an angle either 173° or 90° ⁵⁰.

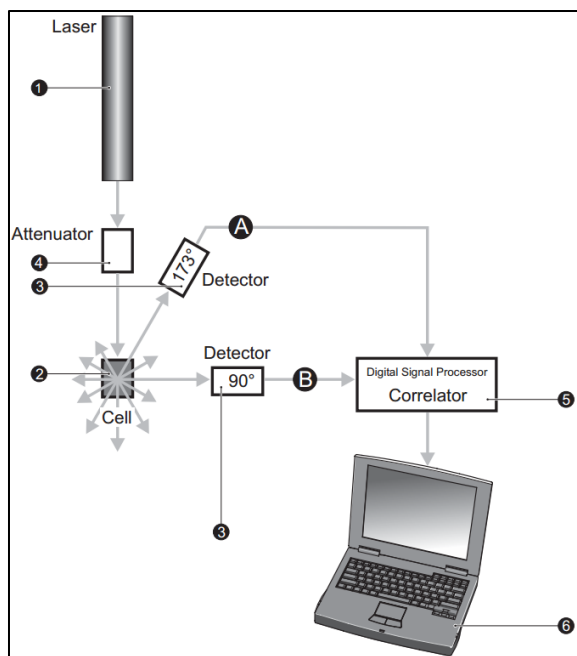


Figure 1.16. The schematic diagram of main components of DLS ⁵⁰.

DLS are made on Malvern Zetasizer Nano-S instrument with a detection angle 173° . This instrument is equipped with a 4.0 mW He–Ne laser ($\lambda = 633 \text{ nm}$) and an Avalanche photodiode detector. All measurements were taken at a temperature of $25.0 \pm 0.1^\circ\text{C}$. At least 3 repeat measurements on each sample were taken for result repeatability.

DLS is an excellent method to measure the diameters of spherical particles. However, it cannot be used to calculate the length of CNC particles from the translational diffusion constant. Therefore, the method which is proposed by Boluk and Danumah based on using STEM and DLS was used to calculate particle width and length (Appendix C).

1.4.2.5 Zeta Potential

Since negatively charged sulfate groups exist on CNC particle surfaces, the surface potential has to be determined. A surface of a charged particle represents schematically in Figure 1.17. For instance, a negatively charged particle has a Stern layer consisting of positive charges. The amount of positive charges decreases when the distance from the particle increases and this opposite charged generates a layer called diffuse layer. Surface potential of particle cannot be

measured directly, however; the zeta potential of particles can be measured experimentally. Zeta potential of nanoparticles will determine by measuring electrophoretic mobility (U_E)⁵⁰:

$$U_E = \frac{2\varepsilon z f(Ka)}{3\eta} \quad \text{Equation 1.62}$$

where z is zeta potential, ε is dielectric constant, η is viscosity and $f(Ka)$ is Henry function. Smoluchowski approximation which referred to $f(Ka)$ that is 1.5 as electrophoretic determinations of zeta potential are mostly made in aqueous media and moderate electrolyte concentration. Malvern Zetasizer Nano-S instrument is used to measure zeta potential of particles.

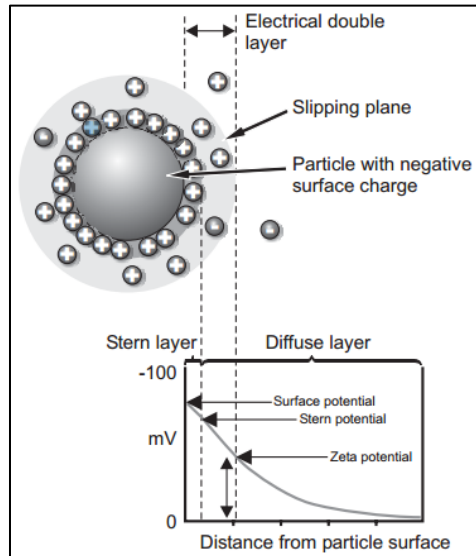


Figure 1.17. Schematic representation of the ionic concentration as a function of distance from the charged particles in suspensions⁵⁰.

1.4.2.6 Rheological Measurements

We discussed the flow behavior of colloidal suspensions and polymer solutions in previous sections. This part will focus on experimental method to determine steady-state shear flow properties using a cone-and-plate rheometer. The fundamental parts of the cone-and-plate rheometer are the flat stationary plate and the rotational cone (

Figure 1.18). The flow behavior can be determined by rotating a cone while the other surface is fixed. The geometry of the cone is important as flow properties are calculated by using general momentum balance equation. In steady-state shear flow measurements, instrument measures the torque, T_r and the angular velocity, Ω . By neglecting inertial forces and edge-effects, the

relationship between the shear stress, σ and the torque, and between shear rate and the angular velocity are computed as ⁵¹:

$$\sigma = 3T_r/2\pi R_r^3, \quad \text{for } \theta_c < 2^\circ \quad \text{Equation 1.63}$$

$$\dot{\gamma} = -\Omega/\theta_c \quad \text{Equation 1.64}$$

where R_r is the radius of cone, θ_c is the angle between the cone and the plate.

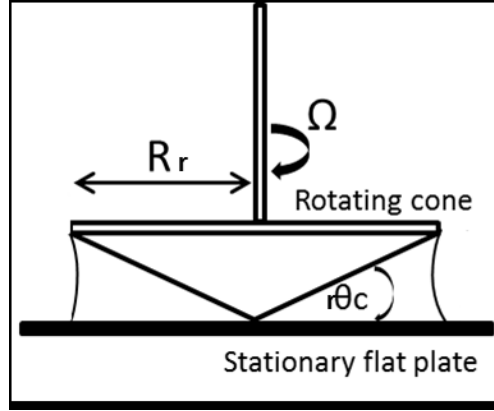


Figure 1.18. Schematic representation of cone-and-plate rheometer ⁵¹.

We use AR-G2 rheometer (TA Instruments, USA) to measure flow behavior of CNC suspensions in aqueous polymer solutions. Cone-and-plate geometry (2° nominal angle) was used to measure the steady-state flow and viscoelastic behavior. Temperature control is established with a ThermoCube200/300/400 (Solid State Cooling Systems Co., USA) kept at $25.0 \pm 0.05^\circ\text{C}$.

1.4.2.7 Nuclear Magnetic Resonance

Solvent relaxation NMR spectroscopy is a common method to determine interactions between polymer and surfactant with nanoparticles. NMR is based on nuclear magnetic moment of nuclei with external applied magnetic field (B). The initial applied field (B_o) encounters energy difference between the spin states (ΔE):

$$\Delta E = \gamma h B_o / 2\pi \quad \text{Equation 1.65}$$

where: h is Planck's constant and γ is gyromagnetic ratio. NMR relaxation is a measurement technique by which an excited magnetic state returns to its equilibrium distribution. Two mechanisms involved in relaxation NMR: (1) spin-lattice relaxation time and (2) spin-spin

relaxation time. The spin-lattice relaxation time (T_1) occurs due to the change in spin orientations resulting from restoration equilibrium magnetization. The spin-spin relaxation time (T_2) is caused by the energy exchange around the nuclei without a loss of energy to the surrounding lattice. For the T_1 relaxation the situation is more complex to define interactions. The applied oscillating magnetic field frequency is higher than the Larmor frequency (magnetic moment of nuclei) as a result of fast tumbling solvent molecules, which leads to a longer T_1 . Solvent molecules bounded with solids leading to a shorter correlation time, so the oscillating magnetic field frequency is lower than the Larmor frequency, indicating a longer T_1 (Figure 1.20). The chain mobility can be defined in terms of T_2 relaxation time as stronger dipolar couplings in the rigid phase shorten the relaxation time of strong dipolar $^1\text{H}-^1\text{H}$ couplings, whereas the higher mobility of solvent molecules results in a longer relaxation time⁵²⁻⁵⁴.

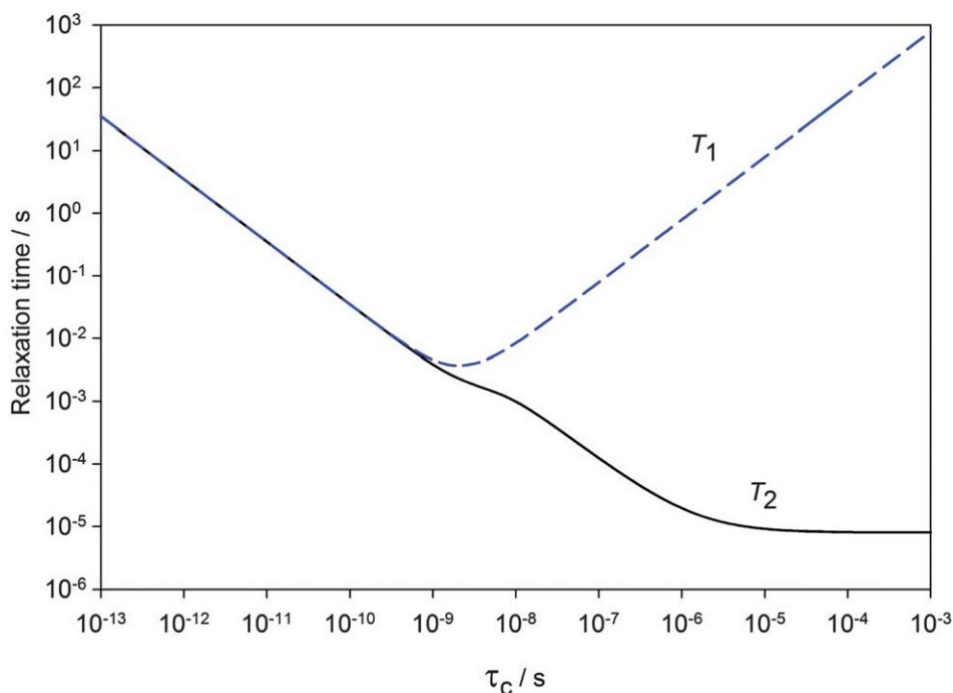


Figure 1.19. Behavior of T_1 and T_2 as a function of correlation time (τ_c)⁵³ Reprinted from: Cooper, C. L.; Cosgrove, T.; van Duijneveldt, J.; Murray, M.; Prescott, S. W. The use of solvent relaxation NMR to study colloidal suspensions. *Soft Matter* 2013, 9, 7211-7228.

The H^1 relaxation measurements are carried out using a Varian Inova 400 MHz spectrometer is used at 26.9 °C. The standard CarrPurcell-Meiboom-Gill (CPMG) sequence is employed.

1.4.2.8 Atomic Force Microscopy

The atomic force microscope (AFM) system is a tool to observe structure of the surface of the material in nanoscale by measuring intermolecular forces with atomic-resolution characterization. A typical AFM system consists of a cantilever probe, a sharp tip, a Piezoelectric (PZT) actuator and a position sensitive photo detector (Figure 1.20). A sharp tip, which is on the mounted PZT, scans the surface. Intermolecular forces between the tip and the surface result in a position change in the cantilever, and the laser beam deflected from the cantilever leads to the difference in light intensities between the upper and lower photo detectors. To get high resolution image of soft surfaces such as polymers, the tapping mode technique is generally used. In this mode, the cantilever is oscillated using a PZT actuator⁵⁵.

In our experiments, we obtained the images of CNC coated mica surfaces by using tapping mode technique to investigate whether polymers are adsorbed or non-adsorbed and also CNC orientation.

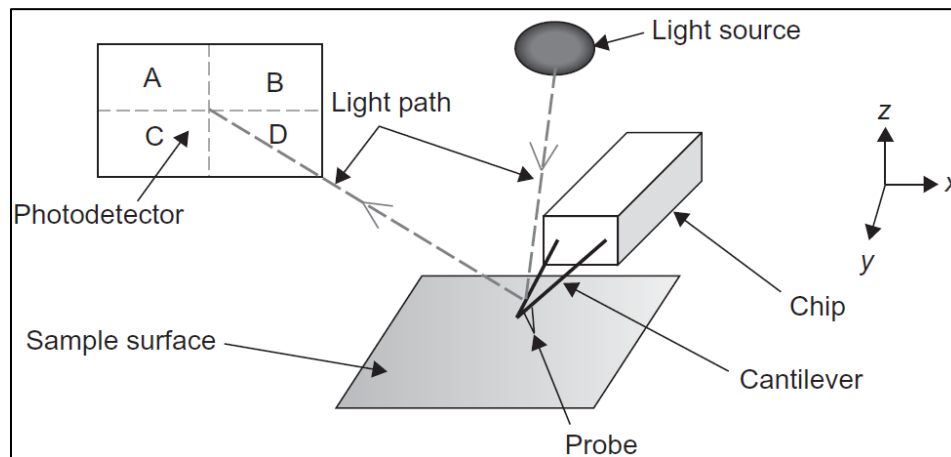


Figure 1.20 Schematic of typical AFM system⁵⁵ Reprinted from: Bowen, W. R.; Hilal, N. *Atomic force microscopy in process engineering: introduction to AFM for improved processes and products*; Oxford ; Burlington, MA : Butterworth-Heinemann, c2009; 1st ed: 2009.

1.4.2.9 Polarized Optical Microscopy

The mesostructure of crystals, liquid crystals, polymers, and other transparent, optically anisotropic materials can be observed with the polarized light optical microscopy. Intensity distribution of a light beam is captured as a microscope image is the intensity distribution, and spatial variation in the intensity is called contrast. Contrast in images produced by polarized light microscopes corresponds to the phase change of material⁵⁶. Therefore, the phase change of CNC

suspensions and CNC suspension in aqueous polymer solutions will be observed by using polarized optical microscopy (POM) that enhanced contrasts to get advance the image quality of birefringent materials. The polarized optical microscopy (POM) analysis of samples with various concentrations was observed with Olympus BX50 equipped with a JVC 3-ccd video camera (Olympus, Japan).

1.4.2.10 Stability Measurements

Interactions of CNC suspensions in polymer solutions may result in different phase behavior or different CNC orientation in suspension by the time passes. The long-term stability behavior of CNC suspensions with polymers can be determined by using light ⁵⁷. The schematic illustration of stability behaviors of CNC suspensions with polymers for bridging flocculation and depletion interactions can be seen in Figure 1.21. When the light send to suspensions, light can either transmit or scatter. The light beam is blocked any time that it encounters a light intensity depending on the stabilization and the distribution of light intensity. The recorded intensity change by time can be interpreted as flocculation or depletion.

Optical analyzer, Turbiscan Lab Expert is used to evaluate stability of CNC suspensions with polymer solutions. Instrument consists of the detection head and transmission (T) and back scattering (BS) detectors. Detection head is composed of a pulsed near-infrared light source ($\lambda=800$ nm) and scans the entire height of the sample in each minute during at least 1 h.

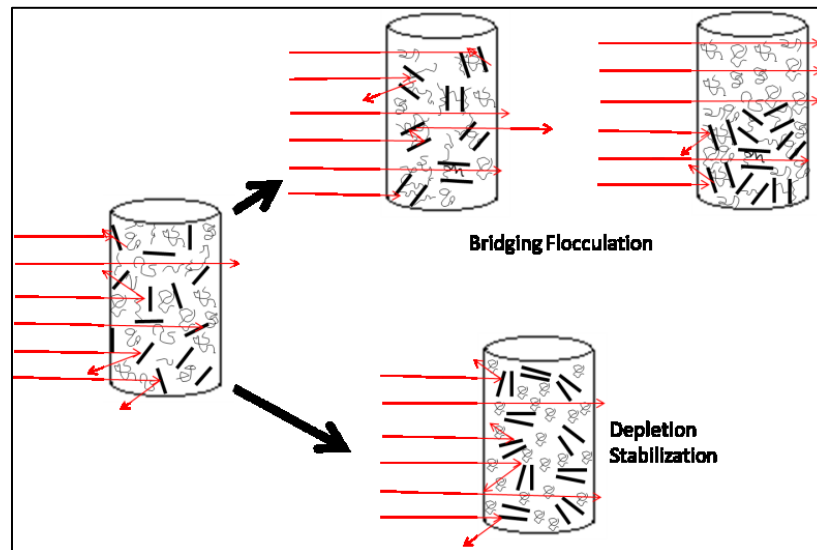


Figure 1.21 Schematic representation of stability behaviors of CNC suspensions.

Chapter 2. The Role of Dilute and Semi-Dilute Cellulose Nanocrystal (CNC) Suspensions on the Rheology of Carboxymethyl Cellulose (CMC) Solutions

The material shown in Chapter 2 has been previously accepted by Canadian Journal of Chemical Engineering. This chapter investigated shear thickening mechanism of CNC suspensions with the presence of CMC polymer. The experiments have been personally conducted; and the images of Figure 2.3 were taken by Dr.Christophe Danumah. The authors of this publication are me, my colleague Dr.Christophe Danumah and my supervisor Dr.Yaman Boluk. The material published is the following.

2.1 Abstract

Non-Newtonian flow behavior of dilute and semi-dilute carboxymethyl cellulose (CMC) solutions in the presence of spindle shaped cellulose nanocrystal particles (CNC) was investigated. Scanning transmission electron microscopy, dynamic light scattering, and polarized optical microscopy and turbidity measurements of CNC suspensions in CMC solutions were also carried out. By adding CNC particles only within the range of 0.33 - 2.0 vol% into the dilute and semi-dilute CMC polymer solutions increased the viscosities at low shear rates between 10^3 - 10^5 time s. The flow curves of CNC suspensions in CMC polymer solutions turned highly non-Newtonian, and their viscosities at high shear rates ($>10^3$) still converged to the flow curves of CMC solutions. The viscosity increase comes from the nematic flocculation of CNC particles in the presence of a non-adsorbing CMC polymer, which results CNC flocs with water-entrapped pockets.

2.2 Introduction

Cellulose with its linear, regular polysaccharide structure and strong intermolecular hydrogen bonds form crystalline microfibrils and fibres. Such unique structure makes cellulose infusible at high temperatures and insoluble in conventional organic solvents. Therefore, since 1870, cellulose has been used as a polymer only after conversion to cellulose derivatives such as cellulose ethers and esters or regeneration to such as viscose⁵⁸. Later advancement of synthetic polymers from petrochemicals eclipsed the utilization of cellulosic polymers and plastics.

Nevertheless cellulose becomes an attractive material again for several reasons. First of all, it is renewable, carbon neutral and also available from abundant wood and other plant fibers supplies. Secondly it is a non-toxic and biocompatible material for the human body and biodegradable. And last but most importantly, cellulose can be converted to spindle shaped nanosized particles which will reveal unique bulk, surface, and colloidal properties⁴⁶. Spindle shaped CNC particles are typically prepared by employing concentrated (65%) sulfuric acid⁵⁹⁻⁶¹. The hydrolysis process removes the amorphous segments of cellulose fibrils and releases homogenous and defect free crystallites. In addition, sulfuric acid also creates negatively charged sulfate ester groups on crystallite surfaces. CNC particles are typically 6-10 nm in width and 100-220 nm in length⁴⁷. Cellulose nanocrystals based products are expected breathe new life into cellulose. Although there are many excellent studies on CNC which were reviewed by Habibi et.al⁶², most of the existing researches on high volume applications are on nanocomposites, films and coatings with desired mechanical, optical and barrier properties⁶³⁻⁶⁵. Yet, the aggregate free dispersion of hydrophilic CNC particles in hydrophobic organic materials is the problem for those CNC applications hence requires additional surface modification and grafting⁶². Sulfonated CNC particles with negative surface charges result stable suspensions in water. CNC suspensions generate birefringence and ordered liquid phase at sufficiently high concentrations⁶⁶. In addition to particle geometry, addition of electrolytes and nonadsorbing macromolecules also govern the formation of nematic phase^{67,68}. Rheological properties of aqueous suspensions of cellulose nanocrystals were investigated in the literature to characterize their particle sizes²¹ and structural changes as a function of CNC concentration under different conditions^{22,23,69}. According to those studies, typical cellulose nanocrystals (length =100-220 nm and width = 5-10 nm) do not show any thickening effect in aqueous solutions unless above 7% concentration. Besides, thickening behavior at high concentrations is not sufficiently shear thinning (pseudoplastic), which is always a required rheological property in paints, coatings, drilling fluids and other functional fluid formulations. Therefore cellulose nanocrystals as opposed to cellulose nanofibrils have never been considered as thickeners. In our laboratories, the synergetic thickening of cellulose nanocrystals in certain water soluble polymers was discovered⁷⁰. Later, the thickening mechanism of cellulose nanocrystals in certain cellulose ethers have been discussed⁷¹. Hence, spindle shaped CNC particles likely self-organize into mesoscopic physical structures in polymer solutions, properties and interactions of these mesoscopic structures determine the macroscopic

behavior of these systems. CNC based such soft matters will play important role in commercial applications and new technologies, however it shall be noted that they behave fundamentally different from traditional liquids and solids. In this study, it is our objective to investigate non-Newtonian flow behavior of carboxymethyl cellulose with the presence of cellulose nanocrystals.

2.3 Experimental

2.3.1 Materials

2.3.1.1 Cellulose Nanocrystals (CNC)

Spray-dried CNC, which was obtained through sulfuric acid hydrolysis of commercial dissolved softwood pulp, was used. A detailed preparation method was described elsewhere⁷¹. CNC particles were suspended in deionized water by using mechanical stirring and sonication (Branson ultrasonic cleaner model 1510, frequency 40 kHz). Furthermore, CNC suspensions were filtered through a 0.45 μ pore-sized membrane. The particle density of CNC was taken as 1.5 g/cm³ to calculate the volume fraction (vol%) from the weight fraction (wt%).

2.3.1.2 Carboxymethyl Cellulose (CMC)

Anionic polyelectrolyte sodium salt of carboxymethyl celluloses (Na-CMC) with 700 kDa molecular weight and 0.80-0.95 degree of substitution was purchased from Sigma–Aldrich (St.Louis,MO, USA). CMC was dissolved in deionized water and CNC suspensions at 25 °C.

2.3.2 Methods

2.3.2.1 Scanning Transmission Electron Microscopy (STEM)

Hitachi model S-4800 apparatus equipped with a field emission source and operating at an accelerating voltage of 30 kV in transmission mode were used to investigate the morphologies of samples. A drop of the CNC aqueous suspension and CNC suspensions in aqueous CMC solutions were deposited on a carbon-coated copper TEM grid for 3 min, and the excess of suspension was wicked off using filter paper. The TEM grid was allowed to dry at room temperature for 3 min. The sample was then stained by depositing a drop of uranyl acetate solution (2 wt% in water) on the grid for 5 min. The excess solution was wicked off using filter paper, and the grid was dried at room temperature prior to imaging.

2.3.2.2 Dynamic Light Scattering (DLS)

DLS measurements were made on Malvern Zetasizer Nano-S instrument with a detection angle 173° . This instrument was equipped with a 4.0 mW He-Ne laser ($\lambda = 633 \text{ nm}$) and an Avalanche photodiode detector. All measurements were taken at a temperature of $25.0 \pm 0.1^\circ\text{C}$. At least 3 repeat measurements on each sample were taken for result repeatability.

2.3.2.3 Rheology

Steady state shear viscosity measurements of the CNC suspensions, CMC solutions and CNC suspensions in aqueous CMC solutions were conducted with AR-G2 rheometer (TA Instruments, USA). Cone and plate ($2^\circ 0' 22''$ nominal angle) geometry was used and temperature control was established with a ThermoCube200/300/400 (Solid State Cooling Systems Co., USA) kept at $25.0 \pm 0.05^\circ\text{C}$. All experiments were performed at least two times for result repeatability.

2.3.2.4 Polarized Optical Microscopy (POM)

The quiescent state birefringence phenomenon of CNC suspensions and CNC suspension in aqueous CMC solutions were examined by viewing the sample glass vials between crossed polarizers. The polarized optical microscopy (POM) analysis of samples with various concentrations was observed with Olympus BX50 equipped with a JVC 3-ccd video camera (Olympus, Japan).

2.3.2.5 Stability Measurements

Optical analyzer, Turbiscan Lab Expert was used to evaluate stability and structure of CNC suspensions with polymer solutions. Instrument consisted of the detection head and transmission (T) and back scattering (BS) detectors. Detection head was composed of a pulsed near-infrared light source ($\lambda=800 \text{ nm}$) and scanned the entire height of the sample in each minute during 2 hours.

2.4 Results

Dimensions of CNC particles were determined with a method explained in detail elsewhere⁴⁷. In this method, STEM and DLS measurements were combined to calculate the length of CNC particles from diameter (obtained from STEM pictures) and translation diffusion coefficient values. The diameter of CNC was determined as $8 \pm 0.8 \text{ nm}$. The length of CNC was calculated as

214 nm. Besides, the average zeta potential of CNC suspension was obtained as -56.6 ± 0.4 mV at neutral pH.

Figure 2.1 shows the flow curves of CNC suspensions at different concentrations, which are reported in terms of volume fractions. Suspensions of CNC particles with a length of 214 nm and width of 8nm are expected to be isotropic up to around 5-6% volume concentrations. Therefore, at dilute (0.33 vol% and 0.67 vol%) and semi-dilute (1.34 vol% and 2.00 vol%) concentrations, CNC suspensions did not exhibit any significant thickening characteristics as expected. The Newtonian flow behavior of Brownian CNC suspensions are directly related to concentration dependent rotational diffusion constant of CNC spindles. In semi-dilute concentration range (1.34 vol% and 2.00 vol%), interactions among CNC spindles restrict the rotational diffusion of rods. Hence, rods become entangled and resulted in a slightly shear thinning flow behavior.

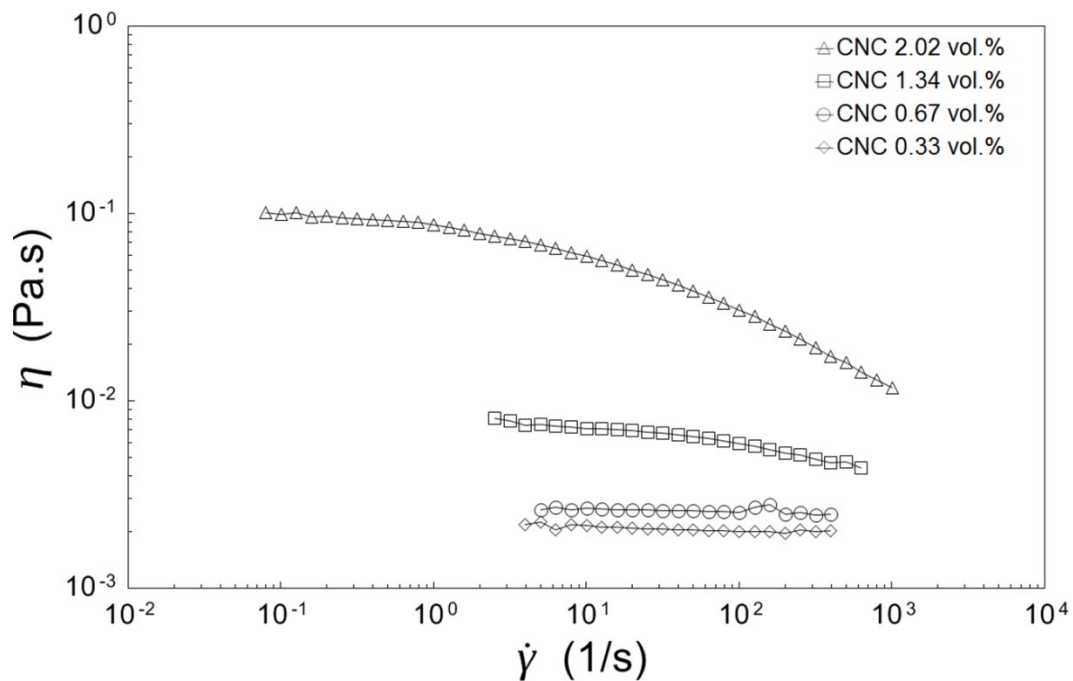


Figure 2.1 Shear viscosities of CNC suspensions measured at 25°C

In a similar way, viscosity versus shear rate curves of CMC polymer solutions are given in Figure 2.2 at various polymer concentrations. Again, depending on the CMC concentration, either Newtonian or shear thinning behavior was observed. The CMC solution at 0.5wt % was in semi-dilute state without any entanglement and exhibited a Newtonian flow behavior. CMC concentration of 1.0 wt. % was the onset of the non-Newtonian behavior. Above 1.0 wt% concentration, the viscosity curves of CMC solutions showed both a drastic viscosity increase

and higher shear thinning profiles with increases in polymer concentration. From the shape of CMC solutions flow curves, it can be argued that 1.0 wt% CMC is the entanglement concentration, c_e and it represents the transition from semi-dilute unentangled solution state to semi-dilute entangled solutions state. Indeed, polymer concentration versus viscosity plots of CMC solutions for $c > 0.01$ (in the semi-dilute entangled regime) followed the scaling law ($\eta_0 \sim c^{4.5}$) which was within the predicted range⁷². Since the polyelectrolyte concentrations is more effective at dilute concentration, the polyelectrolyte flow behaviors with and without addition of monovalent salts and neutral polymers were similar above the semi-diluted entangled state.^{28,30} CMC concentrations of 1.0 wt% and 2.0 wt% solutions showed a typical shear thinning behavior with an initial Newtonian plateau. However, at 3.0 wt% CMC concentration, a slight degree of initial shear thickening was observed at very low shear rates. Then a shear thinning flow followed at higher shear rates ($> 10^{-1} \text{ s}^{-1}$). A similar “shear thickening at low shear rate” behavior were also reported for CMC solutions in the literature³⁷. According to Liu et al. it is due to the “flow-induced formation of polymeric associations”⁷³.

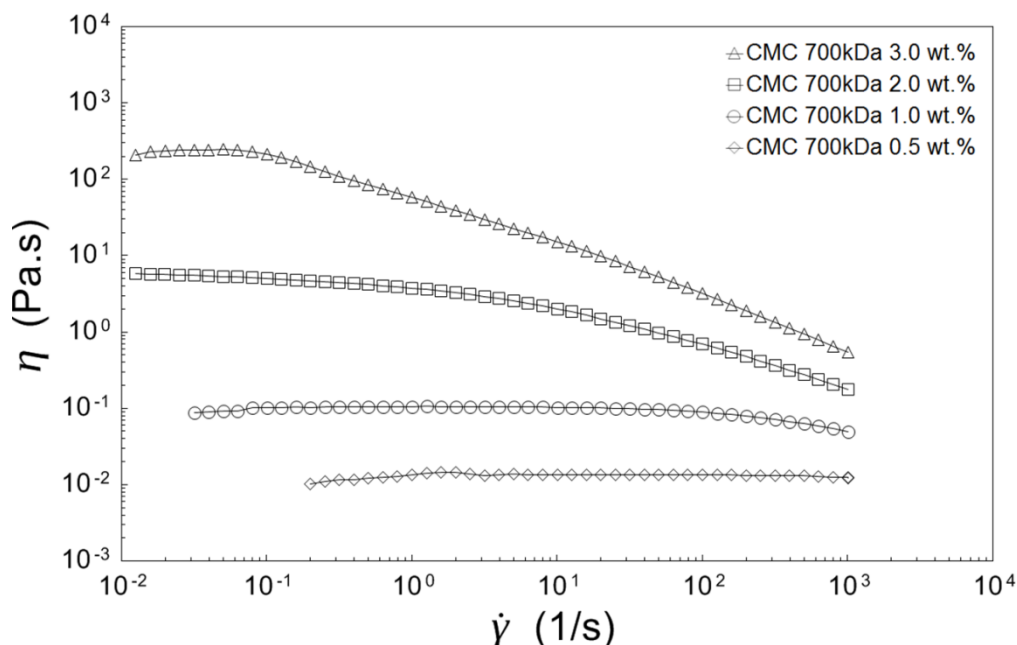


Figure 2.2 Shear viscosities of CMC polymer solutions measured at 25°C.

Additions of very low amount of CNC in dilute and semi-dilute CMC polymer solutions generated a dramatic thickening effect. When sample cuvettes shown in Figure 2.3 were rotated 180°, 0.50 wt%, 0.75 wt% and 1.0 wt% CMC solutions with 0.33 vol% CNC were self-

sustaining due to the structure formation. Among those samples, only 0.25 wt% CMC did not produce any self-sustaining structure by addition of 0.33 vol% CNC.

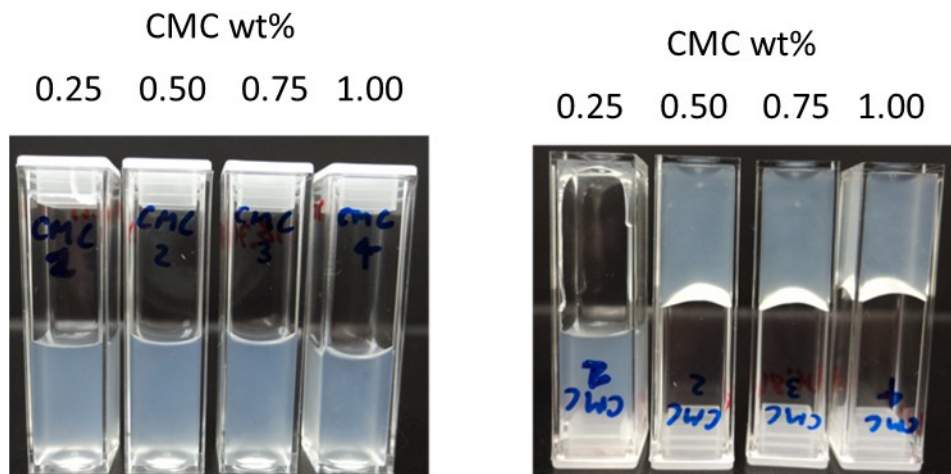


Figure 2.3 Photographs of 0.33 vol% CNC suspension in CMC (700 kDa) solutions. Cuvettes are in (a) upward position; (b) 180° rotated position.

Viscosity versus shear rate curves in Figure 2.4 show the synergistic behavior of needle shaped CNC particles in 0.5 wt%, 1.0 wt% and 2.0 wt% CMC polymer solutions. The viscosity of CMC solutions increased between 10^3 - 10^5 times at low shear rates ($\sim 10^{-2} \text{ s}^{-1}$) by the addition of only between 0.33 vol%- 2.02 vol% of CNC particles. The flow curves of CNC suspensions in CMC solutions turned highly non-Newtonian and their viscosities at high shear rates ($>10^3$) still converged to the flow curves of CMC solutions. Nevertheless, different non-Newtonian flow curves were observed, depending on CMC polymer and CNC suspensions concentrations. As shown more clearly in Figure 2.4.a and 4.b, unlike Newtonian low shear rate plateau-shear thinning behavior of 0.5 wt% and 1.0 wt% CMC polymer solutions, CNC suspensions in CMC polymer solutions caused first a viscosity increase with shear rate then followed by shear thinning at a certain shear rate. Additions of CNC from 0.33 vol% to 2.02 vol% showed both shear thickening at low shear rates and then shear thinning during the rest of shear rates. Increase in CNC concentration also shifted the inflection point to lower shear rates which corresponds the change from shear thickening to shear thinning. Figure 2.4.c shows that CNC suspensions in 2.0 wt% CMC solution behaved differently than CNC suspensions in 0.5 wt% and 1.0 wt% CMC solutions. The shear thickening behavior at low shear rates were not clearly visible within the measured lowest shear rate ($>10^{-3} \text{ s}^{-1}$) as entanglements of polyelectrolyte chains are more dominant compared to CNC polyelectrolyte interactions.

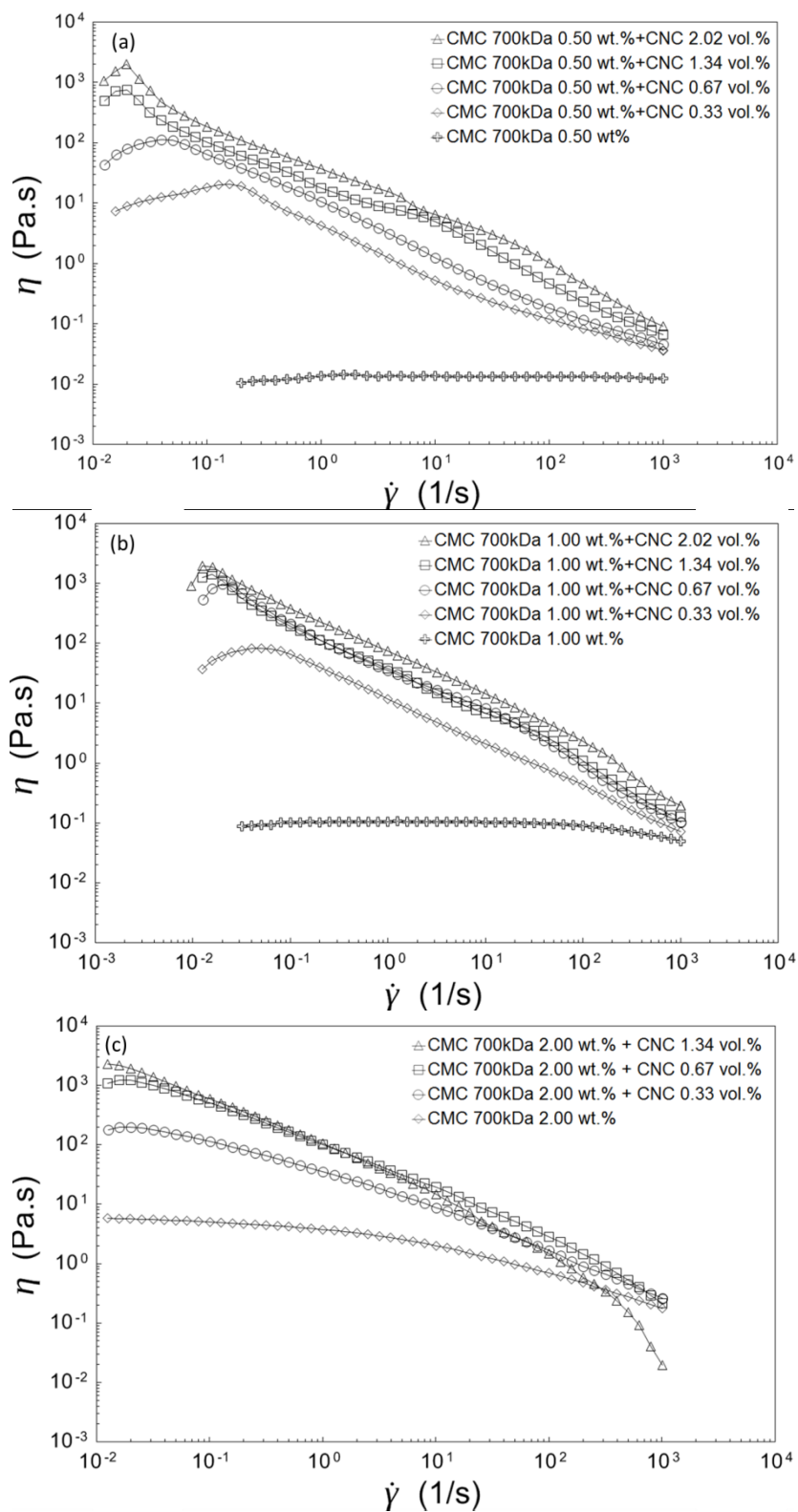


Figure 2.4. Shear viscosities of (a) 0.5 wt%, (b) 1.0 wt% and (c) 2.0 wt% CMC polymer solution with various CNC concentrations measured at 25°C.

Maximum viscosities of CMC solutions with and without CNC additions are plotted in Figure 2.5. Viscosity versus CMC solution concentration data points without any CNC addition agreed with the Newtonian viscosity-Molecular weight- concentration master curve formulated by Clasen and Kulicke ³⁵.

$$\eta_0 = 0.891 + 7.82 \cdot 10^{-3} c M_w^{0.93} + 1.77 \cdot 10^{-5} c^2 M_w^{1.86} + 4.22 \cdot 10^{-12} c^{4.09} M_w^{3.80} \quad \text{Equation 2.1}$$

where η_0 is the zero shear rate viscosity, M_w is the molecular weight and c is the CMC concentrations. Here molecular weight of CMC is taken as 700,000 Da. It is worth to note that this equation was devised for CMC polymer in 0.01 M NaCl solution. Nevertheless, as pointed out by Clasen and Kulicke, the viscosity curves of CMC solutions at different saline concentrations and salt free water converge above the polymer concentration of 1 wt%³⁰. Therefore our viscosity data of CMC solutions in salt free aqueous solution was expressed very well with Equation 1. The addition of CNC even at very low concentrations resulted in a very drastic viscosity increases both in dilute (0.5%) and semi-dilute entangled (1.0%, 2.0% and 3.0%) CMC solutions. CNC additions into CMC polymer solutions let them to reach the asymptotic viscosity value, which is expected to reach only at very high CMC concentrations without CNC. It appears that additions of CNC particles cause CMC solutions behave as highly concentrated polymer solutions.

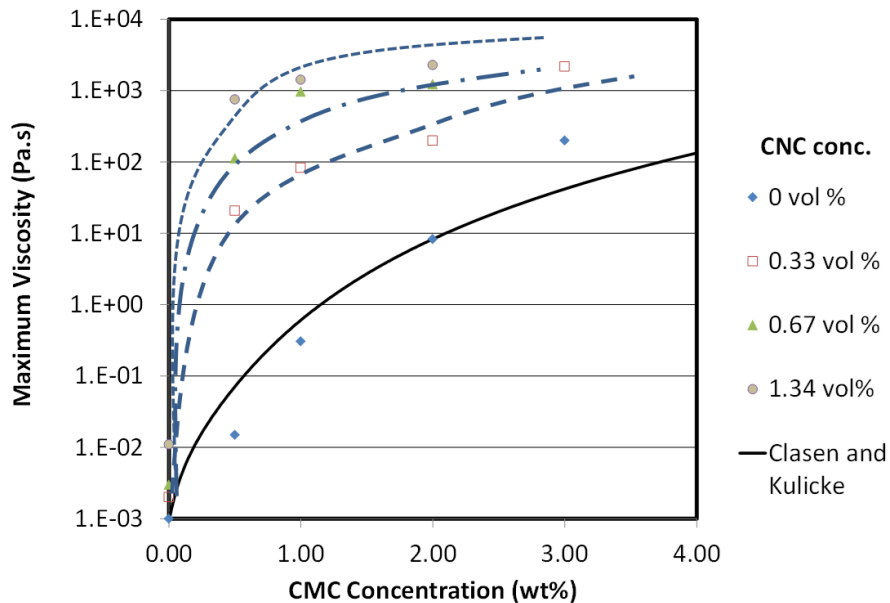


Figure 2.5 Maximum shear dependent viscosity versus CMC polymer concentration at various CNC additions.

The flow curve gradients were calculated in the linear segment of $\log \eta$ (viscosity) versus $\log \dot{\gamma}$ (shear rate) flow curves by fitting them to a power-law fluid (the Ostwald–de Waele relationship), $\eta = K\dot{\gamma}^{n-1}$. The term $n-1$ was taken as flow curve gradient, m and plotted against CMC concentration at various CNC additions in Figure 2.6. Graessly's theoretical gradient value of $m = -0.82$ for highly concentrated polymer solutions and bulk polymer melts were also included into Figure 2.6⁷⁴. In the case of CMC solution without CNC addition, the flow curve gradient, m rises from zero to the predicted value of $m = -0.82$ for high overlap parameter values linearly. According to Clasen and Kulicke³⁰, CMC solutions reach to the asymptotic value of -0.80 at $c. [\eta] = 70$ which corresponds to 4.4% CMC concentration in our case of 700,000 Da molecular weight. In the case of CNC particles presence, the rise to the asymptotic value is dramatic. All of CNC additions caused the CMC solution only at 0.5wt.% polymer concentration to reach the asymptotic gradient.

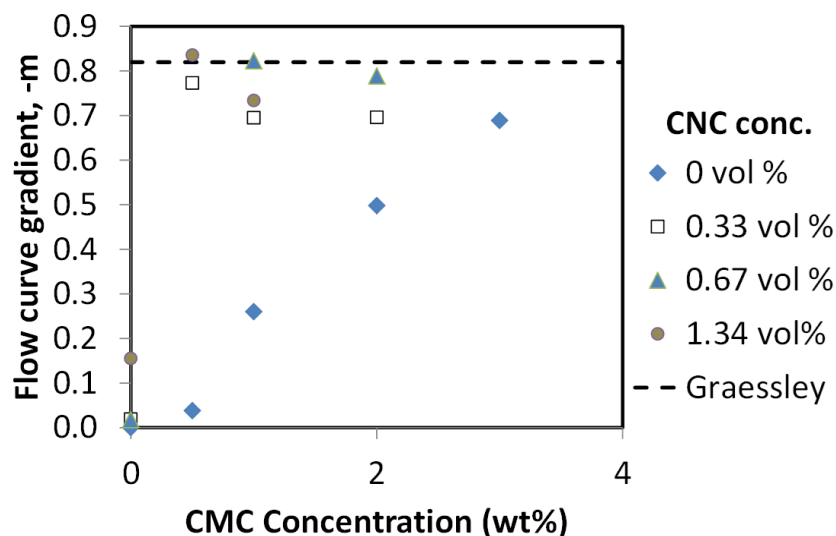
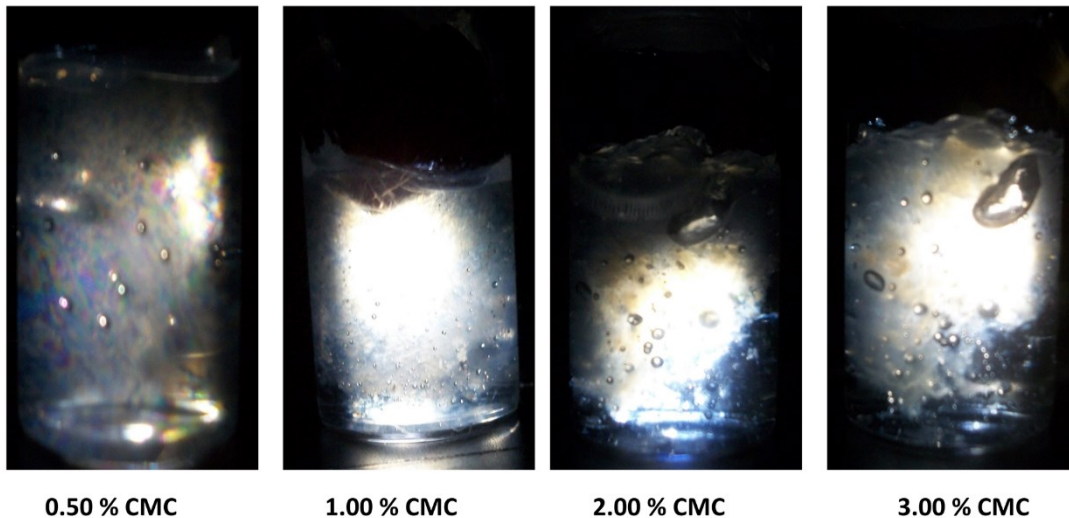


Figure 2.6 Flow curve ingredient of CMC solutions at various CNC additions.

CNC suspensions in CMC polymer solutions which show thickening behavior also exhibits a permanent birefringence with the observation between two cross polarizers (Figure 2.7) and under polarized optical microscope (Figure 2.8). The birefringence became more pronounced both by increasing CMC and CNC concentrations while still staying in semi-dilute concentration range. Images of 0.67 vol% and 1.34 vol% CNC suspensions in 3.0 wt% CMC shows thick isotropic CMC rich phase at the bottom and birefringent nematic CNC rich phase on the top. This arrangement is the opposite of other observations reported in the literature^{68,75}. Edgar and Gray reported dextran rich isotropic phase in the upper layer and cellulose nanocrystal rich chiral

nematic liquid crystalline phase in the bottom layer. However the difference is due to the viscosity of polymer rich phase. Unlike dextran, CMC polymer solution is getting extremely thick once its concentration is increased in CMC rich phase. Samples prepared three years ago are still stable and their thickening characteristics are still intact. Polarized optical micrographs also showed the oriented nematic phase of CNC in CMC polymer solutions very clearly.

(a) 0.67 vol. % CNC in CMC polymer solutions



(b) 1.34 vol. % CNC in CMC polymer solutions

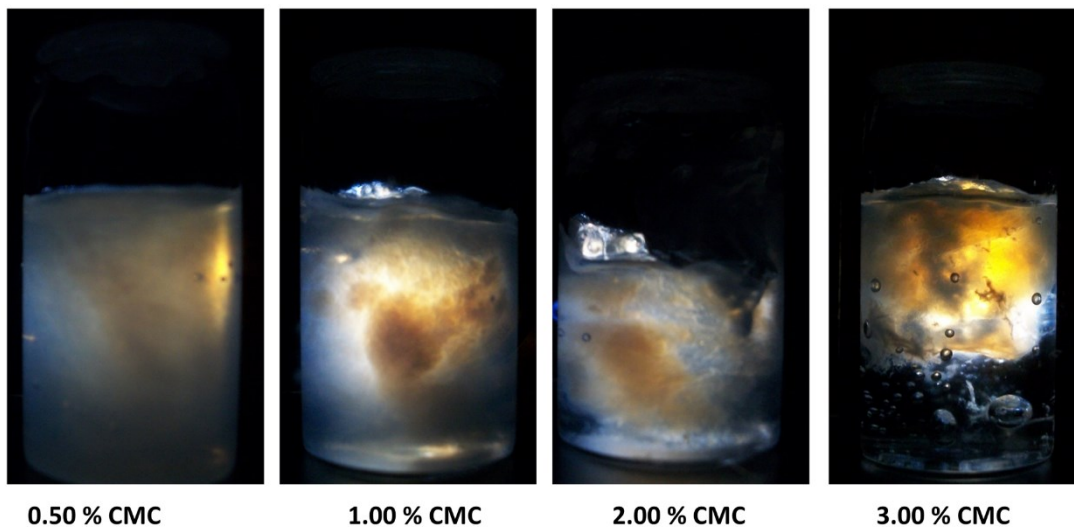


Figure 2.7. Nonisotropic structures of (a) 0.67 vol% and (b) 1.34 vol% CNC in CMC polymer solutions placed between crossed polarizers showing birefringent domains

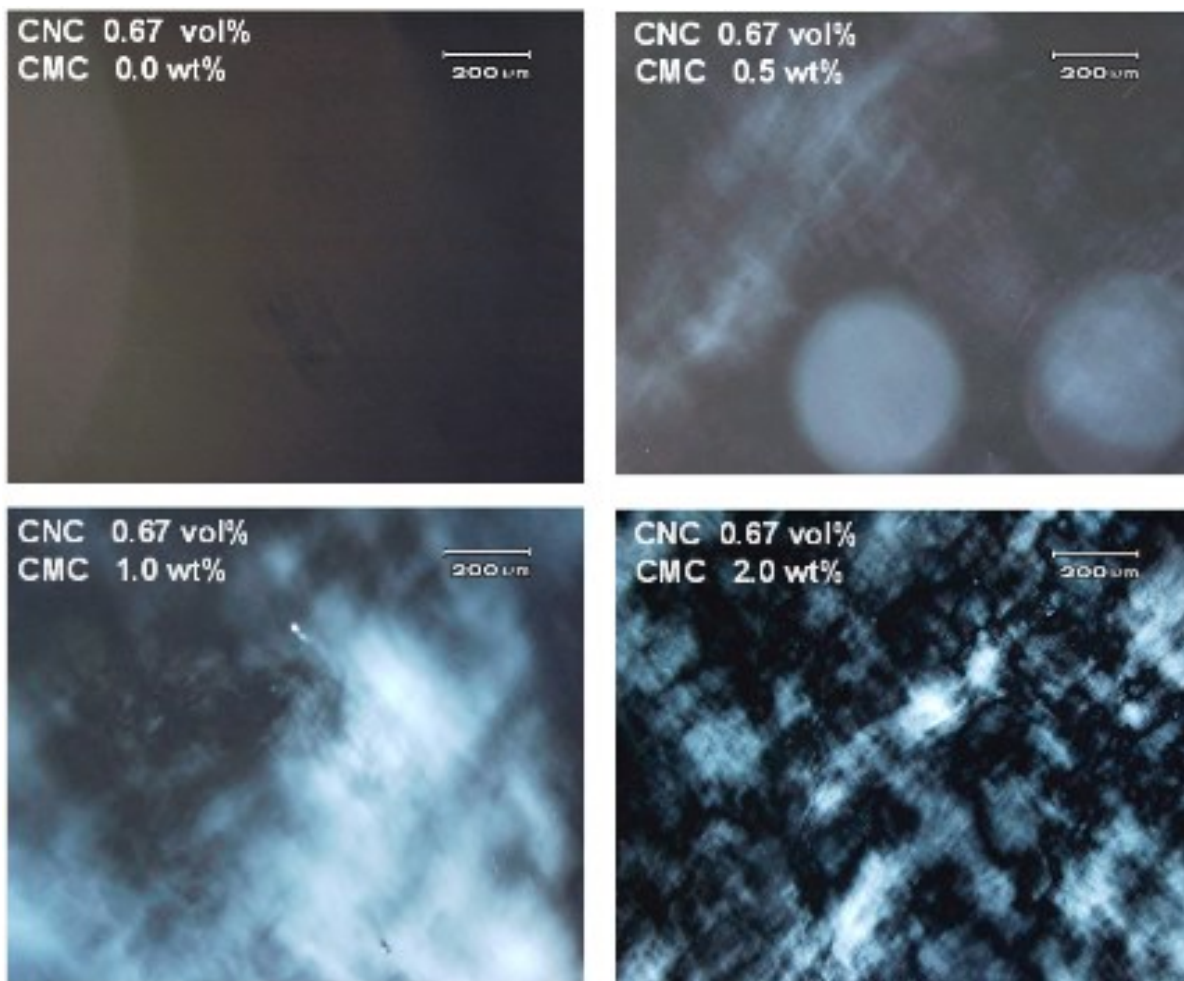


Figure 2.8 Nonisotropic structures of CNC in CMC polymer solutions as shown under POM.

Figure 2.9 shows turbidity results of 1.0 wt.% CMC polymer solution with and without CNC additions during two hours of scanning. Without the presence of CNC, CMC solution was a clear solution and resulted a very high level of light transmission. CNC addition decreased not only the transmission of light but also caused non-uniform transmission along the height of the tube. Nevertheless CNC particles did not cause any time dependent change in turbidity of CMC solutions.

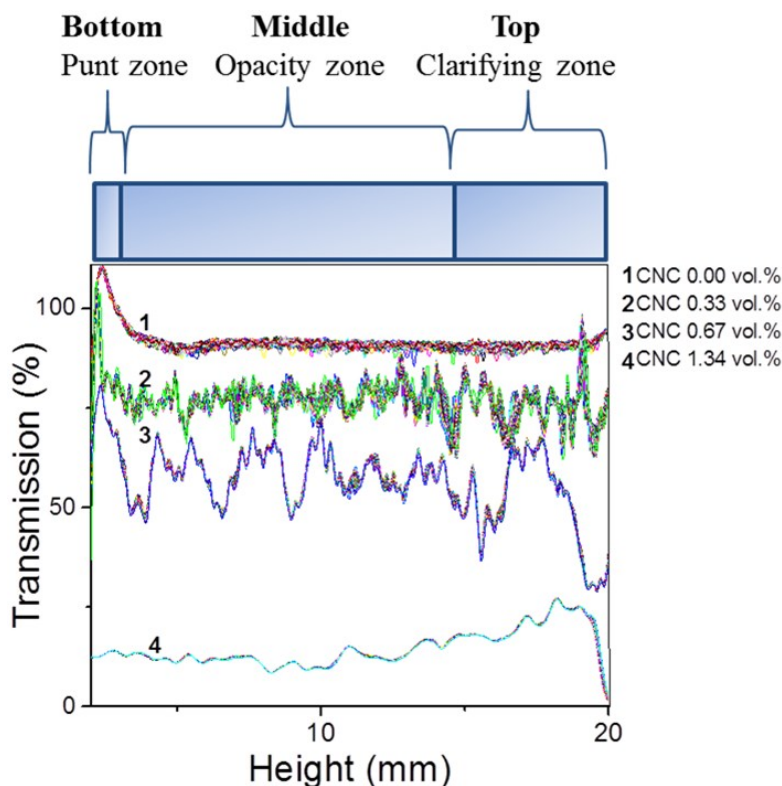


Figure 2.9 Light transmission of 1.0 wt% CMC solution along the sample cell height with various CNC concentrations.

2.5 Discussions

The visual inspections and rheological characterizations showed that the addition of a small amount of CNC particles (which falls within the dilute to semi-dilute suspension concentration range again) into the dilute or semi-dilute CMC polymer solutions resulted significant thickening increases in CMC solutions. Two alternative mechanisms can be considered to explain the dramatic enhancements of the rheological behavior of CNC particles in polymer solutions⁷¹: As a first mechanism, polymer chains adsorb on CNC particles and can cause weak CNC networks by polymer-bridging of CNC particles. In polymer solutions, if particle surfaces prefer macromolecules to aqueous medium, polymers can adsorb onto particle surfaces. If polymer chains are long enough, some segments adsorb in the form of trains while tails protrude into the solution and are available to adsorb on other particles. By applying polymer self-consistent field theory and a “saturable” adsorption model to capture the effect of the particle size, Surve et al. demonstrated that polymers are adsorbed on nanoparticles significantly higher than larger particles⁷⁶. Nevertheless, according to their prediction, interparticle interactions by polymer bridging tend to weaken with an increase in the concentration of polymers. Hence, polymer

adsorption on particle surfaces is not likely in the case of CNC particles with negative surface charges and anionic carboxymethyl cellulose. Besides, if isotropic CNC particles are bridged by adsorbed CMC particles, there shall not be any non-isotropic pockets when inspected the samples between cross-polarized filter and polarized optical microscope. Bridging of particles has to result a well dispersed and transparent systems, which also did not agree with our light scattering data. Polymer bridging of particles such as laponite and silica dispersions containing polyethylene oxide showed shear induced thickening mechanism^{77,78}. The viscosity versus shear rate profiles of CNC added CMC solutions do not suggest any polymer bridged colloidal particle suspensions. Even for the case of adsorbing polymers, our lowest concentration of 0.5 wt% CMC polymer concentrations in the highest CNC concentration of 1.34 vol% suspensions is extremely high to observe bridging. Since polymer bridging occurs at low surface coverage (polymer additions of 0.0001%) bridging by adsorption mechanism is highly unlikely for CNC particles in CMC solutions. Therefore flocculation by bridging cannot be considered to explain unusual thickening behavior of CNC suspensions in CMC solutions.

As a second mechanism, flocculation of particles by depletion in the presence of non-adsorbing polymers can be considered. If macromolecules do not adsorb at particle interfaces, the exclusion of the polymer segments from the particulate volumes leads to an effective “entropic” attraction between the particles known as the depletion interaction⁷⁹. Asakura and Oosawa were the first to formulate the qualitative analysis of depletion. They proposed that the exclusion of polymer molecules leads to an effective attractive interaction between the particles. This idea has been tested here in the case of CNC presence in CMC polymer solutions. CMC is an anionic polyelectrolyte and has higher osmotic pressures than non-ionic polymers at the same molecular weight as a result of higher radius of gyration which is caused by intramolecular charge repulsion. Therefore anionic CMC chains do not adsorb on CNC particles and can cause the depletion of CNC particles. This behavior is observed in many other systems such as flocculation of silica in the presence of anionic CMC⁸⁰. When investigated between crossed polarizers, birefringent domains in Figure 2.7 and nematic CNC rich phase pockets under polarized microscope in Figure 2.8 are the results of nematic liquid crystal flocs of CNC in CMC polymer solutions. Light transmission results in Figure 2.9 are also further evidence of flocculation of CNC particles and formation of pockets of flocs. The depletion of CNC in dextran⁶⁸ and filamentous fd virus in dextran⁷⁵ were also observed in the literature. However,

since dextran is not a conventional thickener, there was no synergetic thickening increase due to either CNC or fd virus.

Thus, the unusual rheological behavior of CNC suspensions in CMC polymer solutions is explained by depletion flocculation. Figure 2.10.a which is adopted from Bouldin et.al.⁸¹ shows the distinct solution states as a function of molecular weight and solution concentration of polymer in a good solvent. In the case of the molecular weight of 700 kDa, the CMC concentration range from 0.1 wt% to 1.0 wt% covers the semi-dilute but non-entangled and not networked polymer solution state. This has been verified in our work as well as reported by Benchabane and Bekour⁷³ and Kastner et.al.⁸² for 700 kDa CMC. At the same molecular weight, polymer solution becomes semi-dilute but entangled between above 1.0 wt%. A second polymer solution state transition occurs from semi-dilute entangled solution to concentrated network solution. This change is predicted to occur around 10 wt%³⁵. Figure 2.10.b schematically illustrates the CMC chains in semi-dilute and entangled solution state. Once CNC particles are added, particles occupy volume fraction higher than their real volume fraction due to flocculation and formation of nematic floc pockets with entrapped CMC free water. Therefore, the available volume of water for CMC chains decreases, apparent CMC concentration will become higher in the CNC suspension/CMC solution than the real CMC concentration. As a result, apparent CMC concentration shifts the solution state to concentrated network solution state (Figure 2.10.c) and results an enormous viscosity increase in the suspension/solution system. High overlap parameters of CMC solutions in the presence of CNC particles due to entanglements give a rise both low shear rate viscosity (Figure 2.5) and flow curve gradient (Figure 2.6) close to asymptotic levels expected for highly concentrated polymer solutions and bulk polymer melts.

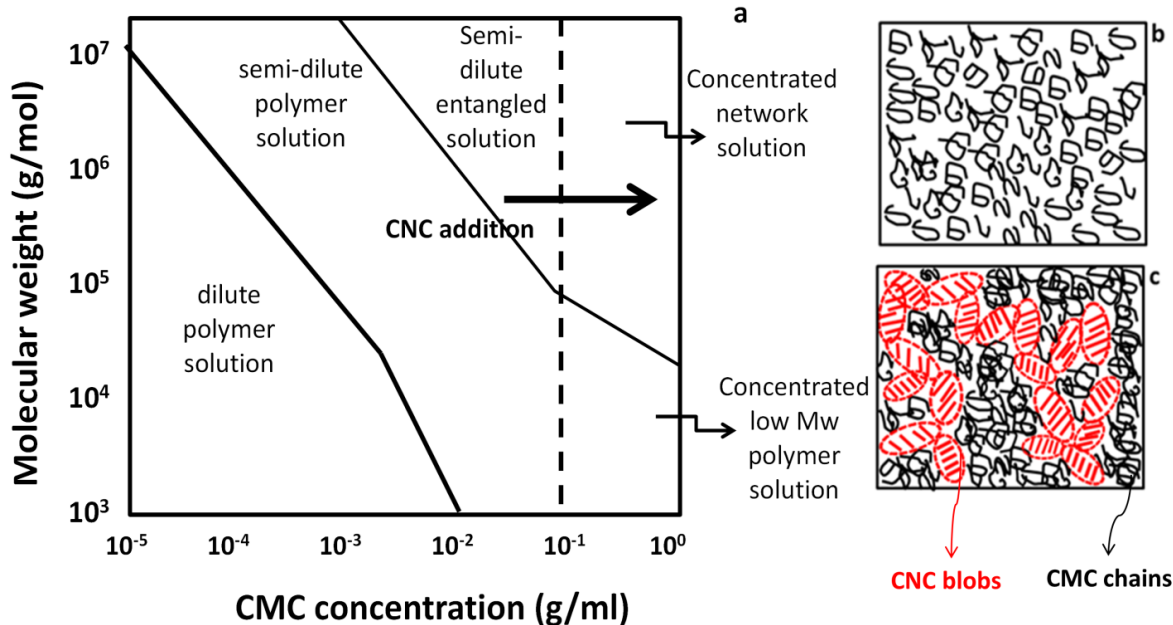


Figure 2.10 The solution states of CMC polymer as a function of CMC molecular weight and concentration and the role of CNC addition to shift from one state to another (a); Schematic representations of CMC polymer solution in semi-dilute entangled state (b); and CMC polymer solution in concentrated network solution state due to the CNC presence (c).

2.6 Conclusion

Spindle shaped CNC particles cause both drastic viscosity increases and steep non-Newtonian flow behavior in CMC solutions despite the use of only dilute or semi-dilute concentration of both CNC particles and CMC polymer in the suspension-solution system. This viscosity increase comes from the nematic flocculation of CNC particles in the presence of a non-adsorbing CMC polymer which turns CNC flocs with water entrapped pockets. As a consequence, the apparent polymer concentration rises to a highly concentrated network solutions state and result in both high viscosity at low shear rate and high degree of shear thinning (high flow curve gradient). CNC suspensions at low concentrations as a rheology modifier in dilute and semi-dilute polymer concentrations has potential applications in coating formulations, drilling and fracturing fluids, personal care and other industrial and household products. The use of such thickening systems shall bring not only desired performance characteristics by tailoring the thickening behavior but also address the operational concerns such as shear, thermal and bacterial degradation of the formulations. Minimizing the concentrations of water soluble polymers in any functional fluid while maintaining the thickening rheology by incorporating relatively shear, thermal and bacterially stable CNC can remedy such problems in operations. Besides cellulose nanocrystals

are easily dispersible in water and easy to formulate with a minimum mechanical action during preparations of product formulations.

Shear thickening behavior of CNC suspensions in the presence of CMC polymer was the main discussion of Chapter 2. Thickening mechanism was investigated in terms of steady-state viscosity and optical measurements. In Chapter 3, rheological properties of CNC suspension with CMC polymers were discussed with the focus on dynamic viscoelastic properties.

Chapter 3. Depletion induced gelling in cellulose nanocrystals (CNC) colloid carboxymethyl cellulose (CMC) polymer mixtures

The material shown in Chapter 3 has been previously submitted to Journal of Rheology. This chapter discussed viscoelastic properties and structure-property relation of CNC suspensions with CMC polymers. The experiments have been personally conducted except viscosity measurements of HEC and hmHEC solutions. These experiments were conducted in Alberta Innovates Technology Futures in the supervision of Dr. Boluk. The authors of this publication are me, and my supervisor Dr. Yaman Boluk. The material submitted is the following.

3.1 Abstract

The flow dynamics and mesoscopic structures of CNC suspensions in CMC polymer solutions were investigated by studying steady shear viscosities, linear viscoelastic behaviors, the applicability of the Cox-Merz rule and STEM and POM images. Addition of 1.34 vol.% CNC in 0.5 %, 1.0 % and 2.0 % CMC polymer solutions resulted in increases in the order of 30,000, 2000 and 800 times if one compares maximum viscosities which occurred below 0.04 s^{-1} shear rate. Both of the ideas of bridging by the adsorption of polymer chains on CNC particles and the depletion of non-adsorbing CMC polymers around CNC particles were tested to explain the dramatic increases in the low shear rate viscosities and strong non-Newtonian behaviors. Our results showed that the flocculation of CNC particles due to the depletion by non-adsorbing CMC polymer molecules resulted in gel formation. STEM image of dilute CMC-CNC solution showed the ordered CNC structures as nematic flocs. Both nematic and chiral nematic phase were observed in POM images of concentrated CNC-CMC solutions. The flocculated structure of CNC particles and formation of non-isotropic flocs in the CMC solution shown in STEM and POM images also supported the depletion mechanism.

3.2 Introduction

Colloidal suspensions are of interest for understanding a wide range of systems such as gels, biological systems, emulsions, foods and coatings. According to application area, the stability of colloidal suspensions is desired property to control by adding adsorbing and non-adsorbing polymers⁸. Polymer adsorption depends on the polymer-solvent interaction, the conformation,

molecular weight and the chemical structure of polymer chain ³⁹. Stability of colloidal suspensions with adsorbing polymer can be described with two mechanisms ⁸³: (1) adsorption flocculation and (2) steric stabilization. In dilute polymer concentrations (at low surface coverage); adsorption flocculation is encountered as polymer chains can form bridges between particles ⁸⁴. At concentrated polymer solutions (saturated surface coverage), steric stabilization occurs due to repulsive interactions. In the case of polymer depletion, non-adsorbing polymers apply osmotic pressure to particles because of entropy loss ^{79,85}. Phase separation ⁸⁶ and phase transition ⁸⁷ occurs at sufficient polymer concentration due to repulsion between polymer and particles ⁸⁸. At higher polymer concentrations, large repulsive barrier leads to depletion stabilization ⁸³. Interestingly, mechanism can be seen in the presence of adsorbing polymer after steric stabilization with further increase polymer concentration depletion after reaching steric stabilization. Fully coverage of particle surface turns adsorbing polymers to non-adsorbing polymers.

The presence of adsorbing and non-adsorbing polymers leads to a change in mesostructure of colloidal suspensions. Below saturation concentration, polymer bridging occurs and can create network structures, gels ⁸⁹. Also, non-adsorbing polymer-particle systems exhibit also gel properties ^{90,91} and phase transitions ^{68,75,92}. Therefore, rheological measurements allow investigating interaction mechanisms in terms of structure-property relations and viscoelastic behaviors. For understanding the mesostructure of particles, microscopy techniques such as polarized optical microscopy and transmission electron microscopy can combine with rheological measurements.

New classes of nanoparticles, cellulose nanocrystals (CNC) are interest of our study to extend application area. Amorphous part of cellulose-based materials such as wood, cotton, etc. are hydrolyzed with sulfuric acid to produce CNCs with a length between a typical length of 100-300 nm and a width of 5-15 nm. Typical rod-like particle, CNC shows isotropic-nematic phase transition and phase separation. This change in mesostructured affects the rheological behavior of CNC suspensions. The flow behavior of CNC suspensions depends on aspect ratio (L/D) of CNC ^{12,93}, surface charge of CNC ^{21,67,67,94} and CNC concentration ^{23,24,95}. The drastic change in shear viscosity and viscoelastic behaviors are obtained at higher CNC concentrations due to isotropic-nematic phase transitions ^{23,24,96}. However, adding polymer in CNC suspensions shows very unique rheological properties and gel formation ^{71,97,98}. The interaction mechanism behind

this unique behavior is still a debate. The aim of this study is to understand interaction mechanism with the use of rheology and microscopy techniques.

3.3 Experimental

3.3.1 Materials

CNC particles were prepared by sulfuric acid hydrolysis and ion-exchange process⁶¹. CNC particles suspensions were mixed with mechanical stirring in deionized water. Mixed solutions were sonicated with Branson ultrasonic cleaner model 1510 (frequency 40 kHz). The diameter of CNC was measured as 8 ± 0.8 nm with a scanning transmission electron microscopy (STEM). The length of CNC was calculated as 214 ± 0.3 nm using the translational translation coefficient, D_t of particles, Broersma's correlations and STEM⁴⁷.

All of the water soluble polymers used in this study, namely sodium salt of carboxymethyl cellulose (CMC), 2-Hydroxyethyl cellulose (HEC), hydrophobically modified 2-Hydroxyethyl cellulose (hmHEC) and polyethylene oxide (PEO) were purchased from Sigma Aldrich (St. Louis, MO, USA). According to supplier's product specification, CMC, HEC, hmHEC, and PEO samples have weight average molecular weight (M_w) of 700, 250, 250 and 600 kDa respectively. Degree of substitution (DS) of CMC was between 0.89-0.90 and molar substitution of HEC and hmHEC was 2.5 ethylene oxide per anhydroglucose repeating unit. hmHEC contained approximately 1.0 wt% C16 alkyl groups. Description, supplier listed molecular weight, degree of substitution (DS), molar substitution (MS) and critical overlap concentration, c^* of polymers are listed in Table 3.1.

Table 3.1 Polymers used for solution preparations in experiments.

Polymer	Acronym	D.S.	M.S.	M_w (kDa)	c^* (mg/L)
Carboxymethyl cellulose	CMC	0.85-0.90		700	11.0
Hydroxyethyl cellulose	HEC	1.0	2.5	250	13.0
Hydrophobically modified Hydroxyethyl cellulose	hmHEC	1.0	2.5	250	6.0
Polyethylene oxide	PEO	-		600	18.3

CNC suspensions in polymer solutions were prepared in two steps. Initially, CNC were suspended in water by using mechanical stirring and ultrasound. After that, polymers were dissolved in CNC suspensions in suitable temperature conditions and time.

3.3.2 Methods

Steady state shear viscosities of aqueous polymer solutions with CNC suspensions were measured with AR-G2 rheometer (TA Instruments, USA). Cone-and-plate geometry with a nominal angle as $2^{\circ}0'22''$ plate geometry of 60mm in diameter was used. The torque resolution is $0.1 \mu\text{N}$. TA Instruments AR-G2 rheometer equipped with a 2° cone and plate geometry of 60 mm in diameter was also used to measure linear viscoelastic properties of colloid-polymer mixtures. First, strain displacement sweep at 1 rad/s was carried out to determine the linear strain range. Then, all of the oscillation mode tests were done sweeping the frequency between 0.1 and 100 rad/s, at the 1.0% strain which was within the linear range. Temperature control was established with a ThermoCube200/300/400 (Solid State Cooling Systems Co., USA) and all measurements were conducted at $25.0 \pm 0.05^{\circ}\text{C}$.

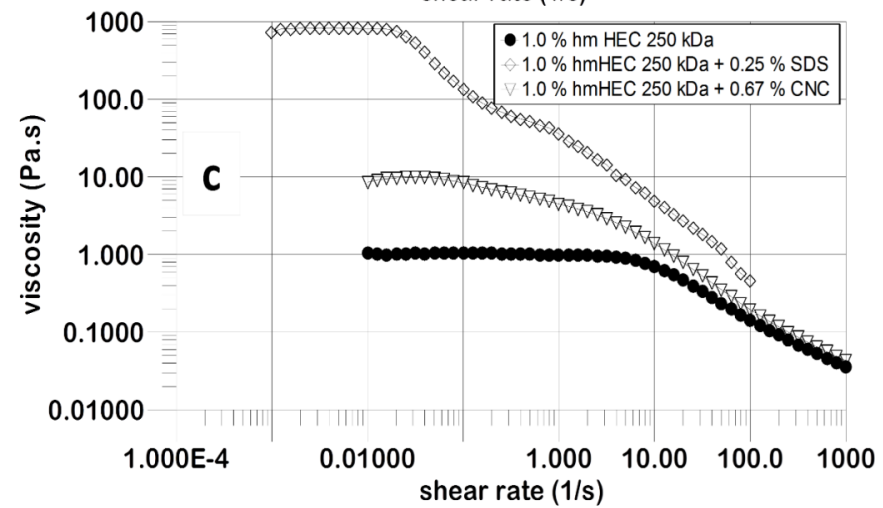
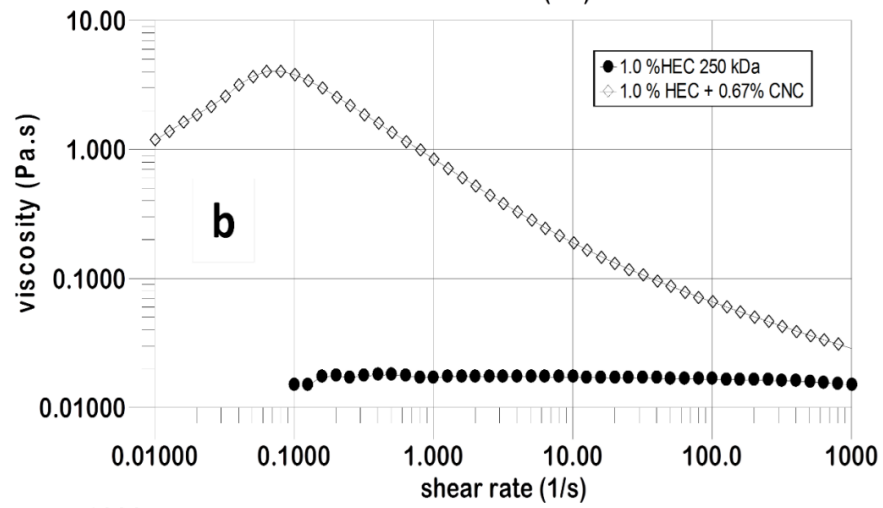
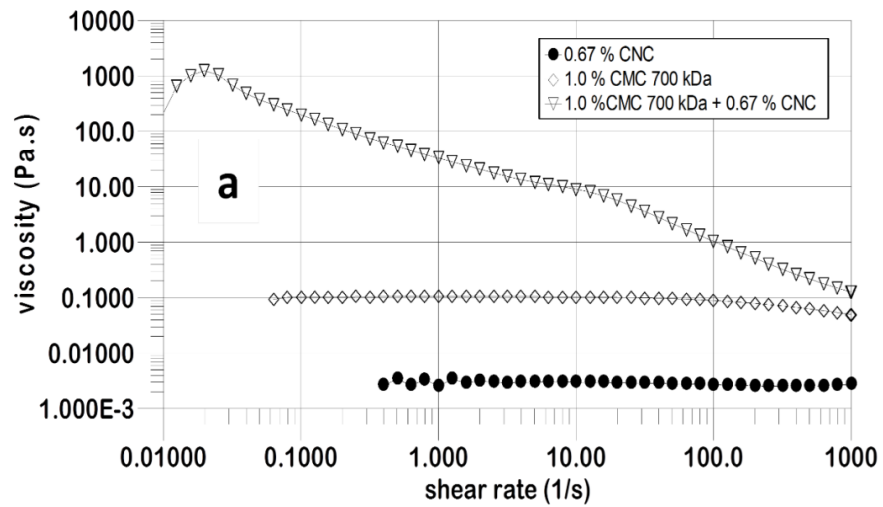
The morphology of the samples were investigated with a Hitachi model S-4800 apparatus equipped with a field emission source and operating at an accelerating voltage of 30kV in transmission mode. The samples were dropped on a carbon-coated TEM grid. After 3 minutes, the excess of liquid was absorbed with a filter paper. The TEM grid was permitted to dry at room temperature for 3 min. A drop of uranyl acetate solution (2.0 wt% in water) was deposited on the grid for 5 min to get a high-resolution image. The excess solution was wicked off using filter paper, and the grid was dried at room temperature prior to imaging. Birefringent structures were observed with an Olympus BX50 equipped with 20x microscope objective lenses and a JVC 3-ccd video camera (Olympus, Japan).

3.4 Results and Discussion

3.4.1 CNC Suspensions in Aqueous Polymer Solutions

Plots of the steady state viscosity as a function of the applied shear rate for CMC, HEC, hmHEC and PEO polymer solutions with and without CNC particles are shown in Figure 3.1. In addition, for comparison purpose the viscosity plots of 0.67% CNC suspension without any polymer and hmHEC solution with 0.25% sodium dodecyl sulfate (SDS) are also included in the

same figure. Rod shaped particles in suspensions exhibit transition from dilute to semi dilute concentration region at volume fraction of $\leq (\pi/4)(d/L)^2$, where d is the diameter and L is the length of the particles. Hence, the suspension of 0.67 vol% CNC with particle length of 214 nm and width of 8nm was just above the dilute concentration range where particles barely touch each other. Consequently, 0.67% CNC suspension, without any polymer presence, was totally a Newtonian fluid and had a very low viscosity (0.003Pa.s) as shown in Figure 3.1.a. All of the polymer solutions were prepared at 10 g/L (1.0%) concentration which was below the critical overlapping concentration, c^* of HEC ($c^* \sim 13$ g/L) and PEO ($c^* \sim 18.3$ g/L), at c^* of CMC ($c^* \sim 11.0$ g/L), and above c^* of the hmHEC ($c^* \sim 6$ g/L). Expectedly, 1.0% HEC and PEO polymer solutions were all Newtonian, while CMC solutions just started to exhibit shear thinning. hmHEC solution above the overlapping concentration exhibited non-Newtonian behavior due to the association of hydrophobic groups. Addition of 0.67% CNC into such polymer solutions increased the viscosity of solutions of CMC 1000 times, HEC 500 times, and hmHEC 10 times at 0.1 s^{-1} shear rate. Moreover, those CNC suspensions in CMC, HEC and hmHEC solutions exhibited strong pseudoplastic behavior. However, unlike those polymer solutions, the addition of CNC in PEO solution barely budged the polymer solution viscosity.



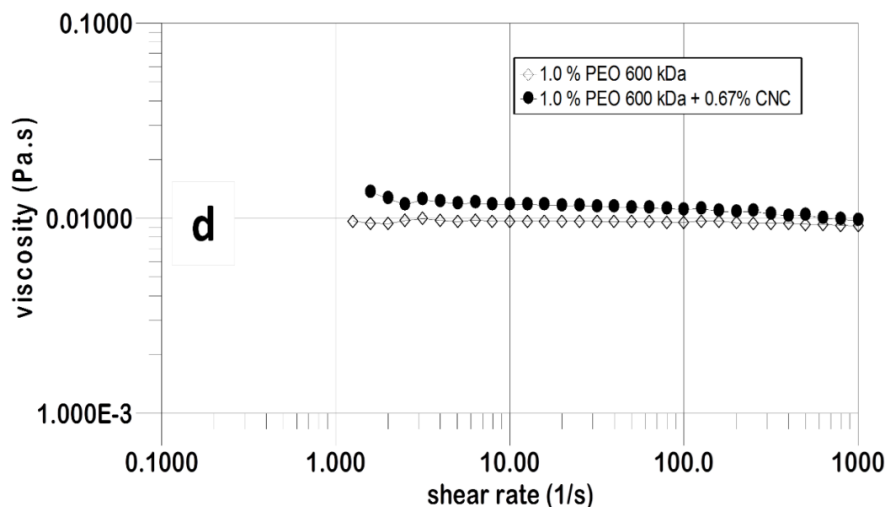


Figure 3.1 Steady shear rate viscosity as a function of shear rate of: (a) 1.0% CMC 700 kDa with and without 0.67% CNC; (b) 1.0% HEC 250 kDa with and without 0.67% CNC; (c) 1.0% hmHEC 250 kDa with and without 0.67% CNC and 0.25% SDS; (d) 1.0% PEO 600 kDa with and without 0.67% CNC.

The dramatic increases in the low shear rate viscosities and strong non-Newtonian behaviors of CNC suspensions in CMC, HEC and hmHEC polymer solutions must come either from the adsorption of polymer chains on CNC particles and forming network junctions or from the depletion of CNC particles due to non-adsorbing polymer chains and flocculation. To test the idea of polymer adsorption and junction formation, flow behavior solutions of hmHEC were also included in this study. It is well known that hydrophobically modified hydroxyethyl cellulose (hmHEC) consists cellulose backbone onto which hydrophobic groups are attached through ethoxylated side chains in a comb-like structure. The hydrophobic moieties of hmHEC associate dynamically with another to form reversible hydrophobic junctions^{99,100}. As shown in Figure 3.1.c, hmHEC solution above the entanglement concentration formed network consisted of hydrophobic associations, yielding also a large increase in the solution viscosity, compared to the unmodified HEC without the hydrophobic groups (see Figure 3.1.b). Besides, the interactions of hmHEC with anionic SDS at 0.25% concentration resulted in even more drastic increased in rheological properties of the solution due to the strengthening of the junctions^{101,102}. hmHEC solutions with or without SDS showed a long distinct region of almost a constant viscosity at low shear rates (Figure 3.1.c), followed by viscosity decrease at higher shear rates. The polymer network was totally destroyed above the critical shear rate and the value of critical shear rate decreased with the addition of SDS. However in the case of CNC added CMC, HEC and hmHEC

solutions there was not any long distinct constant viscosity region at low shear rates, on the contrary there was a shear thickening at the low shear rate region. It was also clear that CNC particles did not result in any viscosity increase in PEO solution. If there were adsorption of polymer molecules on CNC particles and a particle-polymer network formation, one would expect nonionic PEO molecules had a better chance than anionic CMC and hydrophobic hmHEC molecules to adsorb on negatively charged CNC particles. Indeed, the thickening due to the adsorption of polymer molecules on CNC particles were ruled out and the second thickening mechanism, flocculation of particles by depletion in the presence of non-adsorbing polymers were shown in our previous publications by using different experimental techniques^{71,98}. The rheological behavior of CNC in CMC suspensions will be the focus of the rest of this article.

3.4.2 CNC Suspensions in CMC Solutions

3.4.2.1 *Steady State Shear Viscosity*

Figure 3.2 shows the viscosity vs. shear rate plots of CMC solutions, independently varying CNC particle and CMC polymer concentrations. CMC concentrations of 0.5%, 1.0% and 2.0% were below, at and above the critical overlap concentration of CMC of 700 kDa respectively. Nevertheless, addition of 1.34 vol.% CNC in 0.5 %, 1.0 % and 2.0 % CMC polymer solutions resulted in increases in the order of 30,000, 2000 and 800 times if one compares maximum viscosities which occurred below 0.04 s^{-1} shear rate (see Figure 3.2.a). An initial shear thickening behavior was observed when the shear rate was increased above a critical value, followed by very drastic shear thinning. Interestingly, similar initial shear thickening behavior of CMC polymer solutions above a critical concentration (around 2.0%) is observed frequently and one of its plausible interpretation is “flow-induced formation of macromolecular associations”^{103,104}. The possible role of CNC particles on this particular shear thickening was excluded by considering Peclet number of CNC at those very low shear rates. 1.34 vol.% CNC in 2.0% CMC reached its maximum viscosity of $>4,000 \text{ Pa}\cdot\text{s}$ at around 0.02 s^{-1} which corresponds to approximately the viscosity of 8% CMC polymer solution without CNC addition, however dropped drastically above 500 s^{-1} shear rate. Various CNC concentrations (0.67%, 1.34% and 2.0%) in 1.0% CMC polymer solutions resulted in at least 100,000 times increase, while the 0.33% CNC addition still resulted in a respectable 10,000 times increase if one compares again the maximum viscosities

(see Figure 3.2.b). It is worth to note that 0.33% concentration was at the very low end of semi-dilute concentration range of CNC.

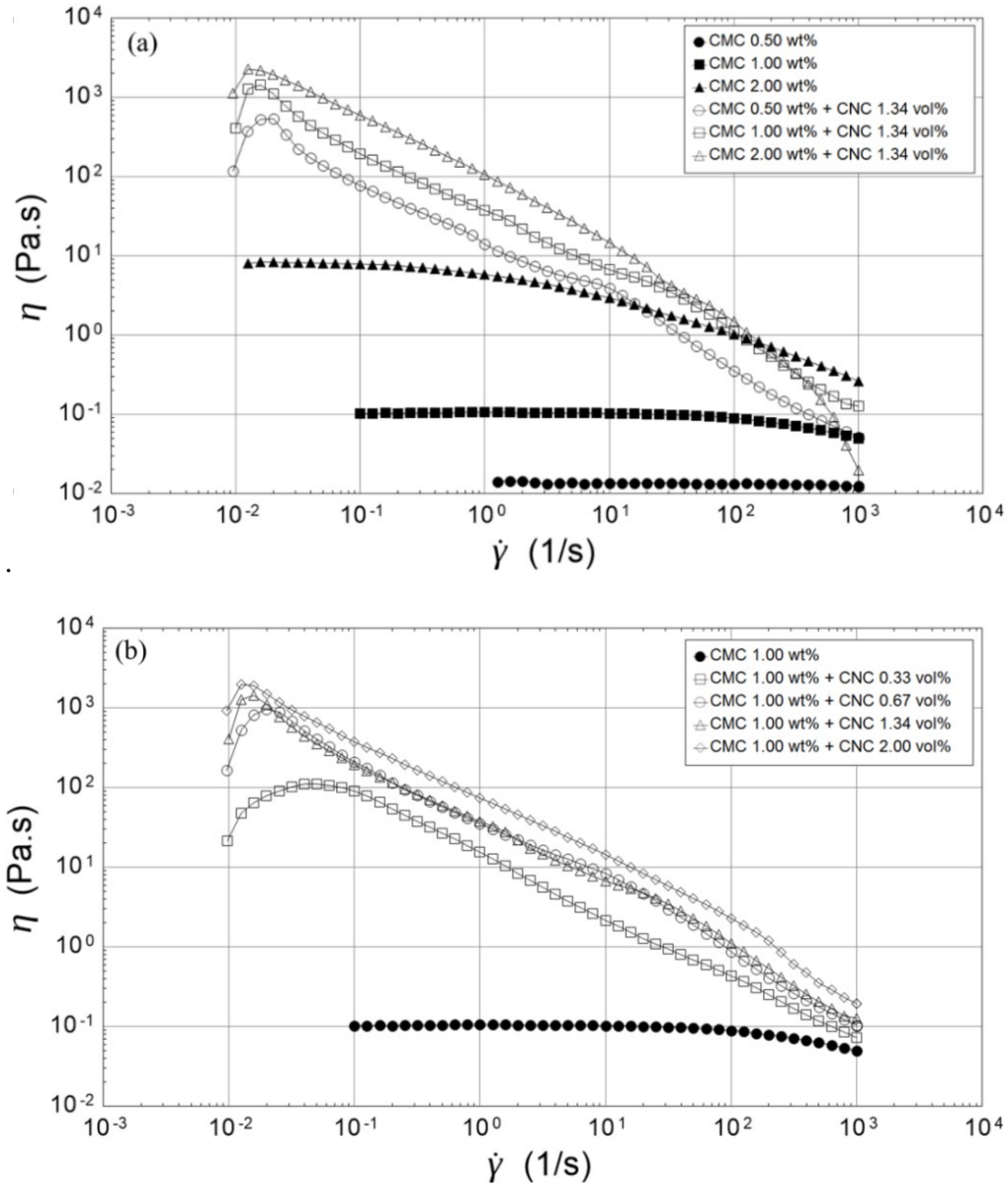
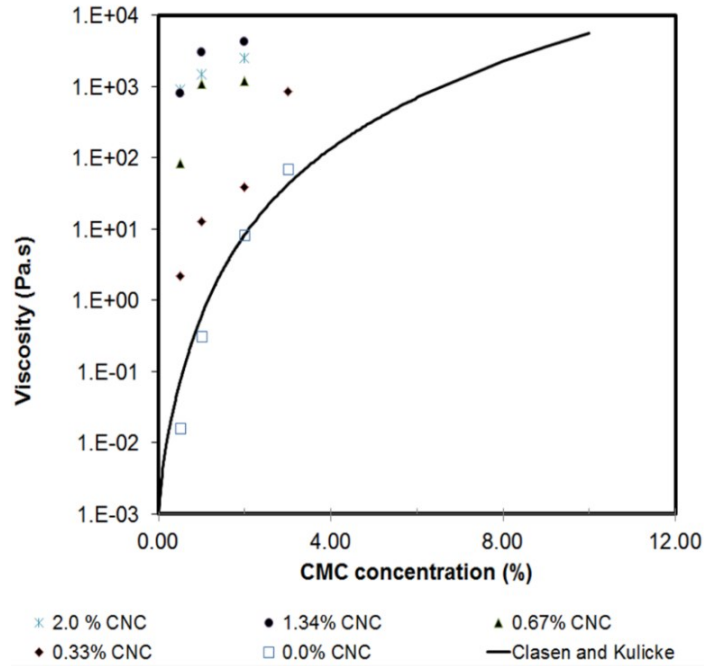


Figure 3.2 Steady state shear viscosities of (a) CMC solutions with and without 1.34 vol.% CNC addition; (b) Various 1.0 wt.% CMC solutions with various CNC concentrations.

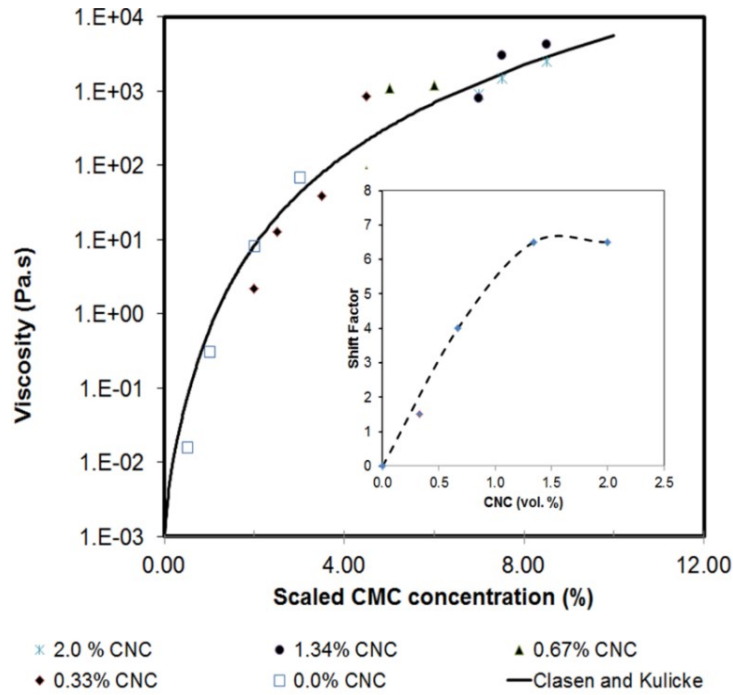
Maximum shear viscosities of CNC suspensions in CMC polymer solutions are plotted as a function of CMC concentration in Figure 3.3.a along with the Newtonian viscosity-Molecular weight- concentration master curve formulated by Clasen and Kulicke³⁰:

$$\eta_0 = 0.891 + 7.82 \cdot 10^{-3} c M_W^{0.93} + 1.77 \cdot 10^{-5} c^2 M_W^{1.86} + 4.22 \cdot 10^{-12} c^{4.09} M_W^{3.80} \quad \text{Equation 3.1}$$

where η_0 is the zero shear rate viscosity, M_w is the molecular weight and c is the CMC concentrations. Here, the molecular weight of CMC is taken as 700,000 Da. It is worth noting that this equation was devised for CMC polymer in 0.01 M NaCl solution. Nevertheless, as pointed out by Clasen and Kulicke, the viscosity curves of CMC solutions at different saline concentrations and salt free water converge above the polymer concentration of 1 wt.%. Therefore our viscosity data of CMC solutions without CNC addition in salt free aqueous solution agreed very well with Equation 3.1. While the CNC concentration in CMC polymer solution increased from zero up to 1.34%, viscosity vs. CMC concentration curves become steeper and then levelled off around 2.0%. Remarkably, all of the data were shifted onto the Clasen-Kulicke master curve; this was accomplished by scaling the CMC concentration at each CNC concentration (Figure 3.3.b). We can explain the rationale for the observed scaling behavior by using a simple model: CNC particles flocculate, entrap water and thus flocculated CNC blobs occupy more volume than their prepared concentration. Hence, the real available volume (reservoir) for CMC polymer solutions becomes less than their corresponding prepared weight (volume) fraction. Indeed, according to our scaling of viscosity data, 0.34, 0.67%, 1.34, and 2.0 vol% prepared CNC concentrations behaved as 1.73, 4.67, 7.84 and 8.50 vol% respectively in CMC solutions and reduced the available volume for CMC molecules. The shift factor at each CNC concentration is displayed in the inner box of Figure 3.3.b.



a



b

Figure 3.3 Low shear rate viscosities of CNC suspensions in CMC solutions: (a) before scaling; (b) after scaling with inner box shows scaling factor at each CNC concentrations.

3.4.2.2 *Linear viscoelasticity*

The storage and loss moduli of CMC polymer solutions with varying amount of CNC particles are shown in Figure 3.4. CMC solutions at 0.5% (not shown in the figure) and at 1.0% polymer concentrations without any CNC particles displayed weak viscoelastic behavior with G' being lower than G'' for the whole frequency range measured. Crossover point was observed in the case of 2.0% CMC solution around 20 Hz. As expected, those polymer solutions had the terminal part of their dynamic spectrum within the measure frequency range. It is worth to note that CMC concentration of 0.5% was below the overlap value and 2.0% was above the overlap concentration of 700 kDa. CMC. The addition of CNC particles into CMC solutions caused monotonic increases in both G' and G'' . By the addition of CNC particles (except 0.33% CNC in 0.5 % CMC) CNC particle-CMC polymer systems became more like physical gels with G' values were always higher than G'' for the whole measured frequency range. Spectra of those samples were within the plateau and transition regions while G' displayed a broader constant plateau with increasing CNC concentration. At 1.34% and 2.0% CNC in 0.5% CMC and 0.67%, 1.34% and 2.0% CNC both in 1.0% CMC and 2.0% CMC solutions G' also remained almost constant. By increasing the CNC concentration, the dynamic moduli plateau was independent of the angular frequency, which is the characteristic of gel formation with strong physical bonds. This behavior was due to the strong gel formation and the characteristic relaxation times of those systems were longer than the longest measurement time of 10 s/cycle of oscillation. The flocculated, water entrapped CNC blobs caused an increase in the apparent polymer concentration in the reservoir of pure polymer solution (as discussed in shear viscosity data) led to higher dynamic moduli values and to the elastic behavior even for the polymer concentration of 0.5% which was below c^* . In this model the terminal and longest relaxation time may be due to the disengagement of polymer chains from entangled network. Shorter relaxation times were due to the disruption of flocculated CNC particles. The intercept of $G'' > G'$ of 0.33% CNC in 0.5% CMC is believed to be related to the disruption of CNC aggregates in relatively low structured polymer solution.

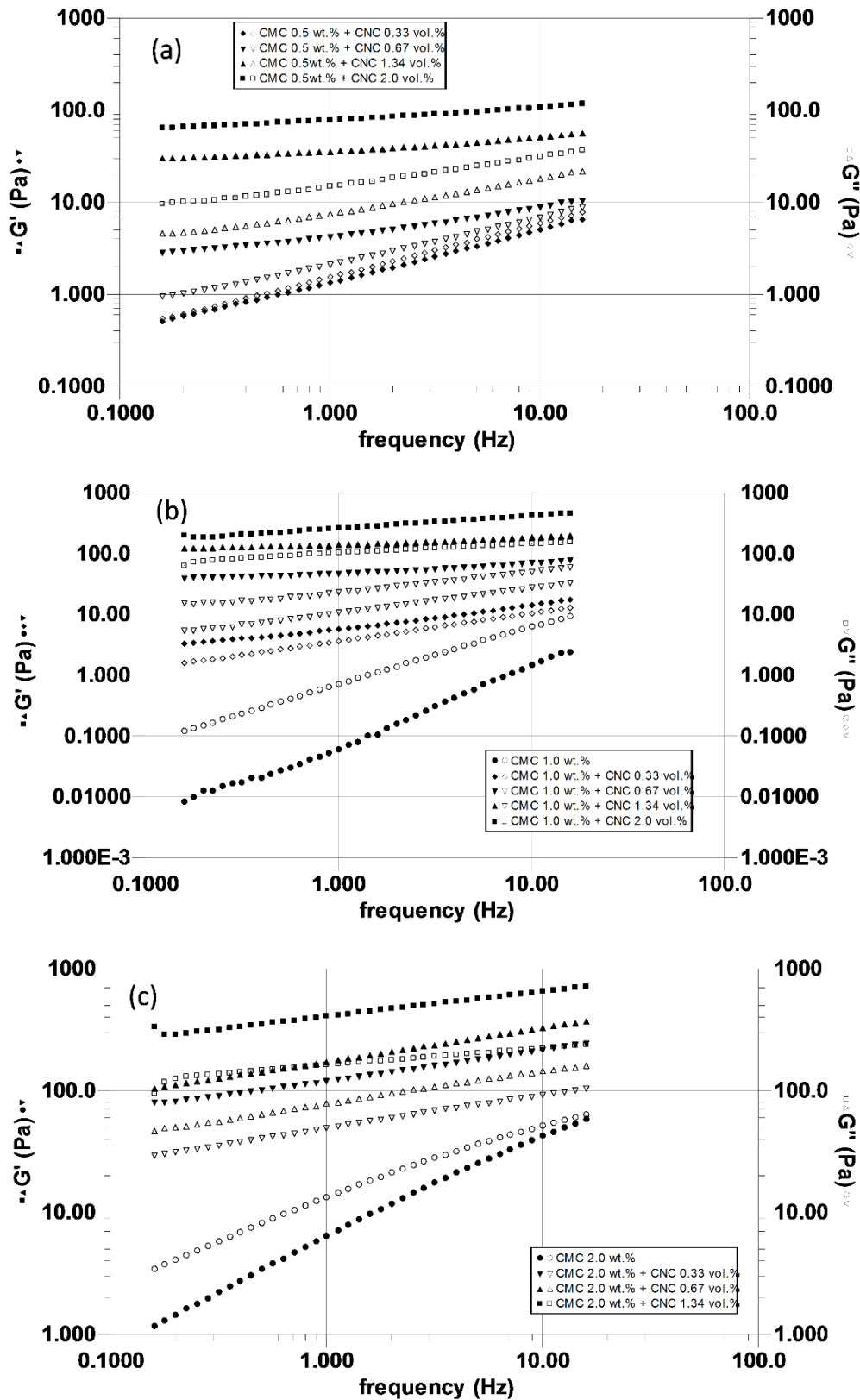


Figure 3.4 Dynamic storage and loss moduli versus oscillatory frequency of CNC suspensions in: (a) 0.5 wt.% CMC solution; (b) 1.0 wt.% CMC solution; (c) 2.0 wt.% CMC solution.

The measured dynamic mechanical data of G' and G'' were converted from the frequency domain into the time domain (linear relaxation modulus $G(t)$) to interpret the data. For this purpose, the discrete relaxation time spectra were extracted by fitting the data into following model with “n” selectable terms to interconvert linear viscoelastic material functions $G'(w)$, $G''(w)$ to $G(t)$:

$$G(t) = G_e + \sum_i^n G_i e^{-t/\tau_i} \quad (2)$$

where G_e is the equilibrium relaxation modulus, and n is the number of relaxation modes and G_i and τ_i are relaxation strength and relaxation time at mode respectively. It is worth to note that the calculation of the relaxation time spectrum from experimental data may become an ill-posed problem. The automatic mode selection of TA Instruments Trios™ software was used to optimize the solution and determine the optimum number of modes. Figure 3.5 shows the equilibrium relaxation modulus of CNC suspensions in polymer solutions while varying CNC concentration. The addition of even very low concentrations of CNC resulted in a very drastic increase in both in dilute (0.5%) and semi-dilute entangled (1.0%, 2.0% and 3.0%) CMC polymer solutions. CNC additions into CMC polymer solutions let them to reach the asymptotic viscosity value, which is expected to reach only at higher CMC concentrations without CNC. A similar behavior in shear viscosity has already been discussed in the previous section. It appears that additions of CNC particles caused concentrations of CMC solutions appeared higher than their formulated values. Non-adsorbing CMC polymer molecules were excluded and depleted from the regions of being closely spaced CNC particles. This caused an increase in the polymer concentration and entangling in “*flocculated CNC free*” solvent reservoir and a drastic enhancement in the G_e moduli values.

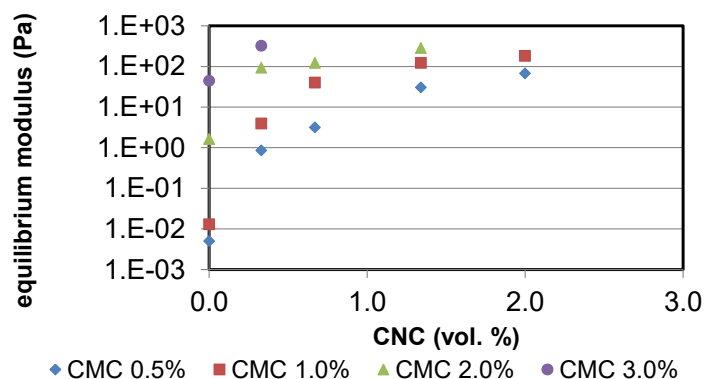
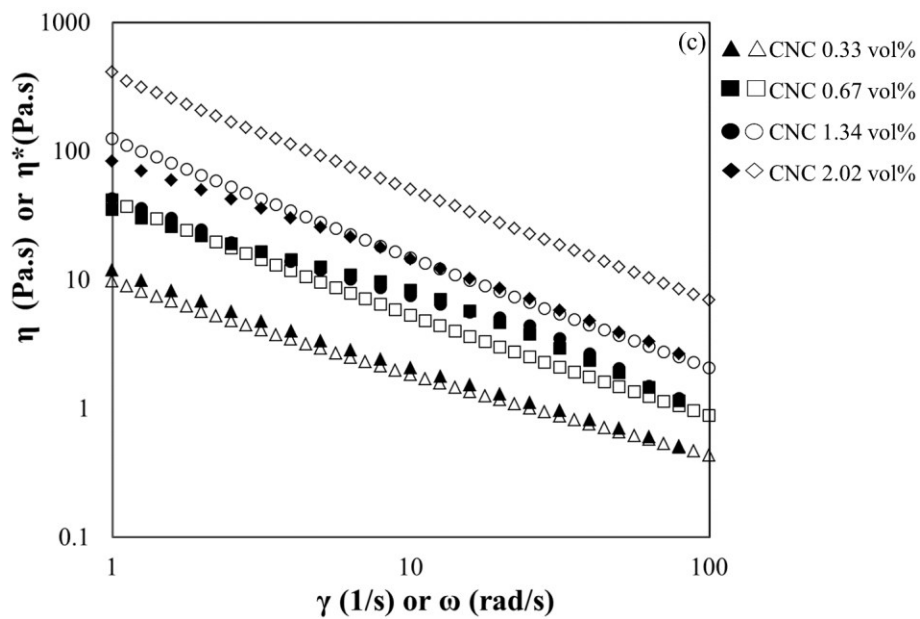
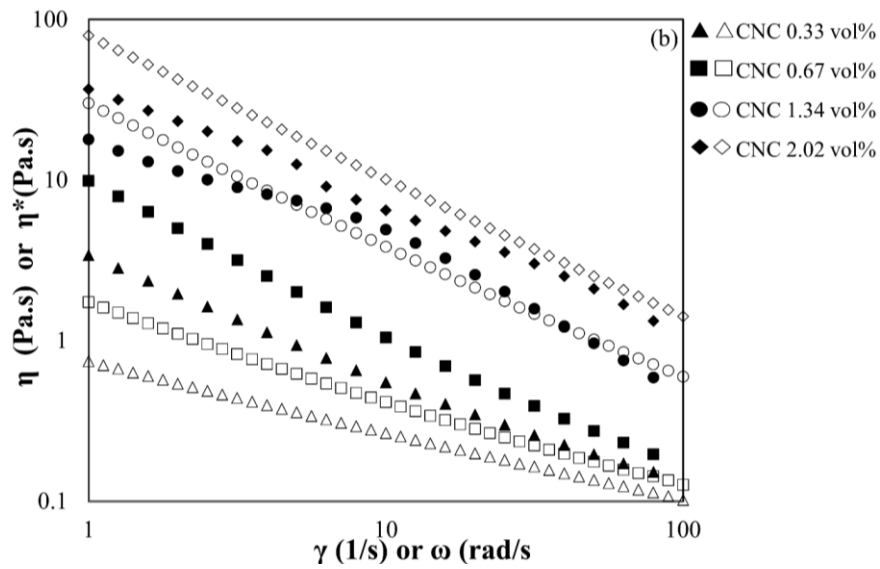
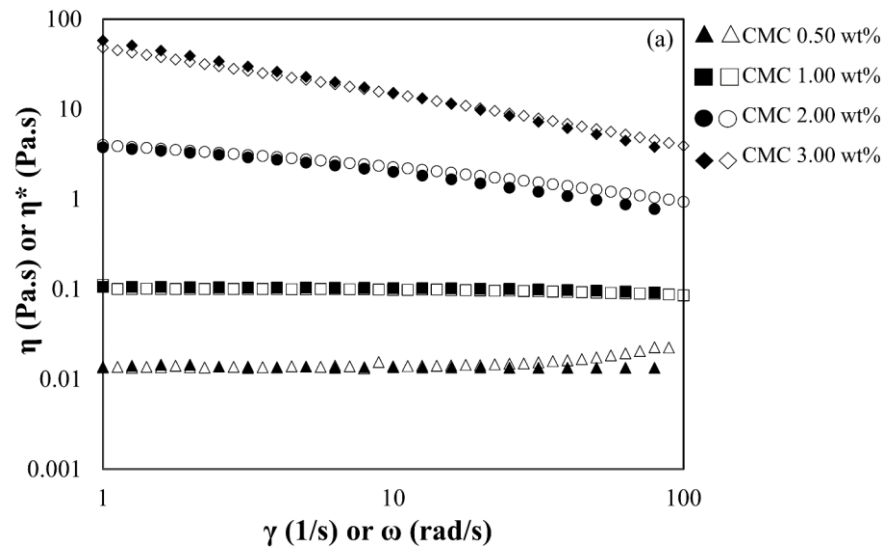


Figure 3.5 Storage (G') and loss (G'') modulus values of (a) 0.5 wt.% CMC, (b) 1.0 wt.% CMC, (c) 2.0 wt.% CMC and (d) 3.0 wt.% CMC with respect to CNC concentration at 1 rad/s.

3.4.2.3 Comparison of steady and dynamic viscosities

Steady state and linear dynamic viscosity data given here were also used to verify whether the Cox-Merz rule applies (Figure 3.6). As expected CMC solutions without CNC obeyed the rule well (Figure 3.6.a). The applicability of the Cox-Merz rule of unentangled semi-dilute CMC solutions with CNC suspensions is tested in Figure 3.6.b. η^* values were smaller than η values in the cases of 0.33 vol.% and 0.67 vol.% CNC suspensions in 0.5% CMC solution indicating disperse systems. Kulicke and Porter (1980) mentioned that ionomeric clusters resulted in higher η values than η^* values. Depletion interactions between negatively charged CNC particles and CMC chains led to ionomeric disperse systems. In the case of 1.34 vol.% and 2.0 vol.% CNC in 0.5% CMC polymer, ionomeric clusters formed percolated blob structures of CNC in CMC solutions with the increase in CNC concentrations due to depletion forces. The stronger associations of CNC particles break down with shear rate, so, η^* values is higher than the η values^{105,106}. CMC chains entangle above the critical concentration of 1.1 wt%. Figure 3.6.c shows the case of CNC suspension in 1.0 wt% CMC solutions, which is close to the critical concentration. The Cox-Merz rule is applicable for the cases of 0.33 vol.% and 0.67 vol.% CNC suspension with 1.0 wt% CMC solutions. η^* values were higher than the η values in the cases of 1.34 vol.% and 2.02 vol.% CNC suspension with 1.0 wt% CMC solutions. Depletion interactions between CNC particles results in both CMC chain entanglement and percolated blob structures of CNC. Figure 3.6.d and 6.e show the CNC-CMC solution sets above the critical concentration. Entangled CMC chains and blob structures result in higher η^* values.



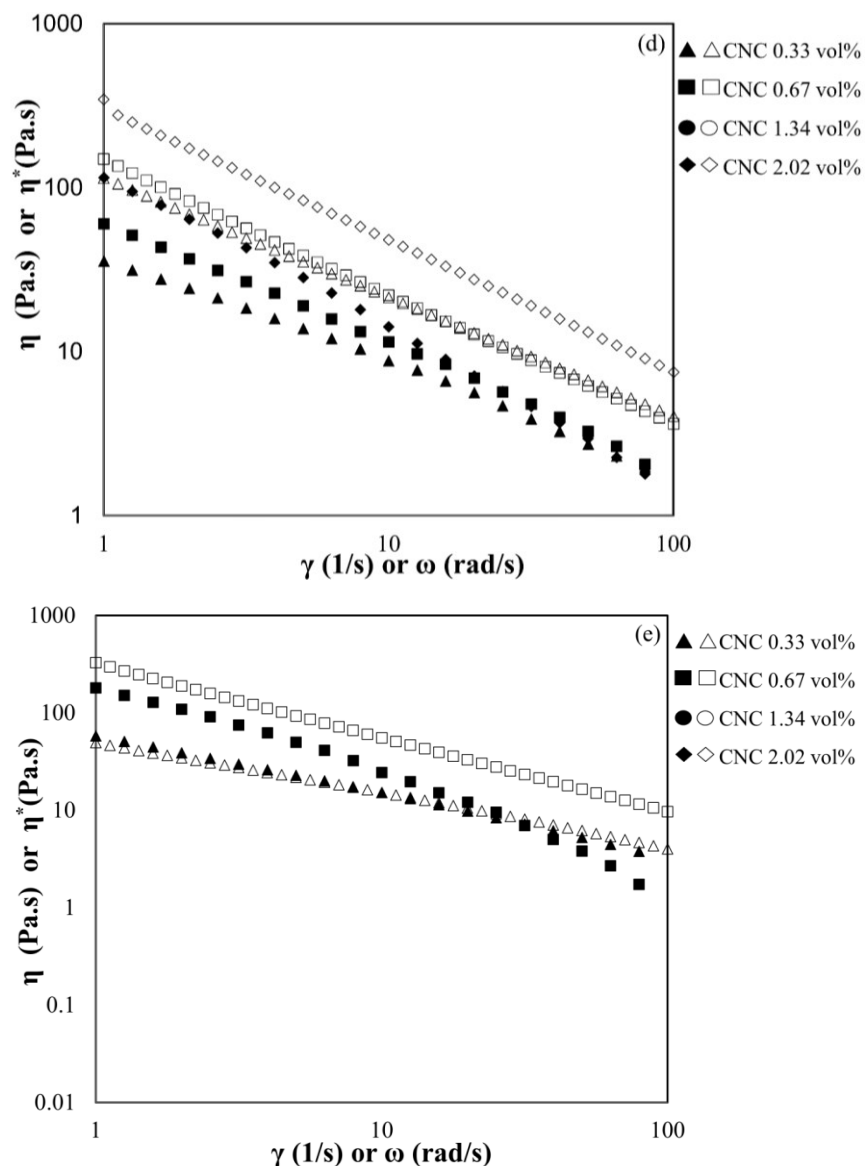


Figure 3.6 The steady-shear (filled) and complex (hallow) viscosity for (a) aqueous CMC (700 kDa) solutions with different concentrations, CNC suspensions with aqueous (b) 0.5 wt.% CMC (c) 1.0 wt.% CMC (d) 2.0 wt.% CMC and (e) 3.0 wt.% CMC solutions at 25°C.

3.4.2.4 Structure formation

It appears that flocculation of CNC particles in the presence of non-adsorbing CMC polymer resulted in enrichment of CMC polymer concentration in the particle free solution reservoir due to the depletion. The flocculated structure of CNC particles and formation of non-isotropic flocs in a CMC solution shown in STEM and POM images supported this view (Figure 3.7). Depletion of CNC particles due to a non-adsorbing anionic CMC polymer chains resulted in nematic flocs

of CNC particles and entrapment of water within⁹⁸. Particle flocs decreased the available solvent reservoir for CMC polymer chains.

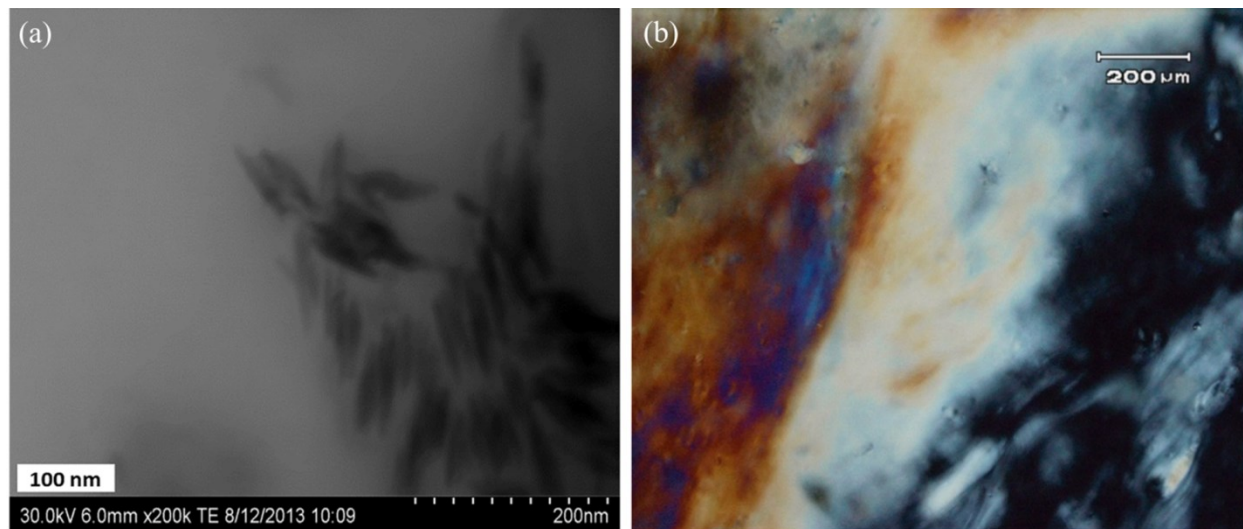


Figure 3.7 (a) STEM image of dilute CNC particles in CMC (700 kDa) solutions and (b) POM image of 2.00 vol% CNC suspensions in 1.0wt% CMC solution.

The role of CNC particles on the formation of CMC solution gels with very high viscosity and finite shear modulus can be depicted by illustrating the depletion and mesoscopic structure of resultant system. The first theoretical interpretation of depletion interactions by nonadsorbing polymer was done by Asakura and Oosawa (5). According to this theory colloidal particles and polymer chains are mutually impenetrable. Thus a nonadsorbing polymer molecule with radius of R_g (radius of gyration of polymer chain) will be excluded from the zone of thickness of the order of R_g from the particle surface, which is called as depleted zone. If the depletion zones of two particles overlap, particles are pushed together due to the unbalanced osmotic pressure. Phase separation in suspensions usually occurs usually due to depletion interactions of nonadsorbing polymers. However colloidal–polymer gel is a special state of flocculated CNC systems in which continuous network of polymer blobs formed before settling of CNC particles. Apart from gel formation, the full phase diagrams of CNC in CMC solutions have been investigated by us and to be published separately. Figure 3.8.a and 3.8.b represent CNC suspension and CMC polymer solution respectively. Figure 3.8.c illustrates the depletion flocculation of CNC particles due to nonadsorbing CMC polymer molecules. Non-adsorbing CMC chains apply osmotic pressure causing nematic flocculation of CNC particles. CNC flocs

lead to an increase in the apparent volume fraction of CNC particles and decrease in the solvent reservoir for polymer molecules. As an example, volume of one particle will change from $\pi d^2 L/4$ (where d is particle diameter and L is particle length) to $\pi(d+\delta)^2 L/4$ (where δ is depletion layer thickness due to nonadsorbing polymer). The apparent volume fraction of CNC particles will increase by the second power of depleted layer thickness. Hence, available solvent reservoir for polymer molecules will decrease and the polymer concentration in reservoir increases drastically.

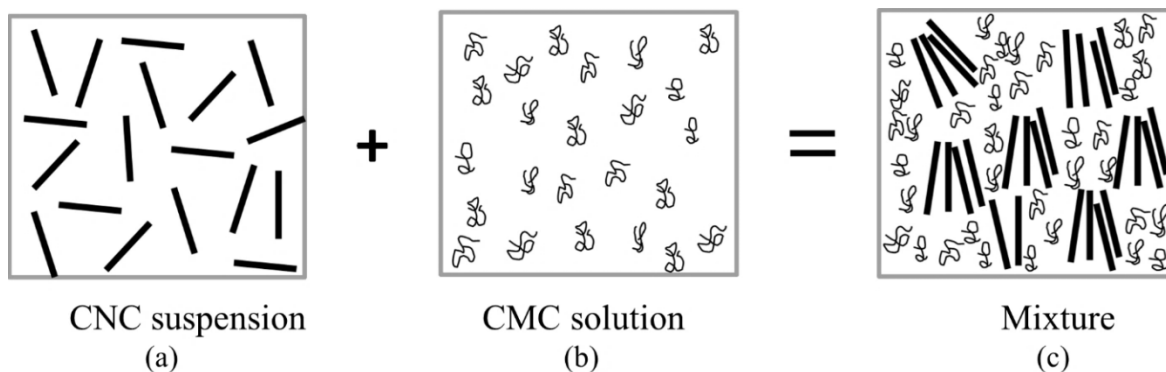


Figure 3.8 Schematic representation of depletion flocculation CNC and increasing the apparent CMC solution concentration.

While increasing the CNC concentration, entrapped water in the blob structure of CNC flocs will also increase. The blob structure formation is mathematically modelled with consideration of polymer chain difference¹⁰⁷. The size difference of polymer chains affects the overlapping volume of the depletion zone resulting in different phase behaviors. Small polymer chain size change a miscible isotropic phase to a miscible nematic phase. For bigger sizes of polymer chains, the phase transition occurs from miscible isotropic phase to immiscible nematic phase. Therefore, bigger CMC chains cannot penetrate between the particles, which may lead to blobs of CNC¹⁰⁷. These blobs may decrease the total volume of polymer matrix, which artificially increases the concentration of polymer and entangles chains. CNC suspensions in CMC solutions exhibit a totally different shear viscosity behavior compared to CNC suspensions in PEO solutions and hydrophobically modified polymers in the presence of surfactants. One has to note that, in the case of thickening due to the hydrophobic interactions in associative polymer/surfactant interactions, polymer concentration has to be above the overlapping threshold. However in the case of CNC addition, drastic thickening effects were still observed while CMC and HEC polymer concentrations were below the overlapping limit. Shear flow can

only brake down nematic flocs at mid-to- higher shear rates, leading to significant decreases in the viscosity. However at lower shear rates, flocs with entrapped water resulted in higher viscosity values.

3.5 Conclusions

The flow dynamics and mesoscopic structures of CNC suspensions in CMC polymer solutions were investigated by studying steady shear viscosities, linear viscoelastic behaviors, the applicability of the Cox-Merz rule and STEM and POM images. Both of the ideas of bridging by the adsorption of polymer chains on CNC particles and the depletion of nonadsorbing CMC polymers around CNC particles were tested to explain the dramatic increases in the low shear rate viscosities and strong non-Newtonian behaviors. Our results showed that the flocculation of CNC particles due to the depletion by nonadsorbing CMC polymer molecules resulted in gel formation. The electrostatic repulsion between negatively charged CNC particles and anionic CMC chains strengthens depletion interactions leading to the chiral nematic order of CNC nanoparticles. Moreover, strong depletion interactions generate an elastic behavior and gelation in CMC-CNC solutions. Addition of CNC particles resulted in the formation of CNC flocs which entrapped water. Therefore, the CMC concentration artificially increased in the bulk state; this caused an increase in the shear viscosity, gelation and produce a different response in the Cox-Merz rule.

STEM image of dilute CMC-CNC solution showed the ordered CNC structures as nematic flocs. Both nematic and chiral nematic phase were observed in POM images of concentrated CNC-CMC solutions. The flocculated structure of CNC particles and formation of nonisotropic flocs in the CMC solution shown in STEM and POM images also supported the depletion mechanism. Those results agreed with our previous investigations (25,27) and presented credible and unfailing argument to explain the gel formation of semi-dilute concentrations of CNC particles in semi-dilute CMC polymer solutions by depletion flocculation of CNC particles. Hence the CMC solutions were dramatically thickened and gelled by adding CNC particles. In the meantime, the collapse of CNC flocs in CMC solutions led to shear thinning behavior at higher shear rates.

The rheological properties of CNC suspensions with CMC polymers were discussed in Chapter 2 and 3. In chapter 4, the flow properties of CNC suspension with PEO polymers were discussed with the focus on steady state viscosity and dynamic viscoelastic properties.

Chapter 4. Rheological Properties of CNC Suspensions in Polyethylene Oxides Solutions

Data in this section will be our further interest to prepare manuscript to explain structure-property relations of CNC suspensions in PEO solutions. The rheological properties and structure formation of CNC suspension with PEO polymers was discussed in Chapter 4.

4.1 Abstract

Adding PEO polymer in CNC suspensions doesn't show any significant thinning behavior in shear viscosities at higher shear rates. For 0.33 vol% CNC nanoparticles in 1.0 wt% PEO solutions thickens 3 times of the viscosity value. However, adding 0.67 vol% of CNCs leads to a decrease in shear viscosity values for the case close to 1.0 wt% PEO solution. This unexpected behavior indicates adsorption of PEO chains onto CNC surfaces. A similar trend is also observed in storage modulus and loss modulus values. The elastic behavior, ($G' > G''$) is only observed in 0.33 vol% CNC-1.0 wt% PEO solution indicating structure formation and adsorption. The reason for the adsorption mechanism is explained as the presence of a cofactor effect and salt. CNC nanoparticles act as cofactor leading to an extension of PEO chains. Adsorption of extended PEO chains occurs in the optimum P:C ratio. The optimum P:C ratio is determined between 0.75 and 2.00 considering the Cox-Merz rule. The bridging mechanism cannot be encountered as CNC particle surfaces are fully covered.

4.2 Introduction

The understanding of rheological properties of colloidal suspensions is a fundamental and challenging task to formulate personal care products, paints, coatings, drilling fluids and other functional fluids. Excluded volume interactions, concentration of colloidal particles, the Brownian motion, hydrodynamic interactions, the shape and charge of colloids are the effective parameters of rheology and stability^{13,14}. Cellulose nanocrystals (CNCs) are unique, non-toxic, biocompatible, and water dispersible colloidal particles^{46,62,108}. CNCs are derived from cellulose by applying concentrated (65%) sulfuric acid⁵⁹⁻⁶¹. The acid hydrolysis technique chops crystallites from amorphous segments creating negatively charged sulfate ester groups on the surface of CNC nanoparticles. According to source and reaction conditions, the dimensions of

CNC vary between 5 to 15 nm in width and 100 to 300 nm in length. CNC aqueous suspensions show ordered birefringent gel-like structure at higher concentration depending on the surface charge and size⁵⁹⁻⁶¹. Therefore, using CNC particles is not sufficient at higher concentrations due to its cost. However, an addition of polymer in CNC suspension may result in unique rheological properties due to the interaction mechanism between CNC particles and polymer chains^{71,97,98}. Therefore, the aim of this study is to understand the interaction mechanism between CNC particles and water-soluble polyethylene oxide chains in terms of structure-property relationship.

4.3 Experimental

Nonionic polyethylene oxide (PEO) with a molecular weight 600 kDa was purchased from Sigma-Aldrich (St. Louis, MO, USA). The properties of PEO are listed in Table 4.1. CNC with dimensions 8 ± 0.8 nm in width and 214 ± 0.3 nm in length were obtained with acid hydrolysis methods. Mark-Houwink-Sakurada relation was used to calculate the radius of gyration (R_g)³⁴. R_g was calculated as 50 nm. The transition concentration (c^{**}) from semi-dilute unentangled regime to semi-dilute entangled regime was determined with the combination of an M- R_G relation, Mark-Houwink-Sakurada viscosity equation and the solution viscosities³¹. By plotting specific viscosity as a function of the concentration,

Steady state shear viscosities of aqueous polymer solutions with CNC suspensions were measured with AR-G2 rheometer (TA Instruments, USA). Cone-and-plate geometry with a nominal angle as $2^{\circ}22'$ plate geometry of 60 mm in diameter was used. The torque resolution is 0.1 μ N. TA Instruments AR-G2 rheometer equipped with a 2° cone and plate geometry of 60 mm in diameter was also used to measure linear viscoelastic properties of colloid-polymer mixtures. First, strain displacement sweep at 1 rad/s was carried out to determine the linear strain range. Then, all of the oscillation mode tests were done sweeping the frequency between 0.1 and 100 rad/s, at the 1.0% strain which was within the linear range. Temperature control was established with a ThermoCube200/300/400 (Solid State Cooling Systems Co., USA) and all measurements were conducted at $25.0 \pm 0.05^{\circ}\text{C}$.

The morphology of the samples were investigated with a Hitachi model S-4800 apparatus equipped with a field emission source and operating at an accelerating voltage of 30kV in transmission mode. The samples were dropped on a carbon-coated TEM grid. After 3 minutes,

the excess of liquid was absorbed with a filter paper. The TEM grid was permitted to dry at room temperature for 3 min. A drop of uranyl acetate solution (2.0 wt.% in water) was deposited on the grid for 5 min to get a high resolution image. The excess solution was wicked off using filter paper, and the grid was dried at room temperature prior to imaging. Birefringent structures were observed with an Olympus BX50 equipped with 20x microscope objective lenses and a JVC 3-ccd video camera (Olympus, Japan).

4.3 Results and Discussion

4.3.1 Shear Viscosity and Structure Relation

Figure 4.1 shows values of shear viscosity for PEO solutions with or without CNC suspensions. PEO solutions in the presence of CNC suspensions show a weak shear thinning behavior at higher shear rates; this is caused by the alignment of CNC particles in the direction of the shear flow and by the lack of a strong structure formation¹².

Figure 4.1.a shows an increase between 3 to 4 times in shear viscosity of 1.34 vol.% CNC suspension in the presence of 1.0 wt.%, 2.0 wt.% and 5 wt.% PEO solutions indicating insignificant effect of PEO concentration on structure formations. The adsorption of PEO chains onto CNC surfaces may lead to weaker depletion interactions preventing the formation of CNC flocs. Figure 4.1.b shows an unexpected viscosity trend for the cases of 1.0 wt.% PEO solutions; these cases were previously reported in various studies^{31,109,110}.

The unexpected viscosity behavior can be better explained using visually explanatory schemes. Interactions between PEO chains and CNC particles are schematically illustrated in Figure 4.2. v and η symbolize free volume and shear viscosity, respectively and η is dependent on v . First of all, Figure 4.2.a represents the cases of 1 wt.% PEO solutions which are below c^{**} . PEO chains are in an unentangled semi-dilute state with a certain excluded volume. The free volume ($v_{f(cnc=0)}$) is so high that the PEO chains don't interact with each other when a shear velocity is applied. Therefore, a non-Newtonian behavior is not reported in Figure 4.1.

Figure 4.2.b illustrates the mesoscopic structure of PEO solutions with 0.33 vol% CNC. An increase in the total number of particles in the solution generates a reduction of the free volume ($v_{f(cnc=0.33)}$). In addition, van de Ven describes a possible PEO adsorption in the presence of cofactor and salt. At an optimum polymer cofactor ratio ($P:C$), the conformation PEO chains is extended¹¹¹. The extended polymer chain with a high molecular weight enables the adsorption of

the polymer chain onto the surface of nanoparticles^{39,112}. The adsorption is possible with a sufficient polymer to particle concentration ratio and a particular size and shape of the polymer chain. A lower free volume and weak adsorption cause the shear viscosity of PEO 1.0 wt% (Figure 4.1.b) to be incremented of twice its original value. Furthermore, polymer concentration for full coverage of 2.02 vol% CNC particles is calculated as 0.56 wt% PEO with the equation, $c_p = \frac{2\Gamma\phi}{R}$. Therefore bridging cannot be observed in 1.00 wt% PEO solutions in every CNC concentration because polymer bridging occurs at the optimum flocculation when half of the surface is covered with polymer molecules³⁹. The adsorption of PEO onto CNC surface results in a larger free volume ($v_{f(cnc=0.67)}$), which produces a lower shear viscosity for the case of 0.67 vol.% CNC in PEO solutions (Figure 4.1.c). Above 0.67 vol% of CNC concentration, PEO chains cannot adsorb because the optimal P:C value is not reached. As a result, the viscosity increases at higher CNC concentrations. Figure 4.2.d illustrates the change in the free volume (v_f) and the number of particles in CNC-PEO solutions for the case of non-adsorption. According to a STEM image of CNC-PEO solution (Figure 4.3.a), no specific alignment of CNC particles in PEO matrix in dilute state is encountered.

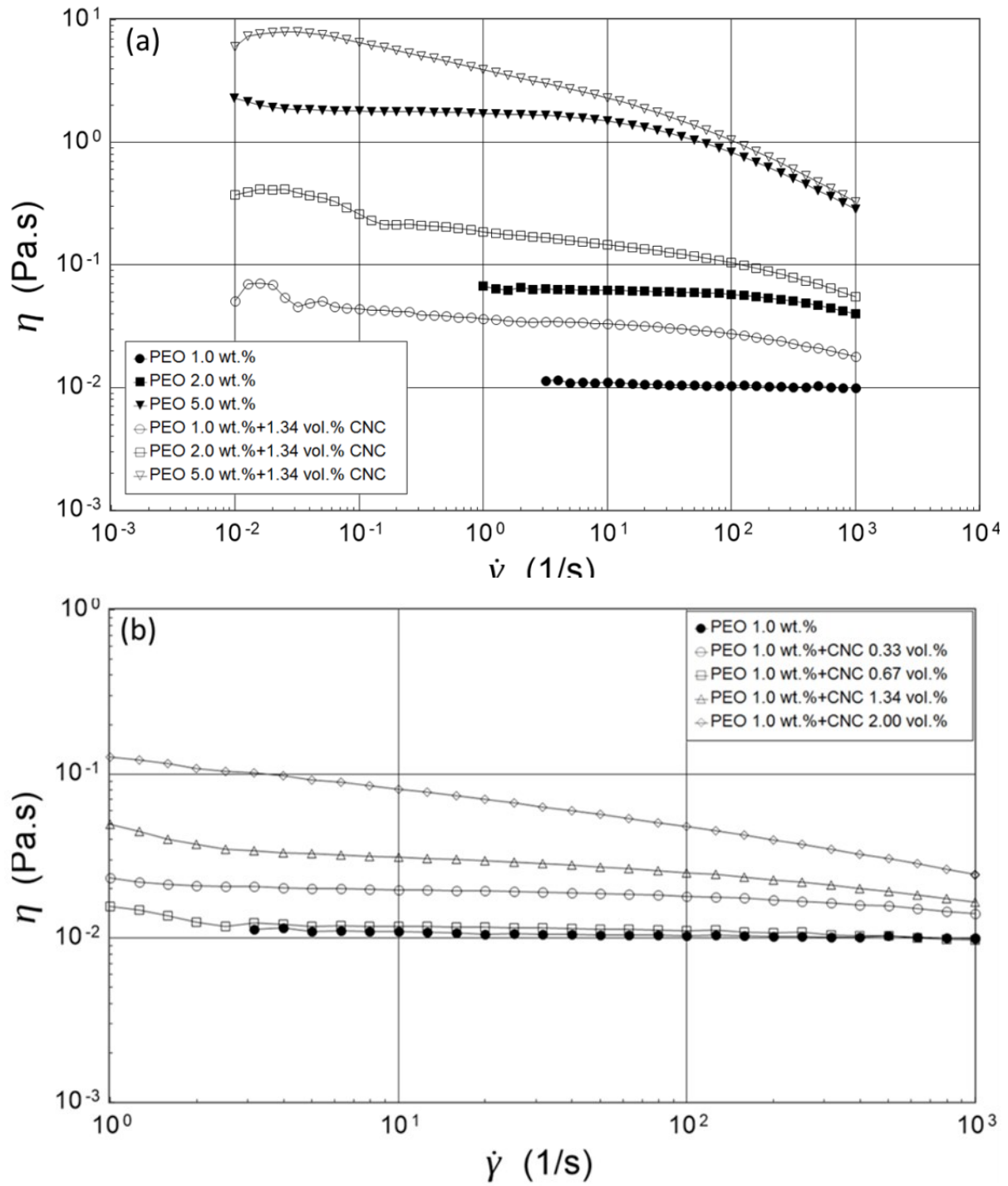


Figure 4.1 Shear viscosity change with shear rate for (a) PEO solutions without and with 1.34 vol% CNC suspensions and (b) CNC suspensions without and with 1.0 wt% PEO solutions.

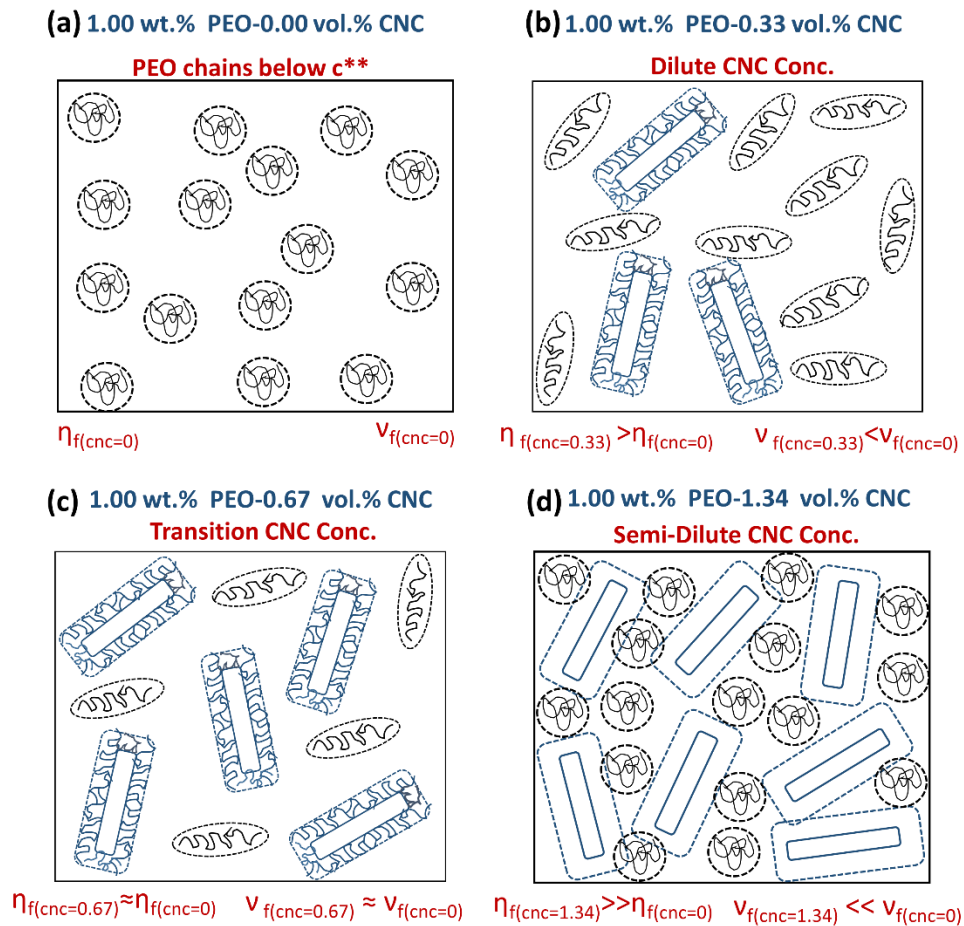


Figure 4.2 Schematic representation of 1.0 wt% PEO solutions with (a) 0.00 vol% , (b) 0.33 vol% (c) 0.67 vol% and (d) 1.34 vol% CNC suspensions and (e) STEM image of CNC-PEO solution.

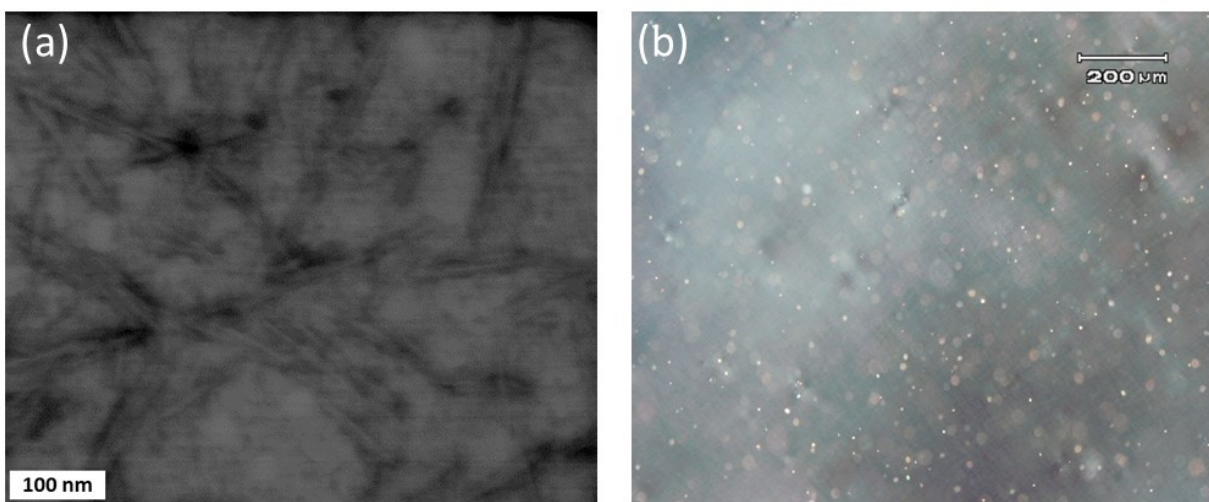


Figure 4.3 (a) STEM image of dilute CNC particles in PEO (600 kDa) solutions and (b) POM image of 2.0 vol% CNC suspensions in 5.0wt% PEO solution.

Figure 4.4 summarizes the molecular weight (M_w) and the concentration influence on the shear viscosity of PEO solutions. Subtracting the CNC suspension viscosity from the bulk solution viscosity eliminates the effect of CNC suspensions. If there are no significant physical interactions between CNC particles and PEO chains, such as depletion flocculation, corresponding curves show typical shear viscosity versus $c.M_w$ diagrams¹¹³ of PEO solutions with CNC suspensions. The PEO solution without CNC suspensions matches with typical η versus $c.M_w$ diagrams. Additions of CNC up to 2.00 vol% in PEO solutions shows similar trend. However, weak depletion interactions lead to unusual behavior for 2.00 vol% CNC suspensions in PEO solutions. Besides, Figure 4.3.b shows birefringence structures of 2.00 vol.% CNC suspensions in 5.0 wt% PEO solutions. Birefringence structures are a sign of the nematic order of CNC suspensions. The isotropic-nematic phase transition concentration is changing between 2.70 vol% and 3.39 vol% for CNCs with aspect ratios between 20 and 50^{62,67,114}. Therefore, weak depletion interactions cause nematic flocs, only when CNC concentration (2.00 vol%) is close to the phase transition concentration (2.70-3.39 vol%).

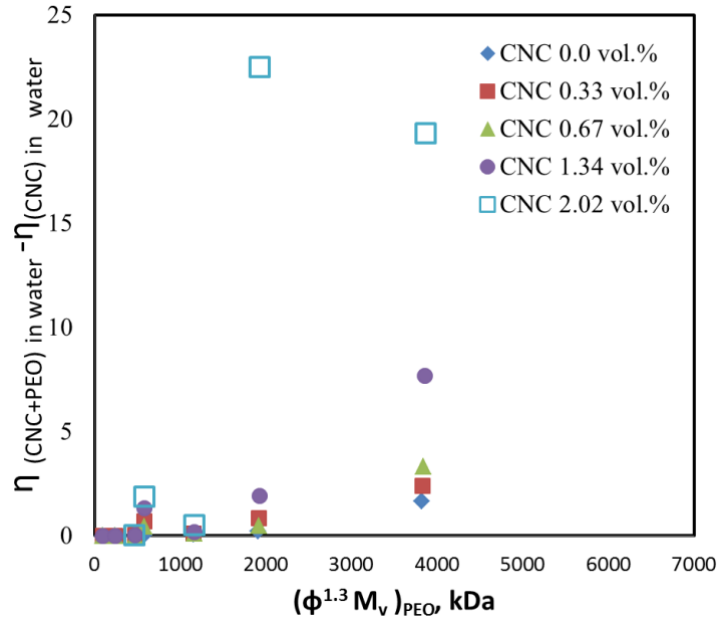


Figure 4.4. Viscosity versus the $\phi^{1.3}M$ product for PEO solutions ($M_w=300$ and 600 kDa) in CNC suspensions at 25°C .

4.3.2 Linear Viscoelastic Behavior

Figure 4.5 indicates a change in dynamic moduli values as a function of oscillatory frequency of PEO solutions in CNC suspensions. Figure 4.5.a and Figure 4.5.b represent the storage modulus (G') and the loss modulus (G'') of PEO solutions below c^{**} at various CNC

concentrations, respectively. Adding 0.33 vol% CNC in 1.00 wt% PEO solution, the response is elastic and $G' > G''$, which agrees with shear viscosity data due to weak adsorption mechanism and structure formation. As the CNC concentration increases, values in dynamic moduli increase due to the presence of more particles and decrease in free volume. Figure 4.5.c and Figure 4.5.d show the case of 5.00 wt% PEO solution, which is above c^{**} . Entangled PEO solution has higher dynamic moduli values than 1.00 wt% PEO solution. Addition of CNC particles in the entanglement network also increases proportionally dynamic moduli values. However, $G'' > G'$ indicates the viscous behavior.

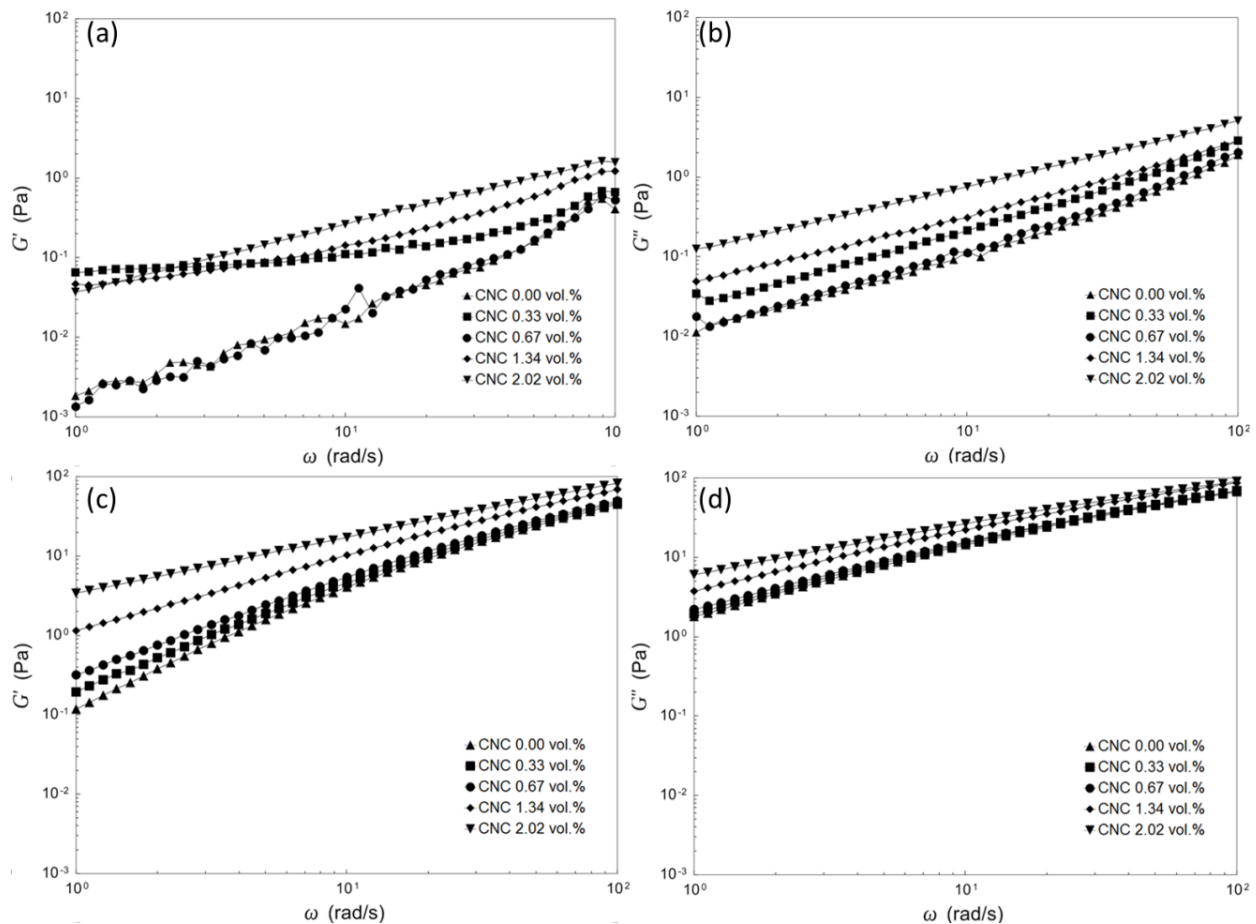


Figure 4.5 Dynamic storage and loss moduli versus oscillatory frequency of (a-b) 1.0 wt% PEO solutions and (c-d) 5.0 wt% PEO solutions in CNC suspensions.

Figure 4.6 shows the G' and G'' values of CNC suspensions in PEO solution at lower frequency, 1 rad/s. An increase in moduli values of PEO solutions without CNC suspensions is observed when PEO concentrations are above the critical concentration due to the entanglement

network. Adding 0.33 vol% CNC in 1 wt% PEO solution results in a solid-like response (Figure 4.6.a) as $G' > G''$ indicates the structure formation. However, liquid-like behavior ($G' < G''$) is observed by increasing the CNC concentration in the 1.0 wt% PEO solution. The adsorption of PEO chain onto the CNC surface weakens the structure formation as the amount of adsorbed PEO chains increases proportionally to CNC concentrations in a constant PEO amount. Figure 4.6.a indicates dynamic moduli values for the transition state from semi-dilute to entangled semi-dilute. Above c^{**} (Figure 4.6.c), the entanglement network of PEO dominates the dynamic rheological behavior.

The power laws, $G' \sim \omega^a$ and $G'' \sim \omega^b$, describe the shear moduli G' and G'' as a function of the angular frequency. The slopes of G' and G'' represent a and b values, respectively. At very low frequencies, the viscoelastic liquid behavior is defined as $G' \sim \omega^2$ and $G'' \sim \omega$. Gelation starts when $a = b = 0.5$ and the solid behavior is reached when a and b values are 0 and 1, respectively¹¹⁵. Table 4.1 indicates the power laws dependency of the PEO-CNC solutions. In PEO solutions without CNC suspensions, a and b values are approximately close to viscoelastic liquid values. Adding CNC into PEO solutions results in decreasing a and b values because of the adsorption of PEO chains and intermolecular interactions PEO chains. The viscoelastic liquid behavior is seen after adding 0.33 vol% CNC in 1.0 wt% and 2.0 wt% PEO solutions. This increases a and b values, which are signs of the PEO adsorption onto the CNC surface. In the case of 2.00 vol% CNC suspensions in 5.0 wt% PEO solutions, a and b values are 0.65 and 0.69, respectively. These values are almost reaching the gelation point due to weak depletion and the entanglement network.

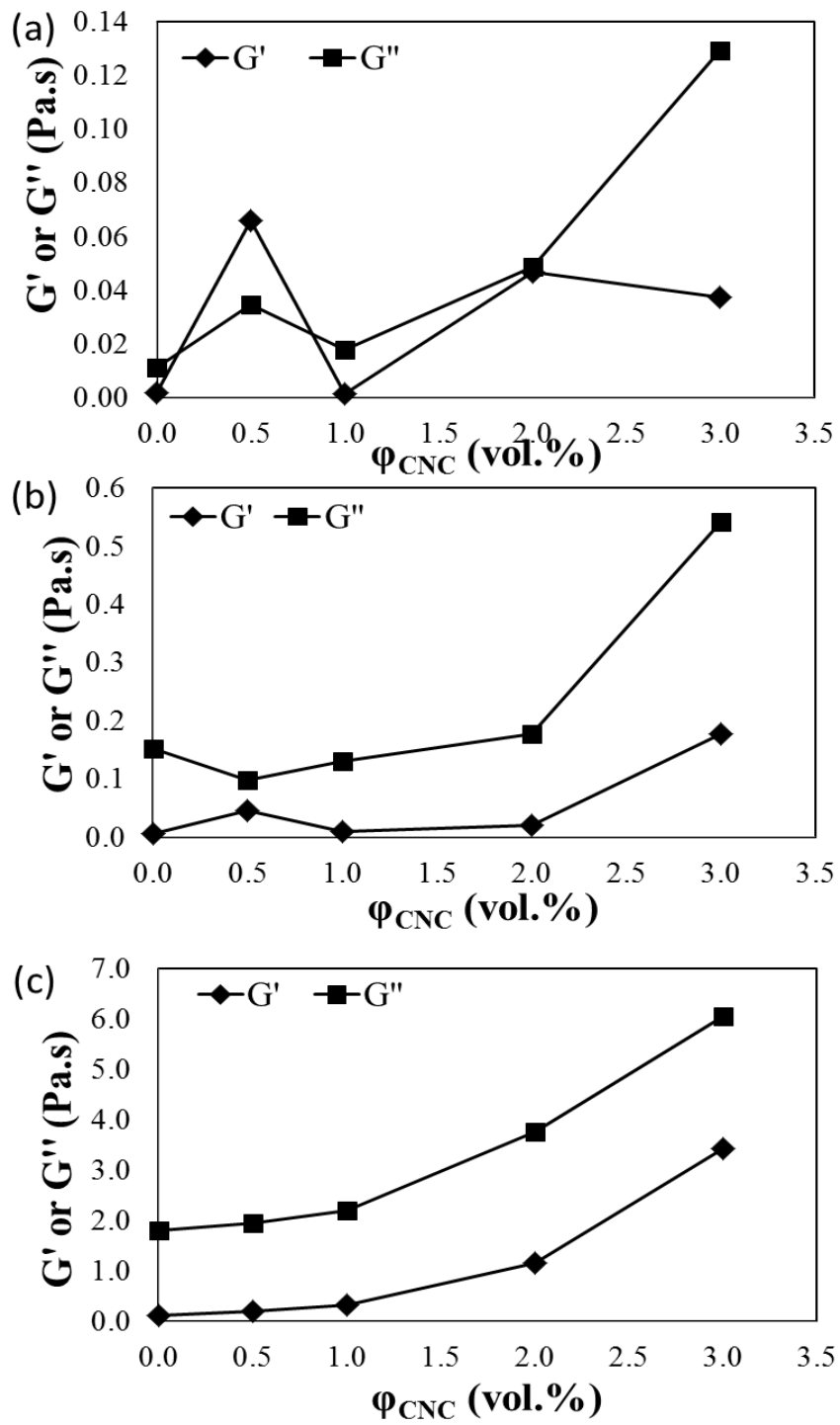


Figure 4.6 Storage (G') and loss (G'') modulus values of (a) 1.0 wt% PEO, (b) 2.0 wt% PEO and (c) 5.0 wt% PEO with respect to CNC concentration at 1 rad/s.

Table 4.1 Terminal slopes of G' and G'' for PEO solutions with CNC suspensions at 25°C.

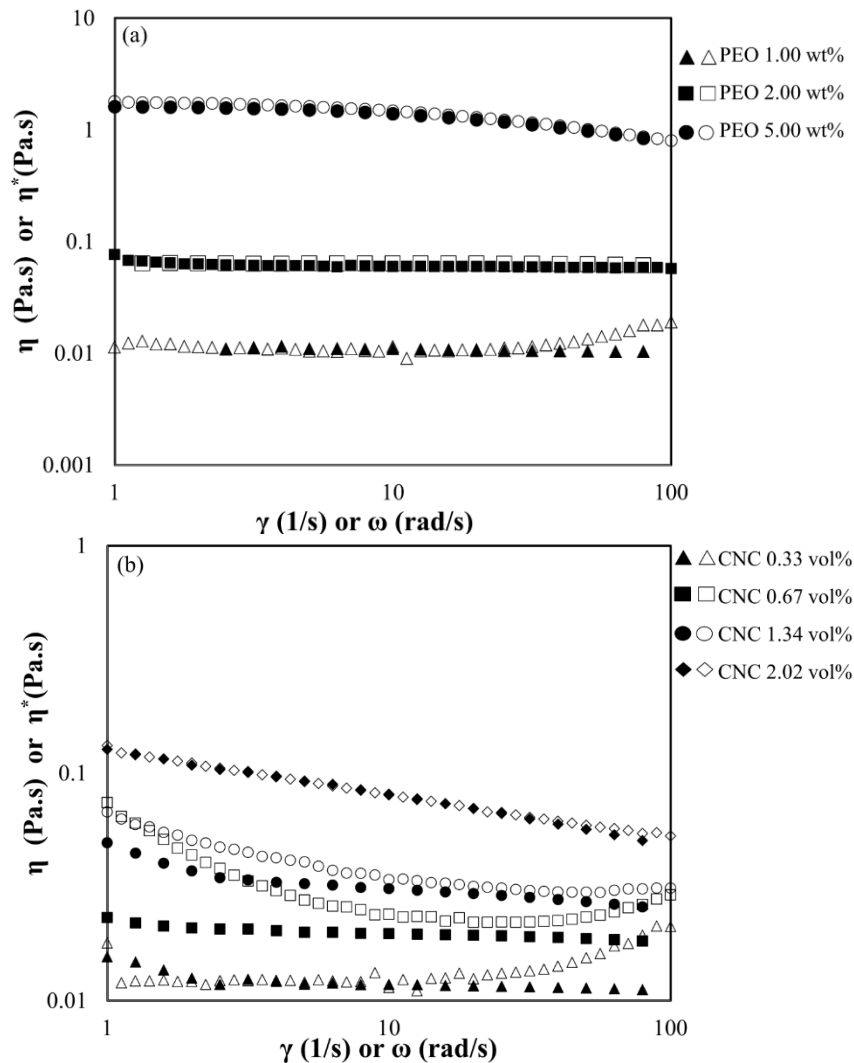
Sample	Polymer Conc. (wt.%)	CNC Conc. (vol.%)	Slope of G'	Slope of G''
PEO1	1.0	0.00	1.61	1.10
PEO1CNC0.5	1.0	0.33	0.23	0.82
PEO1CNC1	1.0	0.67	1.68	1.04
PEO1CNC2	1.0	1.64	0.25	0.80
PEO1CNC3	1.0	2.02	0.84	0.72
PEO2	2.0	0.00	1.75	0.98
PEO2CNC0.5	2.0	0.33	0.25	0.90
PEO2CNC1	2.0	0.67	1.37	0.93
PEO2CNC2	2.0	1.64	1.23	0.90
PEO2CNC3	2.0	2.02	0.92	0.76
PEO5	5.0	0.00	1.69	0.94
PEO5CNC0.5	5.0	0.33	1.40	0.94
PEO5CNC1	5.0	0.67	1.23	0.90
PEO5CNC2	5.0	1.64	0.94	0.81
PEO5CNC3	5.0	2.02	0.69	0.65

4.3.3 Comparison of Steady and Dynamic Viscosities

Figure 4.7 shows applicability of Cox-Merz rule on PEO solutions with and without CNC suspensions. In Figure 6.a, η^* curves are matching with η curves in aqueous PEO solutions. Figure 4.7.b and 7.c show η^* and η curves of CNC suspensions with semi-dilute untangled PEO (1.0 wt% and 2.0 wt%) solution. Cox-Merz rule is inapplicable with 0.33 vol.% and 0.67 vol.% CNC suspensions in 1.0 wt% PEO solution (Figure 4.7.b). A similar behavior is observed for 0.67 vol.%, 1.34 vol% and 2.00 vol% CNC suspensions in 2.0 wt.% PEO solution, Figure 4.7.c. Below critical concentration ($c^{**}=2.65$ wt%), the $P:C$ ratio affects the applicability of the Cox-Merz rule. $P:C$ ratios are 2.00 and 1.00 on weight basis for 0.33 vol.% CNC and 0.67 vol% CNC suspensions in 1.0 wt% PEO, respectively. $P:C$ ratios are 2.00, 1.00 and 0.75 on weight basis for 0.67 vol% CNC, 1.34 vol% CNC and 0.67 vol% CNC suspensions in 2.0 wt% PEO, respectively. van de Ven studied the conformation change and adsorption of PEO chain with cyclic cofactors with the presence of salt solutions. van de Ven showed the optimal PEO-cofactor ratio. At lower $P:C$ ratios, PEO cannot adsorb onto cellulose surface. At higher $P:C$ ratios, negatively charged cofactors increase electrostatic repulsion preventing the adsorption. Besides, NMR studies indicate the adsorption of PEO onto CNC surfaces due to a PEO chain

extension. Therefore, conformations change and adsorption of PEO chains result in the inapplicability of the Cox-Merz rule. According to the applicability of the Cox-Merz rule, the optimal $P:C$ ratio is determined between 0.75 and 2.00.

In 5.0 wt% PEO solutions set, the entanglement of PEO chains dominates the rheological behavior compared to CNC-PEO interactions (Figure 4.7.d). Daga and Wanger (2006) discussed that a modest effect of the adsorption onto laponite particles in rheological measurements can be encountered the removal of PEO chains from the entanglement network ³¹. η^* and η curves of 0.33 vol% CNC suspensions in 5.0 wt% PEO solution do not match due to the adsorption of PEO, 5.0 wt% PEO solution is above c^{**} referring the entanglement of PEO chains.



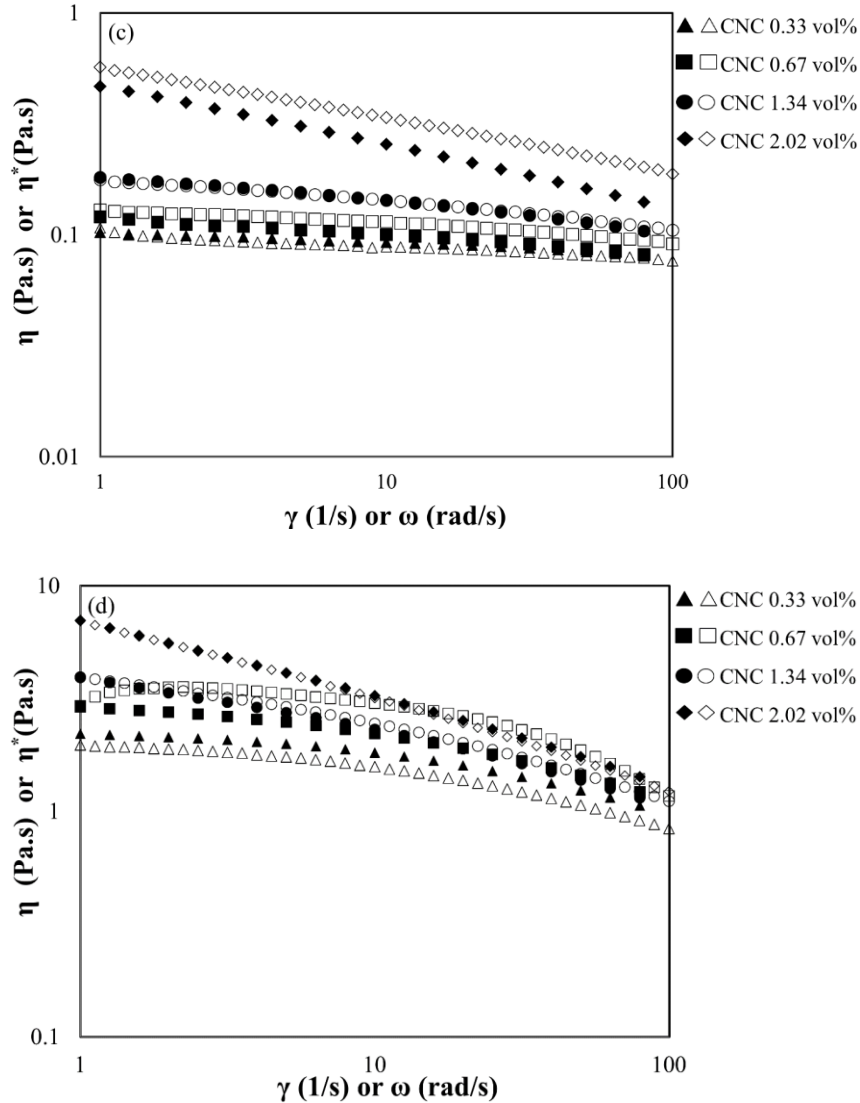


Figure 4.7 The steady-shear (filled) and complex (hallow) viscosity for (a) aqueous PEO (600 kDa) solutions with different concentration, CNC suspension with aqueous (b) 1.0 wt.% PEO (c) 2.0 wt.% PEO and (d) 5.0 wt.% PEO solutions at 25°C.

4.4 Conclusion

The rheology and mesostructured of CNC suspensions with PEO chains were investigated by considering shear viscosities, viscoelastic behaviors and the applicability of the Cox-Merz rule. Adding PEO polymer in CNC suspensions doesn't show any significant thinning behavior in shear viscosities at higher shear rates. For 0.33 vol% CNC nanoparticles in 1.0 wt% PEO solutions thickens 3 times of the viscosity value. However, adding 0.67 vol% of CNCs leads to a decrease in shear viscosity values for the case close to 1.0 wt% PEO solution. This unexpected behavior indicates adsorption of PEO chains onto CNC surfaces. A similar trend is also observed

in storage modulus and loss modulus values. The elastic behavior, ($G' > G''$) is only observed in 0.33 vol.% CNC-1.0 wt.% PEO solution indicating adsorption. The reason for the adsorption mechanism is explained as the presence of a cofactor effect and of salt. CNC nanoparticles act as cofactor leading to an extension of PEO chains. Adsorption of extended PEO chains occurs in the optimum P:C ratio. The optimum P:C ratio is determined between 0.75 and 2.00 considering the Cox-Merz rule. The adsorption is encountered only in 0.33 vol% CNC-1.0 wt% PEO solution due to a sufficient polymer to particle concentration. Even though, STEM image of dilute PEO-CNC solution shows randomly dispersed CNC nanoparticles, birefringent structures are observed by means of POM indicating an isotropic-nematic phase transition. Depletion interactions are the reason for observing a nematic phase below the CNC phase transition concentration (2.70-3.39 vol%). The phase transition occurs only at the highest CNC concentration because PEO chains cannot apply enough osmotic pressure to flocculate CNC particles at lower PEO concentrations. Weak depletion interactions are the results of the adsorption of PEO chains because the presence of PEO chains reduces the applied osmotic pressure.

Structure formation was discussed in terms of rheological properties for CNC suspensions with CMC and PEO polymers in Chapter 2, 3 and 4. In chapter 5, interactions mechanism was discussed in terms of phase behavior and colloidal dynamics.

Chapter 5. Interactions between Cellulose Nanocrystals Suspended in Aqueous Solutions of Anionic and Neutral Polymers

The material shown in Chapter 5 has been previously submitted to Cellulose journal. The experiments have been personally conducted except NMR experiments. NMR experiments were conducted with the help of Mr. Mark Miskolzie. The authors of this publication are me and my supervisor, Dr. Yaman Boluk. The following material focused on determination depletion and adsorption interactions, phase behavior and colloidal dynamics.

5.1 Abstract

Physical structures of aqueous cellulose nanocrystal (CNC) suspensions in anionic polyelectrolyte carboxymethyl cellulose (CMC) and non-ionic poly(ethylene oxide) (PEO) were investigated by studying their cross polarized, polarized optical microscope (POM) images and dynamic light scattering, zeta potential, ^1H spin-lattice relaxation nuclear magnetic resonance (NMR) data. The presence of anionic CMC and nonionic PEO in CNC suspensions led to different kind of interactions. The phase transitions from the isotropic state to nematic and chiral nematic phases were determined with POM. Semi-dilute CNC suspensions showed first gel-like behavior then phase separation by adding only semi-dilute un-entangled CMC polymer solutions, whereas the addition of PEO didn't cause any significant change. Dynamic light scattering, zeta potential and ^1H spin-lattice relaxation NMR data presented further arguments to explain polymer-CNC interactions in CMC and PEO solutions. ^1H NMR solvent relaxation technique determined the adsorption and depletion interactions between polymers and CNC. The minima in spin-spin specific relaxation rate constant showed the depletion of CNC nanoparticles in CMC and somewhat in PEO solutions. It is believed that the depletion flocculation was the case for the effects of CMC polymer chains in CNC suspensions. PEO was weakly adsorbed on CNC surfaces and caused only weak depletion interactions.

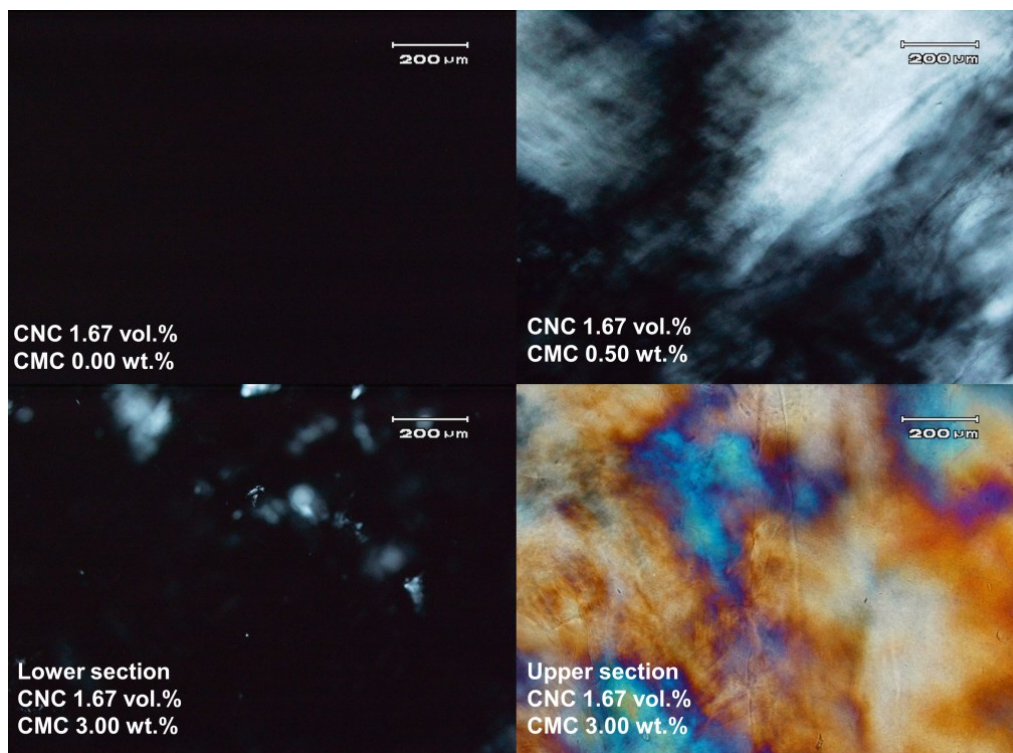


Figure 5.1 POM images of 1.67 vol% of CNC suspensions in 0.0 wt%, 0.5 wt%, 3.0 wt% of CMC polymer solutions.

5.2 Introduction

Cellulose nanocrystals (CNC) are rod-like nanoparticles with a typical length of 100-300 nm and a width of 5-15 nm^{46,62,108}. CNCs are obtained by hydrolyzing the amorphous regions of cellulose with sulfuric acid (65%) and releasing nano-sized whiskers. Acid hydrolyses result in sulfate ester groups which create negative surface charges on rod-like nanoparticles^{60,61}. Due to their short length (100-200 nm), cellulose nanocrystals do not cause any thickening in aqueous suspensions unless they are used at high concentrations (>7vol%)⁶⁹. Nevertheless, CNC can impart specific rheological properties in dilute and demi-dilute solutions of certain polymers, even when they are added in very small amounts. In a remarkable way, CNC particles can substantially increase the low shear rate viscosity without considerably increasing the viscosities at higher shear rates^{70,71,98}. Consequently, CNC can be used as a rheology modifier in aqueous systems such as coatings, drilling fluids and personal care products, where it brings flexibility to tailor the flow behavior which cannot be achieved by classical polymeric thickeners. The distinctive flow behavior of CNC suspensions in polymer suspensions is expected to be the outcome of particle-polymer interactions.

Addition of colloidal particles into polymer solutions can result in two kinds of interactions: (1) adsorption and (2) depletion. Adsorption is defined as an increase in polymer concentration near the interfacial surface of nanoparticles³⁹. The adsorption of polymer chains results in either bridging between nanoparticles and agglomeration or steric stabilization. The conformation of the polymer chains influences the adsorption mechanism. Polymer conformation is affected by the chemical structure of polymer, polymer-solvent interaction and the polymer concentration. The adsorption of polymer on surfaces is a tool to design materials in terms of adhesion, lubrication, and stabilization³⁹. The depletion flocculation is the alternative mechanism for the flocculation, most commonly observed in biological systems⁷⁵ and polymer crystallization¹¹⁶. Asakura and Oosawa were the pioneers, who first demonstrated that entropy driven interactions between non-adsorbing polymers chains and nanoparticles create osmotic pressure leading to flocculation of colloids^{79,117}. Vrij theoretically explained the depletion potential in terms of the size of hard spherical colloids (d), the radius of gyration of polymer chains (R_g), the polymer concentration, osmotic pressure (Π) and depletion layer thickness (δ)⁸⁵. At the presence of sufficient amount of polymer molecules, phase transition and phase separation occur as a result of depletion of colloidal particles¹¹⁸. Onsager explained the phase transition from isotropic phase to nematic phase by using thermodynamical approach⁸⁶ which is applicable to anisometric nanoparticles such as boehmite, fd virus, carbon nanotubes and cellulose nanocrystals. Lekkerkerker and Tuinier⁵ demonstrated that depletion interactions induce a phase transitional of anisometric nanoparticles in the presence of polymer chains⁵. Phase separations are encountered when the colloidal particles are bigger than the characteristic length of polymer chains ($d \gg R_g$).

Not only the size and the conformation but also the surface charge of polymer chains affects adsorption and depletion interactions. Attractions between oppositely charged polymer chains and nanoparticles favor the adsorption. For instance, cationic polymers adsorbed onto CNC surface due to anionic nature of CNC nanoparticles^{119,120}. Of course, the charge density and polymer chain lengths control the conformations of adsorbed chains on particle surfaces. The presence of neutral or similarly charged polymer chains in nanoparticle suspensions may lead to both adsorption and depletion. In this case, differentiating adsorption and depletion interactions is sometimes challenging. Information about the structures formed by colloidal particles in polymer solutions has been provided by an extensive series of rheological measurements

involving silica, and other particles in aqueous solutions^{90,121-123}. There are also direct methods such as atomic force microscopy (AFM), nuclear magnetic resonance (NMR), total internal reflection microscopy (TIRM) etc. to determine the nature of the interactions.^{5,39} ¹H NMR solvent relaxation techniques allows to determine directly the adsorption or depletion of polymer chains by distinguishing interactions of solvent molecules with adsorbed layer segments and the depletion layer^{53,124,125}. Solvent mobility is determined in terms of relaxation time when stronger dipolar couplings in then bound phase induce shorter relaxation time than free molecules in the bulk. In addition, polarized optical measurements are also used as direct methods and the phase transitions between isotropic and nematic states are determined for rod-shaped fd virus⁷⁵, boehmite^{15,92,126} carbon nanotubes¹²⁷ and cellulose nanocrystals^{68,128} solutions.

Very unique rheological properties of CNC suspensions were obtained in the presence of nonionic and anionic polymers^{71,97,98}. Nevertheless, the nature of CNC nanoparticle interactions with nonionic and anionic polymers and mesoscopic structure of CNC nanoparticles polymer solutions are not well understood. Understanding the interactions will allow extending the application areas of CNC nanoparticles by controlling its physical properties. Therefore, the purpose of this study is to investigate interactions between CNC nanoparticles with anionic carboxymethyl cellulose and nonionic PEO in aqueous solutions with the focus on mesoscopic structures, phase diagrams and NMR studies.

5.3 Experimental

5.3.1 Materials

Cellulose nanocrystal (CNC) samples, prepared by sulfuric acid hydrolysis of kraft pulp and neutralized by NaOH in a pilot plant were used in this study⁶¹. CNC sample was in the dried sodium salt-form and completely dispersible in water¹²⁹. Aqueous CNC suspensions were prepared by mechanical stirring in deionized water and then sonicated with Branson ultrasonic cleaner model 1510 (frequency 40 kHz) for 5 minutes. CNC suspensions were filtered through 0.45 μ pore-sized membrane to remove aggregated particles if any left after the dispersion process. The particle density of CNC used as 1.5 g/cm³ to convert the weight fraction (wt.%) to volume fraction (vol.%) from the weight fraction.

CNC suspensions in polymer solutions were prepared by using two types of polymers: anionic sodium salt of carboxymethyl cellulose (CMC) and nonionic polyethylene oxide (PEO). CMC and PEO were purchased from Sigma–Aldrich (St. Louis, MO, USA). The properties of CMC and PEO are summarized in Table 5.1. Chatterjee and Das reported the radius of gyration (R_g) of CMC at 35°C with viscosity measurements³⁶. The radius of gyration (R_g) of PEO was calculated with using a Mark-Houwink-Sakadura relation developed by Devanand and Selser³⁴. The transitional concentration (c^{**}) from semi-dilute unentangled regime to semi-dilute entangled regime was determined with the combination of an M- R_G relation, Mark-Houwink-Sakadura viscosity equation and the solution viscosities³¹. By plotting specific viscosity as a function of the concentration, Benchabane and Bekkour (2008) found the c^{**} value of 700 kDa was 1.0 wt.%, which indicated the accuracy of the theoretical calculation³⁷.

Table 5.1 Properties of polymers.

Polymer	Mw (kDa)	D.S.	$R_g^{35^\circ C}$ (nm)	c^{**} (wt%)
Carboxymethyl cellulose	700	0.85-0.90	153	1.10
Carboxymethyl cellulose	250	0.70	99	2.46
Carboxymethyl cellulose	90	0.70	40	5.47
Polyethylene oxide	600	-	50	1.83
Polyethylene oxide	300	-	34	2.40
Polyethylene oxide	100	-	18	3.81

5.3.2 Polarized Filter Plates

Visibly, the state of a CNC suspension was investigated by shining a flash light through the sample placed between two cross-polarized filters.

5.3.3 Polarized Optical Microscopy (POM)

The phase change of CNC suspensions and CNC suspensions in aqueous polymer solutions was observed by using polarized optical microscopy (POM) that enhanced contrasts to advance the image quality of birefringent materials. POM analysis was performed with an Olympus BX50 equipped with 20x microscope objective lenses and a JVC 3-ccd video camera (Olympus, Japan).

5.3.4 Scanning Transmission Electron Microscopy (STEM)

The samples were investigated with high-resolution STEM using a Hitachi model S-4800. The accelerating voltage of 30kV was applied in transmission mode. A CNC suspension as it was or in a polymer was dropped onto a carbon-coated TEM grid. After three minutes, the excess suspension was absorbed with filter paper. The TEM grid was permitted to dry at room temperature for 3 min. A drop of uranyl acetate solution (2.0 wt.% in water) was deposited on the grid for 5 min to obtain a high resolution image. The excess solution was wicked off using filter paper, and the grid was dried at room temperature prior to imaging. Since the width of CNC particles was monodisperse, STEM micrographs were used as a reliable method to measure the width of CNC particles ⁴⁷. On the other hand, the length of CNC particles was not monodisperse and a statistically meaningful measurement of the length were cumbersome. Therefore, STEM micrographs were not attempted to measure the length of CNC particles.

5.3.5 Dynamic Light Scattering (DLS)

The transitional diffusion coefficient (D_t), zeta potential values (ζ) and electrophoretic mobility (U_E) of CNCs were determined with a Malvern Zetasizer Nano-S instrument with a detection angle of 173° . This instrument was equipped with a 4.0 mW He-Ne laser ($\lambda = 633 \text{ nm}$) and an Avalanche photodiode detector. All measurements were taken at a temperature of $25.0 \pm 0.1^\circ\text{C}$. For repeatability, 3 measurements of each sample were taken.

5.3.6 Nuclear Magnetic Resonance (NMR)

The ^1H spin-lattice relaxation time T_1 and spin-spin relaxation time T_2 were determined by measurements which were carried out using a Varian Inova 400MHz spectrometer set at 26.9°C . The standard inversion recovery pulse sequence and Carr-Purcell-Meiboom-Gill (CPMG) sequence were used to measure T_1 and T_2 , respectively. The spin-lattice relaxation occurs due to the longitudinal direction component of the static magnetic field of the magnetization reaching thermodynamic equilibrium with its surroundings (the "lattice"). T_1 characterizes the rate at which the longitudinal M_z component of the magnetization vector reestablish exponentially towards its equilibrium value of magnetization, $M_z(0)$ according to Equation 5.1:

$$M_z(t) = M_z(0)[1 - \exp(-t/T_1)] \quad \text{Equation 5.1}$$

The spin-spin relaxation is caused by the energy exchange around the nuclei without a loss of energy to the surrounding lattice. The T_2 value was obtained by fitting the decay of transverse magnetization, M_{xy} to $M_{xy}(0)$ following the relation:

$$M_{xy}(t) = M_{xy}(0)\exp(-t/T_2) \quad \text{Equation 5.2}$$

The spin-lattice (T_1) and spin-spin, (T_2) relaxation times were extracted by applying nonlinear least-squares analysis of equations 1 and 2, respectively as long as data fit. If the fit to single exponential was not satisfactory, data was expressed in terms of a double exponential form and relaxation times were extracted as $T_{a,1}$ and $T_{a,2}$, where $a=1$ or 2 representing spin-lattice and spin-spin relaxation respectively.

5.4 Results and Discussion

5.4.1 Structure Formation

The average width of CNC particles was measured as 8.0 ± 0.8 nm from STEM micrographs (Figure 5.2). A CNC particle was assumed cylindrical shape and the measured width was taken as the diameter (d) of CNC rods. Instead of reporting hydrodynamic radius of CNC particles as particle length (70 nm), DLS measurements were used along with STEM measurements to calculate the length of particle (L), following the method described by Boluk and Danumah⁴⁷. Hence, the average length of CNC particles (L) was calculated as 214 ± 0.3 nm, by using the transitional diffusion coefficient (D_t) from DLS and particle diameter (d) from STEM photographs. The transitions from dilute to semi dilute and from semi dilute to concentrated regimes occur at volume fractions of $\phi^* \cong (d/L)^2$ and $\phi^{**} \cong d/L$ respectively based on rigid rod approximation. Those equations suggest that for the radius of 8 ± 0.8 nm and the length of 214 ± 0.8 nm, our experiments with 0.33 vol.% and 0.67 vol.% CNC concentrations were within the semi dilute concentration range where particles barely touch each other.

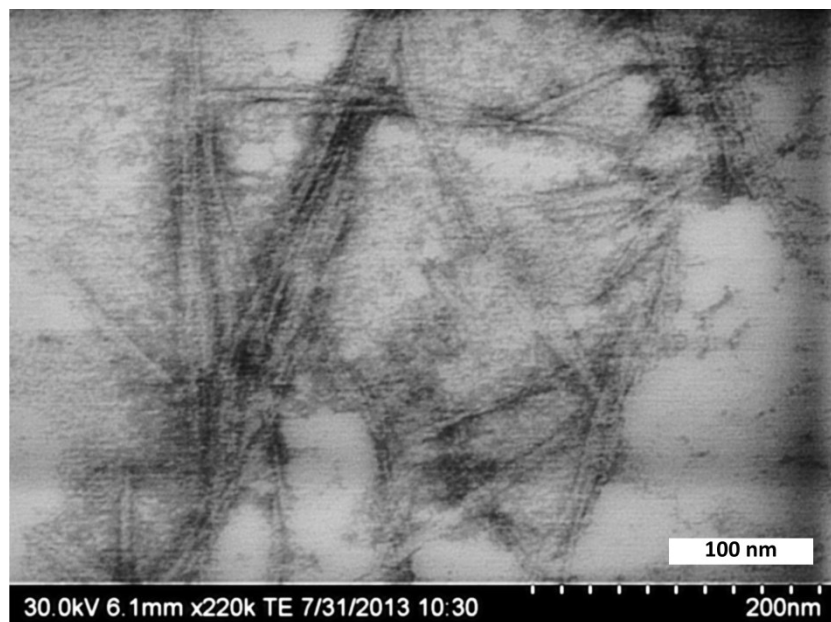


Figure 5.2 STEM picture of CNC.

The CNC suspension at 0.67 vol% without any polymer addition was almost clear and had the viscosity very close to water as also reported previously.⁹⁸ Incorporating CMC polymer molecules in 0.67 vol% of CNC suspension resulted in turbid mixtures (Figure 5.3). Besides, a gel formation was observed starting with 0.5 wt% CMC polymer addition into the 0.67 vol% CNC suspension. When the samples were turned upside down, 0.67 vol% CNC suspension in 1.0 wt%, 2.0 wt% and 3.0 wt% CMC solutions did not flow and suspended from the top which showed that the yield strength in those gels were higher than the stress generated by the gels own weight plus the weight of stirring magnet left in sample bottles. This unusual gelling behavior has already been discussed in detail ^{71,98}. Careful inspection of samples showed that 0.67 vol% CNC suspension in 2.0 wt.% and 3.0 wt.% CMC solutions formed two phases. A transparent portion located in the lower section of bottle indicates CNC deprived phase. A turbid CNC-rich phase located in the upper portion. The phase separation of rod-like nanoparticles in the presence of polymer solutions is also observed in the literature. However the locations of particle rich and deprived phases in our study were the opposite of the other reported observations ^{68,92}. For instance, Gray et al. ⁶⁸ observed that the addition of dextran resulted in a CNC-rich phase in the lower section of vials because dextran is a branched polymer and inherently not a thickener ⁶⁸. Dextran solution depletes CNC particles and lets the flocculated CNC particles to precipitate. In our case of CNC in CMC solutions, increased thickening of CMC prevented the diffusion of CNC rich phase to the bottom part of the vial.

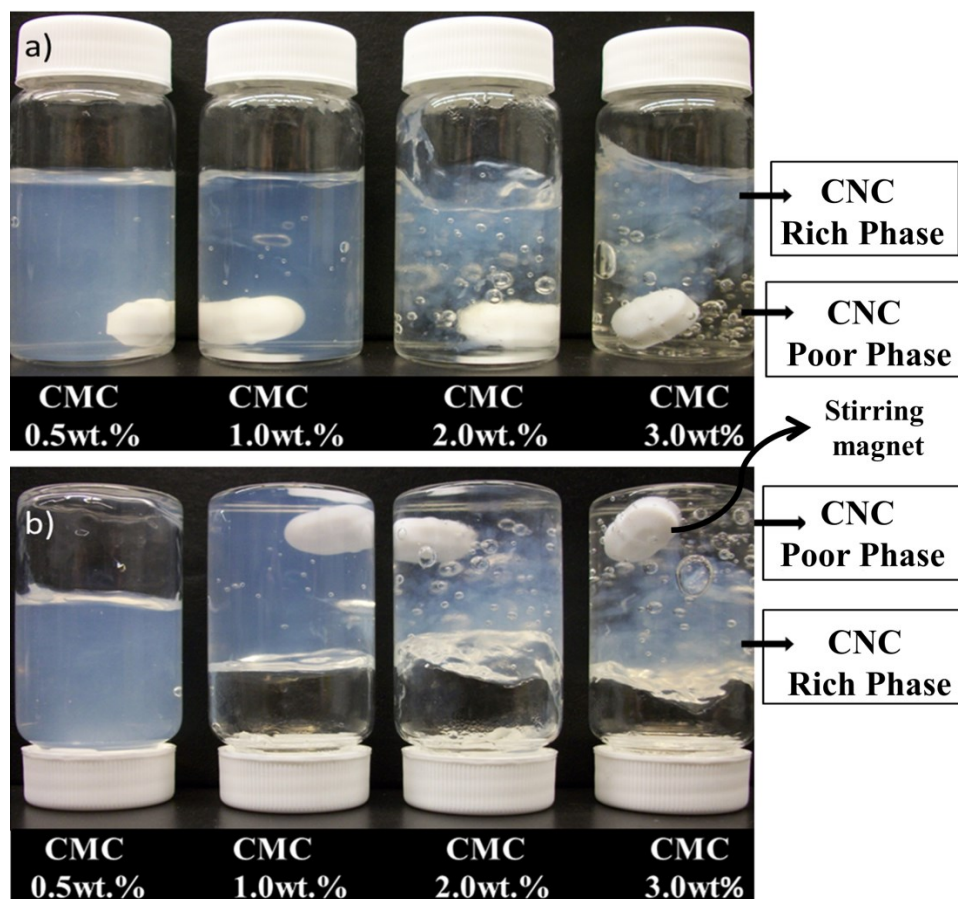


Figure 5.3 Photographs of 0.67 vol.% CNC suspensions in CMC (700 kDa) solutions. Vials are in (a) upward position; (b) 180° rotated position.

As a next step, a polarized filter system was used to observe the unusual structure of CNC suspensions in CMC polymer solutions (Figure 5.4). Shining a light beam through the suspension of isotropic portions between cross-polarized filters generated dark images. On the contrary, in the case of non-isotropic and oriented particles, the light reflected from the ordered CNC suspensions with different angles resulting in brighter areas on images. As a result, 0.33 vol% CNC suspensions in CMC solutions had dark and birefringence areas that correspond to the isotropic and anisotropic phases, respectively. CNC suspensions with the presence of 0.5 wt% and 1.0 wt% CMC have only birefringence areas showing without any physical phase separation. However, dark areas and birefringence areas were seen in CNC suspensions with 2.0 wt% and 3.0 wt% CMC, indicating separation of two phases.

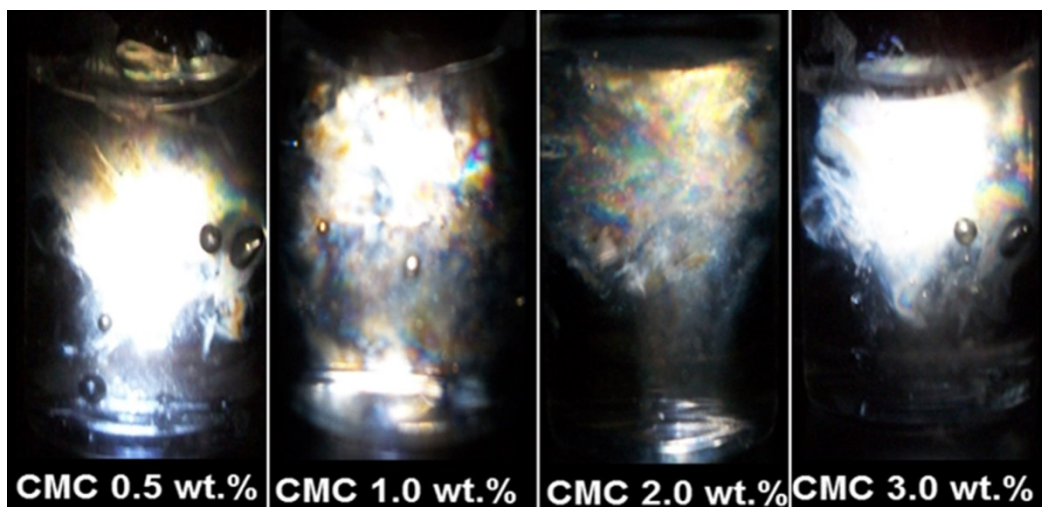


Figure 5.4 Crossed-polarized images of vials of 0.33 vol.% CNC suspensions in CMC polymer solutions showing birefringent domains.

Structure formation of CNC suspensions in CMC solutions were closely surveyed under POM (Figure 5.5). The dark image in Figure 5.5.a was a 0.67 vol% CNC isotropic suspension without any CMC presence. The brighter segments appeared with the addition of 0.5 wt% CMC because of a liquid crystal formation of flocculated CNC particles (Figure 5.5.b). Increasing the CMC polymer concentration to 1.0 wt% caused the brighter areas wider, which correlates with the increase in the amount of ordered CNC particles due to their flocculation (Figure 5.5.c.). Both images of Figure 5.5.b and Figure 5.5.c have dark and bright areas reflecting mixture of isotropic-nematic phases in solutions. Further addition of 2.0 wt% and 3.0 wt% of CMC in solution resulted in separation of phases which was also observed in gelling of 0.67 vol% CNC suspensions with CMC solutions. POM images of the upper and lower parts (Figure 5.5.d-g) indicate the nematic CNC rich and isotropic polymer rich phases, respectively.

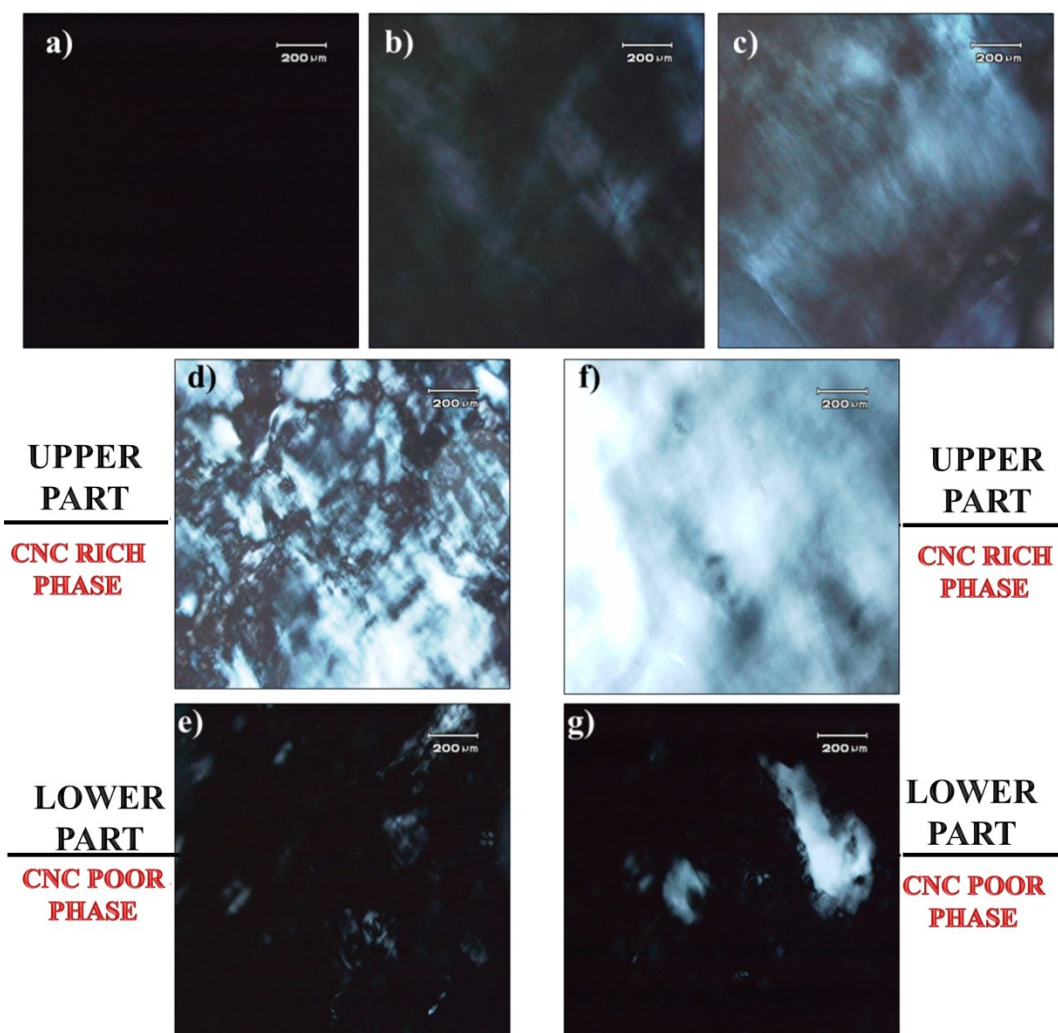


Figure 5.5 (a) POM images of 0.33 vol% of CNC suspensions in (a) 0.0 wt%, (b) 0.5 wt%, (c) 1.0 wt%, (d) upper part of 2.0 wt%, (e) upper part of 3.0 wt%, (f) lower part of 2.0 wt% and (g) lower part of 3.0 wt% of CMC polymer solutions.

Phase separation and gel formation results showed above were due to the flocculation of CNC particles by the addition of nonadsorbing flexible CMC polymer chains. The depletion interactions among CNC particles were believed to be occurred due to the unbalanced distribution of CMC molecules around CNC particles when the particle to particle distance is smaller than the radius of gyration of CMC polymer chains. The strength of the attraction is controlled by the polymer concentration and size. Asakura and Oosawa were the first to formulate the qualitative analysis of depletion ^{79,117}. In their model polymer molecules are assumed to behave as spheres which are behaved rigid with repulsive interactions with colloids but free to penetrate into each other. This assumption only makes depletion interaction between spherical particles strong only if the sizes of colloidal particles are larger than the radius of

penetrable polymer spheres ($d > R_g$). Otherwise, spherical colloidal particles can penetrate into the polymer chains if their sizes are smaller than or equal to the size of polymer chains and weakened depletion. Nevertheless this argument is not exactly valid for rod-like particles even if their diameter is smaller than the size of polymer chains ($d < R_g$) as long as $L > R_g$. According to the simulation results carried out by Dogic et al.⁷⁵, the depletion interaction between cylinders is stronger than between spheres of equal diameter in the presence of much bigger polymer chains⁷⁵. If we apply their simulations to our CNC suspensions, both isotropic and nematic phases were expected to be formed up to 2.0% CNC concentration with the concentration of CMC solutions which were tested in this study. Results of the POM images are summarized by preparing a phase diagram for CNC-CMC mixtures (Figure 5.6). CNC suspensions shown on the abscissa of Figure 5.6 up to 2.0 wt% without any CMC addition were totally isotropic. The Onsager theory proved that a highly anisomeric particles with a sufficient aspect ratio show isotropic-nematic phase transitional as virial-expansion reduces free energy leading to orientation⁸⁶. Besides, the acid hydrolysis process causes a negative charge on CNC; consequently, electrostatic repulsion affects the free energy of the system and decreases the phase transitional concentration.¹³⁰ CNC suspensions without CMC polymer addition are expected to be isotropic within the range of 2.70 vol.% (4.0 wt.%) and 3.39 vol.% (5.0 wt.%) for CNCs with aspect ratios between 20 and 50^{62,67,114}. Addition of CMC led to a transitional from isotropic to isotropic-nematic structures at any CNC concentration shown in Figure 5.6. First an isotropic-nematic structures formed but stayed in a single phase (e.g. 0.33vol.% CNC+0.5wt.% CMC). However increasing polymer concentration further at any CNC concentration resulted in phase separation with a bottom isotropic phase and an upper anisotropic phase (e.g. 0.33vol.% CNC+2.0wt.% CMC). Higher CNC concentration required less CMC addition for the formation of isotropic-nematic structures (e.g. 2.0vol.% CNC+0.5wt.% CMC). In the meantime, increasing the CNC concentration while keeping CMC concentration constant resulted in an increase in the fraction of nematic phase of CNC suspensions. Furthermore, 1.0 wt% CMC in 2.0 vol% CNC and 3.0 wt% CMC in 1.34 vol% CNC samples had a chiral nematic phase. Calculation of Lekkerkerker and Stroobants indicated that long rod particles with relatively small polymer molecules have a phase diagram with one isotropic and two nematic phases.⁸⁷ That explains the existence of isotropic-nematic and chiral nematic phases in the phase diagram of the CNC-CMC polymer system.

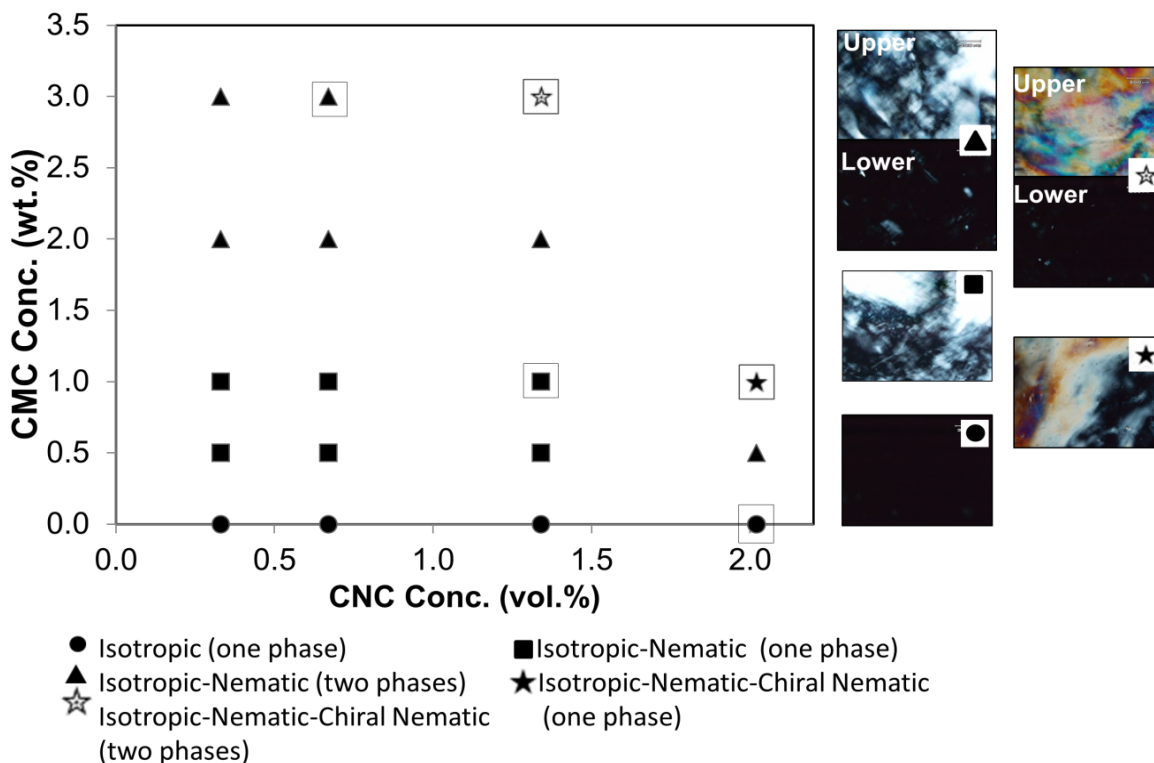


Figure 5.6 Phase diagram for CNC suspensions in CMC solutions.

As discussed, incorporation of nonadsorbing CMC polymer molecules caused the depletion of CNC particles, flocculation, and phase behavior. In theoretical studies, the aspect ratio (L/d) of the rod-like particles and the ratio of the radius of gyration of polymer to rod diameter (R_g/d) are defined as effective parameters for the depletion and phase behavior of colloidal suspensions with polymers.⁸⁷ According to their mathematical calculations, an isotropic and two nematic phase diagrams are obtained for rods with high $L/d \simeq 20$ and $R_g/d \simeq 0.5$. In our case, similar phase behavior in CMC-CNC mixtures was observed with $L/d \simeq 27$ but with $R_g/d \simeq 19$ which was 33 times bigger than theoretical value. However, by replacing the ratio of R_g/d with R_g/L , the phase behavior of rod-like particles in polymer chains could be used to explain our experimental results. The recalculated value of $R_g/L \simeq 0.70$ matched the theoretical calculations.

The second focus of the study was to investigate the structure formation in CNC-PEO mixtures. POM images, digital photographs and crossed-polarized images of CNC-PEO mixtures are shown in Figure 5.7. Spherulites of semi-crystalline PEO were observed at a higher PEO concentration (5.0 wt%). According to Strawhecker and Manias, the presence of nanoparticles in a PEO matrix hinders the spherulites' growth, leading to smaller sizes rather than neat PEO

spherulites; on the other hand, overall PEO crystallinity doesn't change¹³¹. As shown in Figure 5.7.a and b, an increase in the CNC concentration reduced the size of the spherulites but increased the number of PEO spherulites, as reported in the literature. 2.02 vol.% of CNC suspension is close to its isotropic to The Standard Varian s2pul Pulse Sequence 13 nmr transitional (2.70-3.39 vol%) so that birefringence structures came into sight in Figure 5.7.c with the addition of 1.0 wt% PEO. In the meantime, a higher amount of CNC restricts the growth of PEO spherulites. However, spherulites appeared in 2.02 vol.% of CNC while PEO concentration increases from 1.0 wt% to 5.0 wt% (Figure 5.7.d). Birefringence structures were observed in POM images of 2.02 vol.% CNC suspensions with PEO, whereas gelling didn't occur, indicating only weak depletion interactions between CNC nanoparticles and PEO chains.

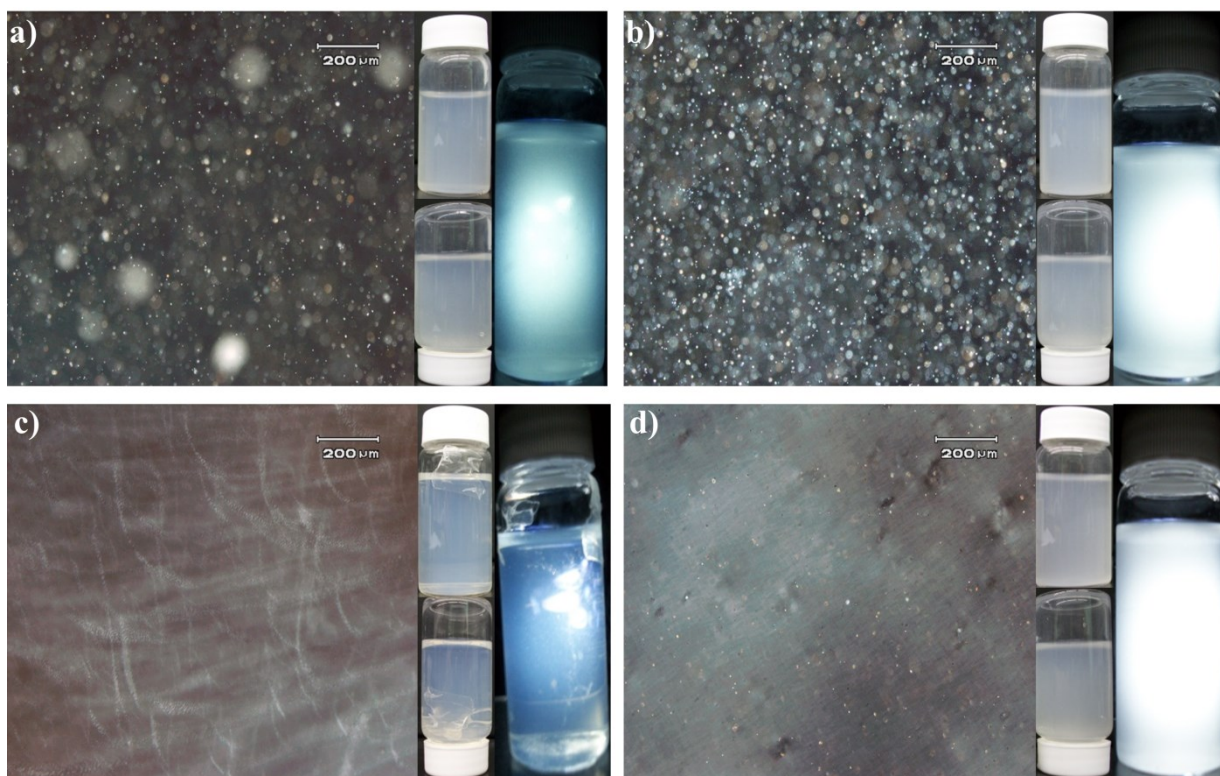


Figure 5.7 POM images, digital photographs and crossed-polarized images of (a) 0.67 vol.% CNC suspensions in 5.0wt.% PEO solution, (b) 1.34 vol.% CNC suspensions in 5.0wt.% PEO solution, (c) 2.02 vol.% CNC suspensions in 1.0wt.% PEO solution, (d) 2.02 vol.% CNC suspensions in 5.0wt.% PEO solution.

5.4.2 DLS and Zeta Potential Measurements

Table 5.2 shows the transitional diffusion coefficient (D_t), zeta potential (ζ) and electrophoretic mobility (u_E) values of CNC suspension with and without polymer presence. Hydrodynamic radius (R_h) values are also placed in the table to indicate the changes in CNC

particle size. Introducing CMC molecules into the CNC suspension decreased D_t of CNC particles and increased the hydrodynamic radius (R_h). The magnitude of increase in R_h was very high to explain in terms of adsorption of CMC polymers on CNC surfaces, despite the commonly held belief that adsorption of CMC on negatively charged CNC surface is possible. The adsorption of CMC on a cellulose surface is the argument because of the reporting by Liimataainen et al.¹³². According to this study, CMC chains adsorb on cellulose fibers but only in the presence of CaCl_2 ¹³². However, in our study, the presence of anionic sulfate groups on CNC, the absence of multivalent counter ions in solutions and narrow surface contact area of CNC particles eliminated the possibility of adsorption of CMC on CNC by compressing the repulsive interactions between anionic particles and anionic polymer chains.

On the other hand, it is more likely that CNC particles were flocculated by depletion due to non-adsorbing CMC molecules (Figure 5.8.a). As illustrated in Figure 5.8.b, electrostatic repulsion between negatively charged CMC chains and CNC particles strengthens depletion of CNC particles. Sharma and Walz (1994) calculated depletion forces between charged particles with charged polymers.¹³³ Electrostatic repulsion contributed the magnitude and the range of the depletion effect. Strong depletion interactions caused increases in both the apparent particle size of CNC due to flocculation and effective viscosity of the “suspended medium” due to the enrichment of polymer concentration in CNC free parts of the medium. The hydrodynamic interactions and their leading to an increase in friction coefficient was also reported by Tuinier et al.¹³⁴. CMC concentration was believed not-exist in depleted layers and enriched in the surrounding of CNC particles. The concentration difference leads to two different kinds of viscosity in solution: viscosity of surrounding zone and effective viscosity of the depleted zone. When CNC particles get closer to each other, a decrease in effective viscosity affects Brownian motions of flocculated CNC particles. Therefore, the particles stick to each other and act as a larger particle, resulting in a slower CNC particle motion in dilute solutions. CMC polymers with higher molecular weights caused the diffusion of CNC particles more slowly, as expected. According to the AFM results of Burns et al., molecular weight has two counter-acting influences on depletion interactions at fixed concentrations¹³⁵. A decrease in molecular weight causes a reduction in the thickness of the depletion layer but an increase in osmotic pressure. Consequently, two opposing effects end with a short-range depletion force. Hence, because of

stronger depletion forces, motions of CNC particles in a 700kDa CMC polymer solution slowed down more than a CNC particle in a 90kDa CMC polymer solution.

Table 5.2 Dimensions and surface charge analysis of CNC with different polymer solutions.

Sample	Mw (kDa)	R _h (nm)	D _t (x10 ¹²) (m ² s)	ζ (mV)	uE (μmV ⁻¹ s ⁻¹ cm)	d (nm) (STEM)
CNC	-	69.37 ±0.34	7.08±0.03	-56.60±0.40	-4.41±0.03	8.24±0.83
CNC-CMC700	700	100.32±2.41	4.89±0.16	n.a.	-6.89±0.03 ?	8.36±1.99
CNC-CMC250	250	94.33±0.20	5.20±0.01	n.a.	-5.94±0.04 ?	n.a.
CNC-CMC90	90	90.04±0.22	5.44±0.01	-62.43±1.01	-4.86±0.08	8.20±1.55
CNC-PEO600	600	72.84±0.09	6.73±0.01	-22.27±1.90	-1.73±0.03	9.37±1.13
CNC-PEO300	300	74.69±1.21	6.56±0.11	-29.57±8.56	-2.03±0.03	n.a.
CNC-PEO100	100	73.08±0.13	6.71±0.01	-27.70±6.71	-2.16±0.03	9.61±1.32

The fifth and sixth columns in Table 5.2 show zeta potentials and mobilities of zeta sizer measurements. The electrophoretic mobility values, -6.89 and -5.94 μ m V⁻¹s⁻¹cm of CNC in 700 kDa and 250 kDa CMC polymer solutions compared to electrophoretic mobility of -4.41 μ m V⁻¹s⁻¹cm of CNC were totally unrealistic even if there were adsorption of negatively charged CMC on negatively charged CNC surfaces. Hence, zeta potential values were not even listed in Table 5.2. These unrealistic results can be explained as follow. While performing zeta sizer measurements, there are two different substances in suspensions: (1) CNC particles and (2) a non-adsorbing CMC polymer. A traditional method of tracking the motion of particles under microscope during the electrophoresis is an accurate zeta potential measurement technique, because it measures the electrophoretic velocity of a particle in the stationery layer where the electro-osmotic flow is zero. In contrast, a Malvern ZetasizerTM performs a measurement at any point in the cell using a laser beam⁵⁰. To obtain the true electrophoretic velocity, a rapid reversing applied field eliminates the electro-osmosis effect in the entire cell so particles reach terminal velocity during fluid flow. In this case, with CNC particle and CMC polymer mixture, the measuring technique failed because the sizes of the two different particles have the same order of magnitude and charge. The radius of gyration of 250 kDa and 700 kDa CMC polymers

are 99 nm and 153 nm, respectively ³⁶. Thus, the readings of electrophoretic mobility in the presence of 250kDa and 700kDa CMCs were not expected to be correct. Since R_g values of CMC chains are much closer to the CNC dimension, the change in electrophoretic mobility values cannot be attributed to the CNC particle alone. On the other hand, the lower molecular weight of CMC (90 kDa) has a smaller radius of gyration (40 nm), leading to an insignificant electro-osmosis effect. Therefore, the electrophoretic mobility values of CNC suspensions in 90 kDa CMC solution were closer to the CNC suspensions.

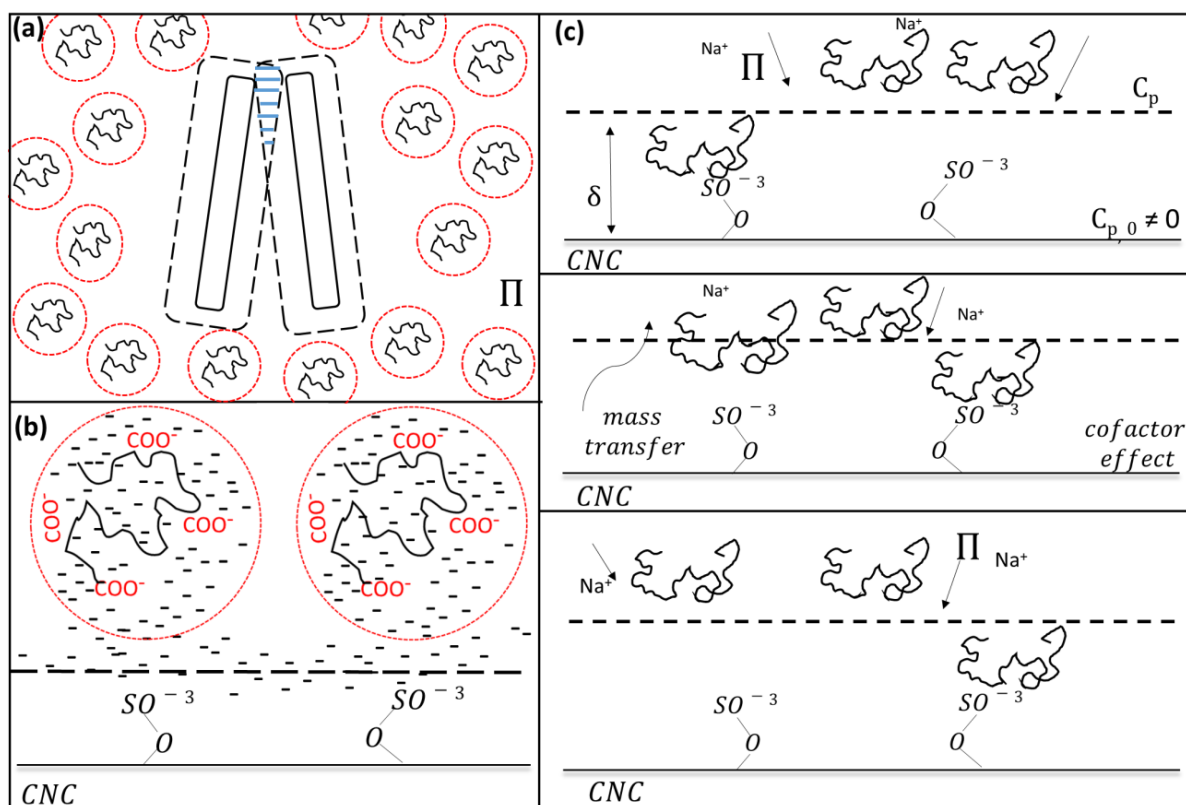


Figure 5.8. Schematic of (a) CMC polyelectrolytes leading to osmotic depletion of CNC particles strengthen with electrostatic repulsion, (b) the zoomed-in view of the depletion zone of the CNC-CMC system, and (c) the presence of salt leading to the kinetic adsorption mechanism of PEO on sulfate groups of CNC (dashline refers to boundary of depletion zone).

In the case of CNC in PEO solutions, the transitional diffusion constants decreased only slightly, which were probably due to the weak adsorption of PEO on CNC particles. Therefore effective hydrodynamic size (R_h) of CNC increased slightly due to PEO adsorption. The zeta potential values of CNC in the presence of PEO decreased from -56 mV to the range of -22/-27 mV. In this case, the size of CNC is bigger than that of the radius of gyration of PEO molecules.

As a result, the PEO matrix scatters very little compared with the total scattered intensity, so all the scattered intensity will be attributed to the CNC particles. Adding PEO with different molecular weights to solutions decreases the negative value of zeta potential to between -29.0 and -22.0 mV, indicating adsorption onto the CNC surface. The thickness of adsorbed PEO is calculated at less than 1 nm using a method explained in detailed elsewhere¹³⁶. PEO's radius of gyration is at least 50 times larger than calculated value of 1nm, which may indicate weak physical adsorption of PEO as pancake structure³⁹. This kind of adsorption behavior of PEO chains can be explained in the presence of salt ions which would work as cofactors. van de Ven (2005) showed that PEO chains extended and associated with cofactors when low amounts of salt were present in the concentration¹¹¹. In the case of our samples, the presence of salt in CNC solutions was a result of ion-exchanging H^+ with neutral monovalent cations such as Na^+ . CNC samples which were obtained in dried sodium salt-form concentration. Therefore free sodium ions and sulfate groups on CNC particles may act as a cofactor. The presence of Na^+ extends PEO chains and PEO chains adsorbs onto CNC surface (Figure 5.8.c). PEO chains are dynamically associated with sulfate groups. PEO chains are desorbed from CNC surface as PEO chains are flexible and very weakly adsorbed onto CNC surfaces.

5.4.3 1H Solvent Relaxation NMR

Mobility of water molecules was expected to be altered at interfaces in multi-component and multi-phase CNC in polymer solutions. Therefore, 1H NMR spin-lattice (T_1) and spin-spin (T_2) relaxation times of protons of water molecules in CNC suspensions were measured to investigate the dispersion state of CNC and roles of CMC and PEO polymers. For small water molecules, the proton spin-spin relaxation time (T_2) always inversely varies with the characteristics time of molecular orientation (correlation time). Unlike T_2 , spin-lattice relaxation time (T_1) decreases first then goes through minimum and increases as a function of correlation time. Therefore, as expected, measured T_2 values of all of the CNC samples were lower than their T_1 values. Water molecules in CNC suspensions, CMC and PEO polymer solutions can be considered in two states: a highly mobile free state in the bulk and the bound state with restricted motions at interfaces. Free water molecules have relatively long relaxation times in contrast to bound molecules which have restricted molecular motions and shorter relaxation times. In the case of spin-spin (T_2) relaxation, the exchanges between those two states are usually fast (fast exchange) and can be described by a single relaxation time. However, in the other case of spin-lattice

relaxation (T_1), exchanges between free and bound water molecules may not be fast and more complex multi exponential decays can arise. In our measurements, single exponential T_1 and T_2 relaxation times were observed in the case of CNC in CMC solutions. In contrast, T_1 and T_2 of CNC in PEO solutions decayed with a double exponential mode, having both fast and slow exchanges. For the rest of the discussion, the spin-spin relaxation data were used and the spin-lattice relaxation data are included into Appendix A.

The spin-spin relaxation times (T_2) of water, 1.0 wt% CNC suspension (without any polymer), 1 wt% CMC (without CNC) and 1 wt% PEO (without CNC) polymer solutions are listed in Table 5.3. For fast exchanges, the observed relaxation time (T_2) in CNC suspensions or polymer solutions can be expressed in terms of relaxation times of free water molecules in bulk (T_{2f}) and bound water molecules which are immobilized on CNC surfaces or polymer chains (T_{2b}):

$$\frac{1}{T_2} = \frac{1}{T_{2f}} (1 - p) + \frac{1}{T_{2b}} p \quad \text{Equation 5.3}$$

where, p is the probability of finding a randomly chosen water molecule in a bound state. Contact area per unit weight is higher for polymer chains than CNC particle surfaces. This suggests that the amount of contact with water molecules, hence the probability of water molecules in the bound state was higher in CMC and PEO polymer solutions than in CNC suspensions. 1.0 wt% CMC polymer solution resulted in a lower relaxation time (T_2) than 1.0 wt% CNC suspension (2.31 s vs 4.12 s). Cellulose molecules on CNC surfaces and caboxymethyl cellulose molecules of CMC polymer share the same backbone and both of them carry anionic functional groups. Hence, CNC surfaces and free CMC polymer molecules were assumed having comparable T_{2b} values and the lower T_2 value of 1.0 wt% CMC solution was attributed to its higher contact area with water (p value). The relaxation time of 1.0 wt% CMC was also lower than 1.0 wt% PEO, due to the presence of charged carboxyl groups. Besides anionic CMC chains have stiffer backbone than uncharged PEO molecules which also resulted less degree of motion of bound water molecules.

Table 5.3 Spin-spin relaxation times and relaxation rate constants of samples with respect to molecular weight, CNC concentration and salt concentration.

Polymer Type	Mw (kDa)	Polymer Conc. (wt%)	CNC Conc. (wt%)	NaCl (ppm)	T₂ (s)	R₂		
-	-	0	0	0	6.75	0		
-	-	-	1	0	4.12	0.64		
PEO	600	1	0	0	2.98	1.27		
CMC	700	1	0	0	2.31	1.92		
CMC	90	1	1	0	2.25	2.00		
CMC	250	1	1	0	1.96	2.44		
CMC	700	1	1	0	1.22	4.53		
CMC	700	1	1	200	1.32	4.11		

Polymer Type	Mw (kDa)	Polymer Conc. (wt%)	CNC Conc. (wt%)	NaCl (ppm)	T_{2,1} (s)	R_{2,1}	T_{2,2} (s)	R_{2,2}
PEO	600	0.1	1	0	3.31	1.04	0.59	10.44
PEO	600	0.1	0.5	0	3.69	0.83	0.58	10.64
PEO	600	0.1	0.05	0	3.23	1.09	0.58	10.64
PEO	600	0.1	0.01	0	3.74	0.81	0.57	10.84

Following van der Beck et al.¹³⁷, spin-spin relaxation time (T₂) is most commonly expressed in terms of relaxation rate constant $R_2 = 1/T_2$ and the specific relaxation rate constant, R_{2sp} which is defined as:

$$R_{2sp} = \frac{R_2}{R_2^0} - 1 \quad \text{Equation 5.4}$$

where R_2^0 is the relaxation rate constant of pure water solvent which is also assumed as the relaxation rate constant for free water molecules in dilute CNC suspensions. Figure 5.9 shows the specific relaxation rate constant (R_{2sp}) for 1.0 wt.% CNC suspension as a function of polymer concentration for CMC and PEO polymers. Addition of polymers in a CNC suspension can increase the specific relaxation rate, R_{2sp} of the systems due to two factors: 1) formation of additional bound water on free polymer chains in the solution; 2) an increase in the bound water on CNC particle surfaces due to polymer adsorption. Both of those factors were considered for an increase of R_{2sp} by the addition of 0.01 wt% of CMC (shown in enlarged section in Figure 5.9). Anionic CMC molecules even if they were adsorbed on negatively charged CNC surfaces,

could not be strongly attached in train and pancake conformations and contribute to the additional entrapment of water molecules. Hence adsorption of CMC molecules on CNC surfaces were ruled out for the increase in R_{2sp} . It is believed that at 0.01 wt% CMC concentration, R_{2sp} was increased only due to the bound water on free CMC polymer chains in the solution (Figure 5.10). Addition of CMC molecules higher than 0.1% resulted a steady increase in R_{2sp} , which was also totally expected again if one considers the increase in bound water on increased number of free polymer chains in the solution. However, a notable opposing trend with a minimum R_{2sp} at 0.05 wt% CMC concentration was observed. Addition of 0.05 wt.% CMC in CNC suspension decreased the R_{2sp} value of CNC suspension to the level of polymer free CNC suspension. This behavior, which was also observed by Cosgrove in other depleted structures: NaPSS added in silica and latex suspensions^{53,124,125}. Again it is believed that minimum point was observed due to the depletion of CNC particles in the presence of CMC polymer chains. Flocculation of CNC particles due to the depletion decreased the total particle-water interface area per unit weight hence the amount of bound water. Such a decrease compensated the presence of additional polymer chains in the solution. Further increases in CMC addition steadily increased the R_{2sp} of the system. However the increase was more drastic than one would expect only due to the presence of additional free polymer chains in the solution. Once CNC particles were flocculated due to the depletion by CMC, gelling and bound water in networked structure resulted much higher R_{2sp} values (schematically represented in Figure 5.10). This explanation also confirms the gel structure that we observed in photographs, cross polarized filter and POM pictures of CNC in CMC solutions.

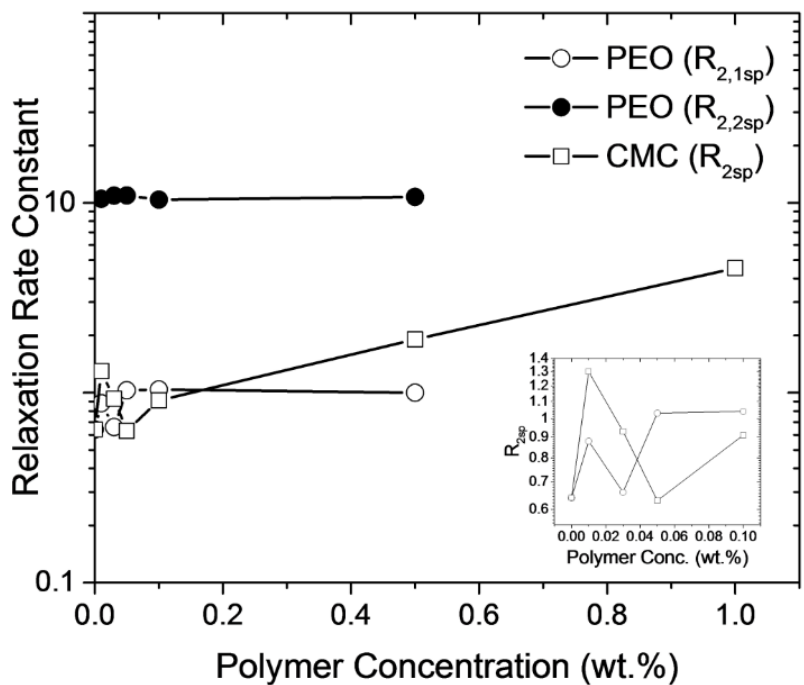


Figure 5.9 Change in relaxation rate constant (R_{2sp}) with respect to polymer concentration of 1.0 wt% of CNC suspensions in aqueous CMC and PEO solutions

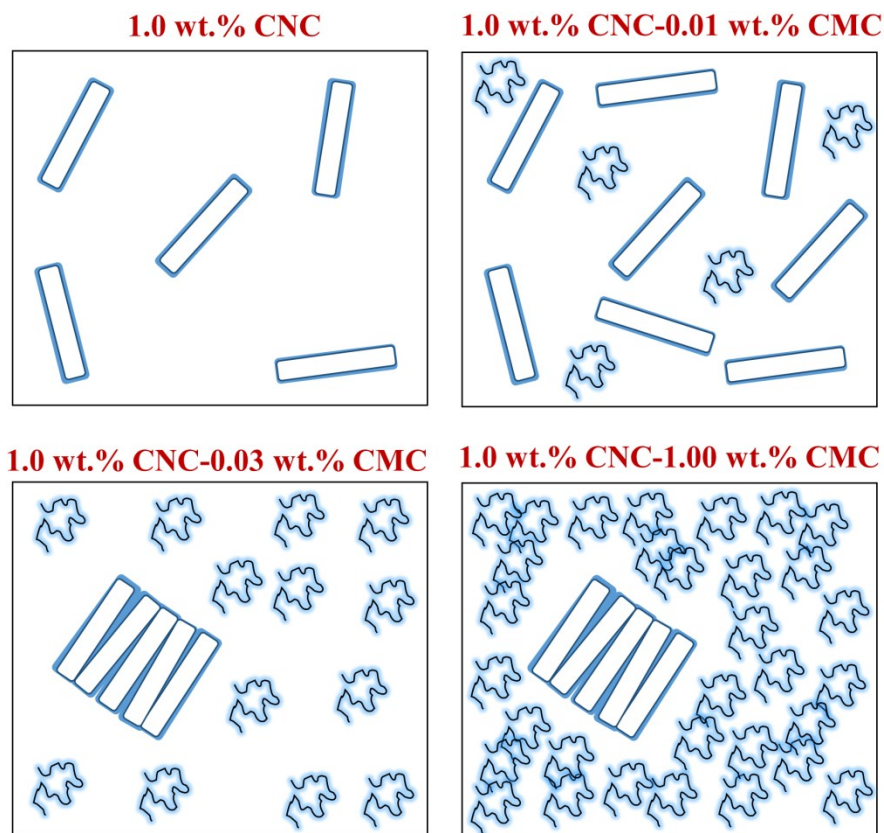


Figure 5.10 Illustration of 1.0 wt% CNC suspensions with various CMC concentration

Relaxation times of 1.0 wt% CNC suspension in 1.0 wt% CMC solution were also measured by using 700kDa, 250kDa and 90kDa molecular weight polymers. R_{2sp} values of CNC suspensions in CMC solutions steadily decreased with using lower molecular weight polymer molecules. Such polymer molecular weight effect also rejected the probability of polymer adsorption on CNC surfaces. If adsorption of CMC chains on CNC surfaces happened, the lower molecular weight CMC could be expected, adsorb better and have higher R_{2sp} . The decrease of R_{2sp} values along with decrease in molecular weight was due to the less effective gel formation. Addition of 200 ppm salt in CNC-CMC system screened the Coulombic repulsive interactions and led to flexible and compact structure of polymer chains. Therefore, R_{2sp} value decreased due to the presence of less bound water around CMC chains.

Unlike in CMC solutions, CNC suspensions in PEO solutions resulted in double exponential decay in relaxation times. The $T_{2,1}$ and $T_{2,2}$ relaxation times were due to fast and slow exchanges between bound and free water molecules, respectively. The slow exchange ($T_{2,2}$) between dipolar couplings on CNC surfaces and the solution was due to the limited degree of freedom of water molecules, which were trapped between CNC surfaces and adsorbed PEO molecules. As shown in Figure 5.9, $R_{2,2sp}$ did only change slightly with respect to the PEO concentration, as PEO adsorption had already reached the saturation in lower concentrations. The $R_{2,1sp}$ values of CNC suspensions as a function of PEO concentration also showed the similar but weaker trend than the case of CNC suspension in CMC solutions. Somewhat less decrease in $R_{2,1sp}$ value of CNC suspension was observed with the addition of 0.03 wt.% PEO which is indicating a weak depletion interaction between CNC and PEO chains. Unlike CMC in CNC suspensions, $R_{2,1sp}$ didn't increase drastically with respect to the PEO concentration as PEO chains couldn't form network structure and gels due to smaller R_g and the compact structure of PEO chains.

No trend was observed while by adding 0.1 wt% PEO into various CNC concentrations (Table 5.3). Such absence of the trend can be explained in terms of relaxation times of free water molecules in the bulk (T_{2f}) and bound water molecules, which are immobilized both on CNC particles ($(T_{2b})_{CNC}$) and polymer chains ($(T_{2b})_{PEO}$):

$$\frac{1}{T_2} = \frac{1}{T_{2f}} (1 - p_1 - p_2) + \frac{1}{(T_{2b})_{CNC}} p_1 + \frac{1}{(T_{2b})_{PEO}} p_2 \quad \text{Equation 5.5}$$

where, p_1 and p_2 are the probabilities of finding bounded water molecules on CNC and PEO, respectively. On the one hand, an increase in CNC particle concentration reduced the value of p_2 while resulted in a higher p_1 value. Adsorption of polymers on CNC would also increase $(T_{2b})_{CNC}$. It is believed that those opposing effects led non-proportional changes of $R_{2,1sp}$ with respect to CNC concentrations.

5.5 Conclusion

By investigating the physical structures of CNC in anionic polyelectrolyte CMC and non-ionic polymer PEO solutions and their cross polarized, POM images, dynamic light scattering, zeta potential measurements and ^1H spin-lattice relaxation rates, we presented credible and unflinching argument to explain the gel formation of CNC in semi-dilute concentrations in semi-dilute un-entangled CMC polymer solutions. Unlike the adsorption, the depletion flocculation was believed to be the case for the effects of CMC polymer chains in CNC suspensions. NMR results, POM images and gel formation have all supported that depletion flocculation was the reason to the structural change in CNC-CMC polymer solutions.

Regarding to CNC suspension in PEO solutions, DLS and NMR measurements showed the adsorption of PEO onto CNC surfaces, although non-ionic PEO could also act as a non-adsorbing polymer. The existence of salt in low concentrations most likely extended the PEO chain and sulfate groups of CNC particles played the role of cofactors leading to adsorption. The cofactor effect of PEO on its adsorption on CNC surfaces needs further investigation. POM images showed the isotropic-nematic phase transitional of CNC-PEO solutions only when CNC concentration is 2.00 vol%. After saturation of PEO chains, weak depletion interactions occurred in CNC suspension with PEO.

Structure formation and colloidal dynamics of CNC suspensions with CMC and PEO polymers were the main discussion of Chapter 5. Interaction mechanisms were determined in terms of different methods up to end of this current chapter. In Chapter 6, we would like to see interaction mechanism effect on self-assembly of CNC particles.

Chapter 6. Atomic Force Microscopy (AFM) Studies on Self-Assembly of CNC Films from Aqueous Polymer Solutions

Data in this section will be the base to prepare a letter about self-assembly of CNC particles in a neutral and anionic polymer medium.

6.1 Abstract

This study investigated the effect of interactions between CNC particles with PEO and CMC on self-assembly of CNC particles. Solvent-cast films were visualized using AFM in tapping-mode. Strong depletion interactions between CNC particles and CMC chains resulted in an ordered structure of CNC particles. Less significant degree of ordering was observed in CNC-PEO samples. The formation of PEO spherulites indicated that PEO polymer was highly crystalline. XRD results showed that the presence of CNC particles decreased the spherulites size. Two separate phases were observed in dilute CNC-CMC sample referring depletion interactions. In case of PEO-CNC samples AFM image of dilute CNC-PEO proved the adsorption of PEO chains on CNC surface visually.

6.2 Introduction

Self-assembly of nanoparticles is a hot topic to study to obtain desired properties of materials. Self-assembly of nanoparticles occurs to keep the Gibbs free energy at the minimum value¹³⁸. Therefore, self-assembly of nanoparticles can be driven due to enthalpic and/or entropic effects¹³⁸. Onsager explained theoretically entropy driven self-assembly of rod particles⁸⁶. According to Onsager theory, rod-like particles such as fd virus⁷⁵, boehmite^{15,92,126} carbon nanotubes¹²⁷ and cellulose nanocrystals^{68,128} exhibits isotropic-nematic phase transition. Cellulose nanocrystals can be considered as rod-like nanoparticles and they are derived from cellulose polymer with acid hydrolysis techniques. The acid hydrolysis results in a negative charged sulfate ester groups on CNC. Therefore, electrostatic repulsion reduces the free energy of the system resulting in a lower the phase transition concentration¹³⁰. CNC suspensions showed the phase transition within the range of 2.70 vol.% (4.0 wt.%) and 3.39 vol.% (5.0 wt.%) for CNCs with aspect ratios between 20 and 50^{62,67,114}. Addition of polymer in CNC suspension results in different phase behaviors due to interactions between CNC particles and polymer chains. Self-assembly of CNC particles with polymers haven't studied in detailed yet. Therefore this study focused on

understanding self-assembly mechanism of CNC particles with carboxymethyl cellulose (CMC) and polyethylene oxide (PEO) in terms of atomic force measurements (AFM) techniques.

6.3 Experimental

6.3.1 AFM Measurements

The surface of each sample was imaged using an AFM instrument (Digital Instruments/Veeco Instruments MultiMode Nanoscope IV). According to the image size, AFM was equipped with an E or J scanner. In order to obtain optimized height profiles, antimony doped silicon cantilevers (Bruker USA, Inc.) with a spring constant of 42 N/m were used in tapping mode (TM-AFM). Clean mica substrates were prepared then a film cast on the mica from droplet of prepared solution. To maintain a slow evaporation, samples were dried in a closed petri dish at room temperature without any external force (Figure 6.1).

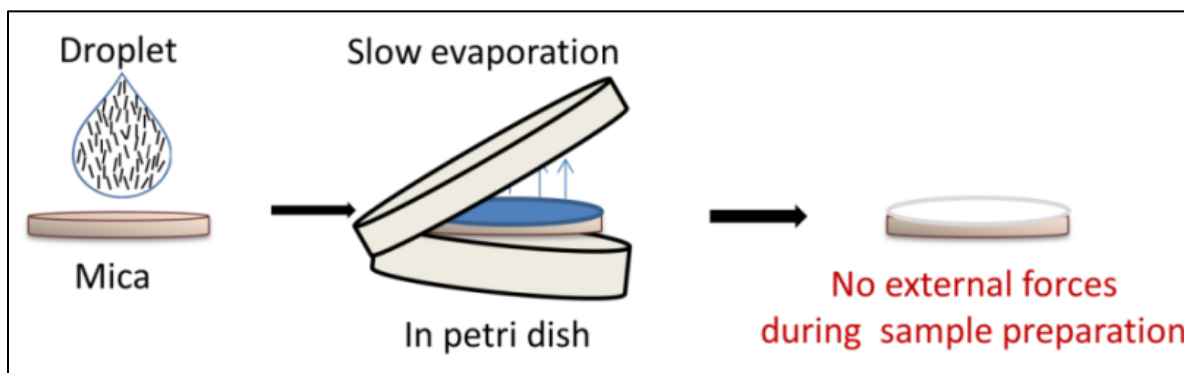


Figure 6.1 Illustration of sample preparation for AFM measurements

6.3.2 X-ray Diffraction Analyses

X-ray Diffraction (XRD) was used to characterize the crystallinity of CNC suspensions, PEO solutions and their mixture. Bruker D8 Discover was conducted (Cu K α radiation, $\lambda=1.54$ nm, 40 kV, 40 mA) between 5° and 70°.

6.4 Results

Figure 6.2 shows the topography of dried film surfaces casting from CNC solutions in different scanning area Figure 6.2.a and Figure 6.2.b show the surface of 0.50 wt% CNC films in two different scanning areas, 100 μm x 100 μm and 50 μm x 50 μm . Figure 6.2.c, Figure 6.2.d, Figure 6.2.e and Figure 6.2.f indicates the surface topography of 1.0 wt% CNC films. The

roughness for the case of 0.5 wt% CNC is higher than in the case of 1.0 wt% CNC indicating the presence of CNC particles.

Figure 6.3.a and Figure 6.3.b show the surface topography of dried film cast from a droplet of 2.00 wt% CMC solution. The surface of CMC is amorphous and smooth. In Figure 6.3.c and Figure 6.3.d The surface topography of 1.0 wt% PEO solution contains spherulites of semi-crystalline PEO matching with POM results in Figure 4.7. Nucleation site, crystalline lamellas and grain boundary were observed in the images (Figure 6.3.c and Figure 6.3.d).

Figure 6.4 shows the surface topography of CNC suspensions with CMC solutions. Figure 6.4.a represents the 0.50 wt% CNC-0.50 wt% CMC solution; in this case the polymer concentration is below the critical concentration level ($c^{**} \approx 1.10$ wt%). Aggregated spots point to CNC blobs. When the concentration of CMC solution is above c^{**} (Figure 6.4.b), the number of aggregated spots increase. Moreover, CMC chains assemble as branches, which is similar to the self-assembled collagen structure (138). At a low CMC concentration (0.05 wt%), the orientation of CNC particles is observed in Figure 6.4.c and Figure 6.4.d. Depletion interactions generate an ordered CNC structure. In Figure 6.3.d, CNC flocs are further more evident compared the previous images (Figure 6.4.a and Figure 6.4.b). Strong depletion interactions lead to produce ordered sets of CNC flocs generating blob structure of CNC particles. This result is in accordance with our discussions in Chapter 2, Chapter 3 and Chapter 4.

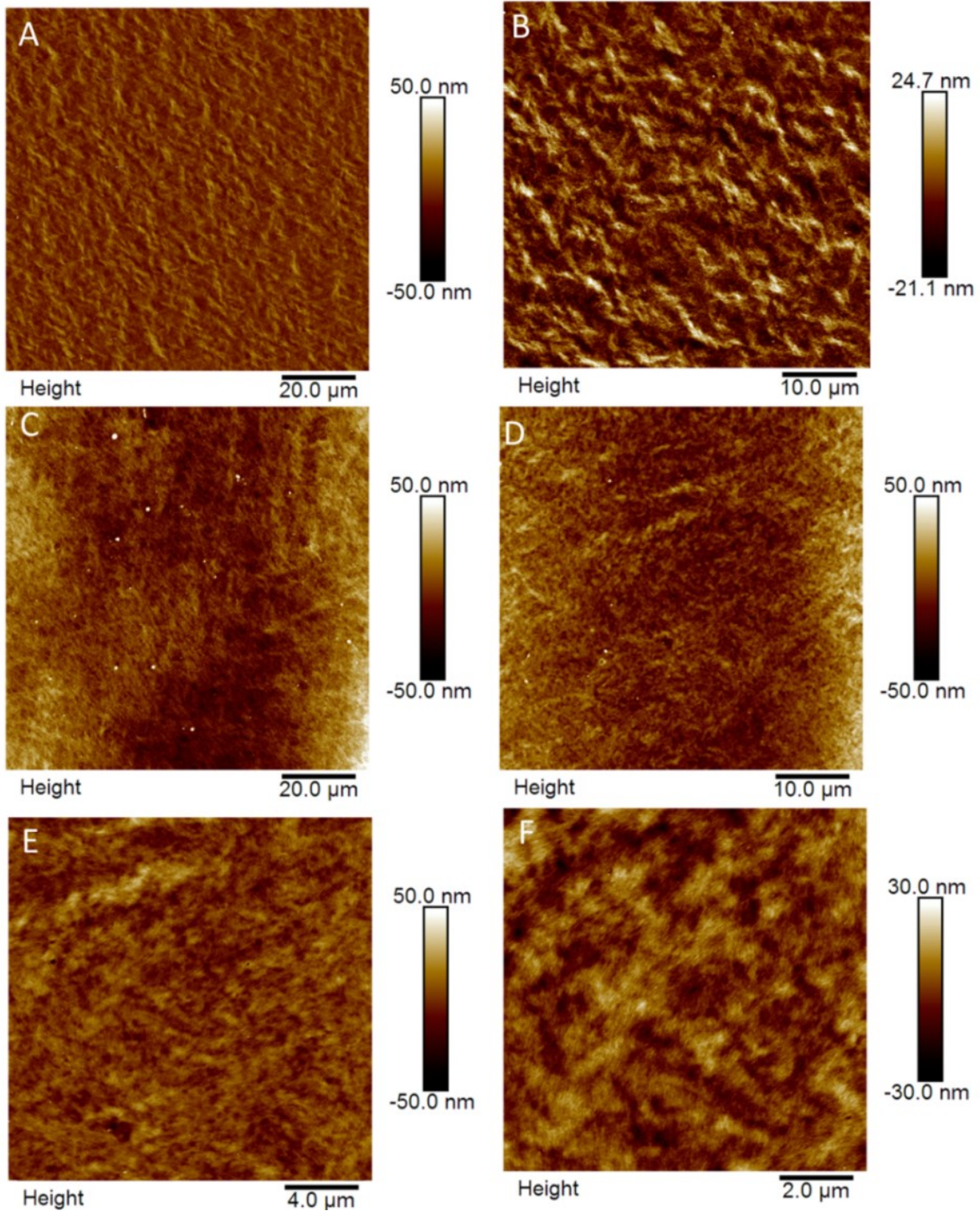


Figure 6.2 AFM Height images of surface of film cast from droplet of 0.50 wt% CNC suspension with the scan size of (a) 100 $\mu\text{m} \times 100 \mu\text{m}$ and (b) 50 $\mu\text{m} \times 50 \mu\text{m}$, and 1.00 wt% CNC suspension with the scan size of (c) 100 $\mu\text{m} \times 100 \mu\text{m}$, (d) 50 $\mu\text{m} \times 50 \mu\text{m}$, (e) 10 $\mu\text{m} \times 10 \mu\text{m}$ and (f) 5 $\mu\text{m} \times 5 \mu\text{m}$.

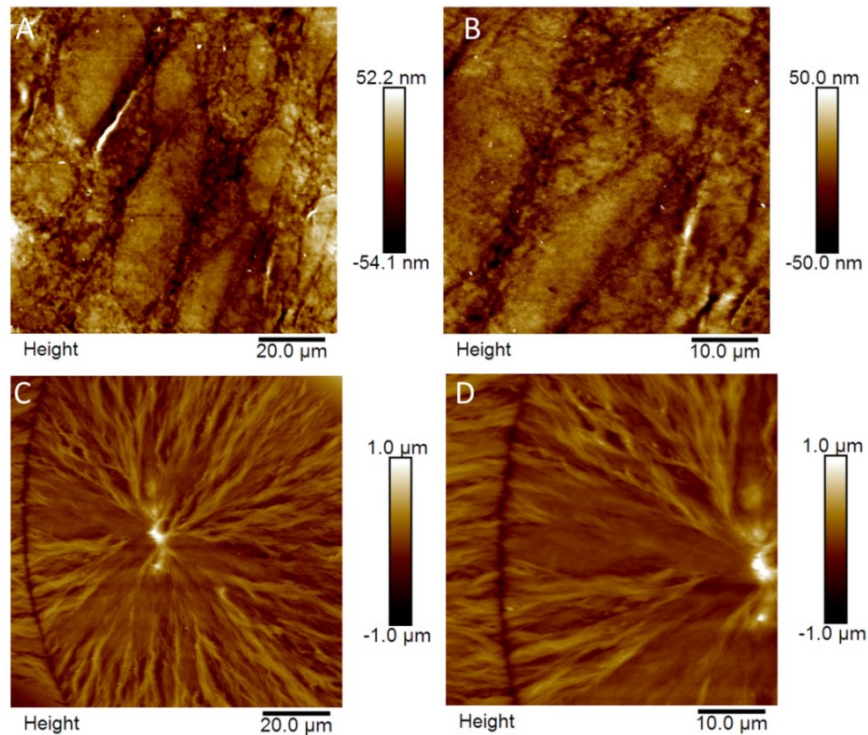


Figure 6.3 AFM Height images of surface of film cast from droplet of 2.00 wt% CMC solution with the scan size of (a) 100 μm x 100 μm and (b) 50 μm x 50 μm and 1.00 wt% PEO solution with the scan size of (c) 100 μm x 100 μm and (d) 50 μm x 50 μm .

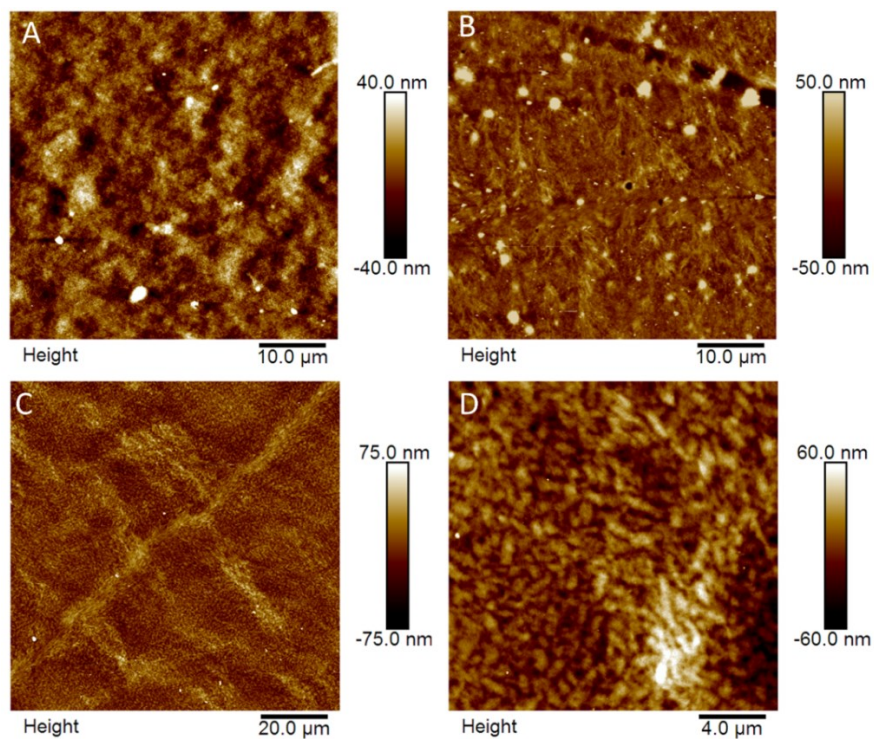


Figure 6.4 AFM Height images of surface of film cast from droplet of (a) 0.50 wt% CMC-0.50 wt% CNC mixture (50 μm x 50 μm), (b) 0.50 wt% CMC-2.00 wt% CNC mixture (50 μm x 50 μm) and 0.05 wt% CMC-1.00 wt% CNC mixture with the scan size of (c) 100 μm x 100 μm and (d) 5.00 μm x 5.00 μm .

In the case of PEO solutions, ordered CNC structures are also observed when the concentration of PEO is very low (0.05 wt%). In Figure 6.5 Figure 5.B.a, Figure 6.5.b and Figure 6.5.c, the degree of ordering is less significant for CNC particles in PEO solution than CNC particles in CMC solutions because of weak depletion interactions between CNC particles and PEO chains. Increasing the concentration of PEO results in CNC flocs (Figure 6.5.d). However, the spherulites of PEO chains are not observed in CNC-PEO solutions because CNC particles limit the formation of spherulites; this observation agrees with our discussion in Chapter 4.

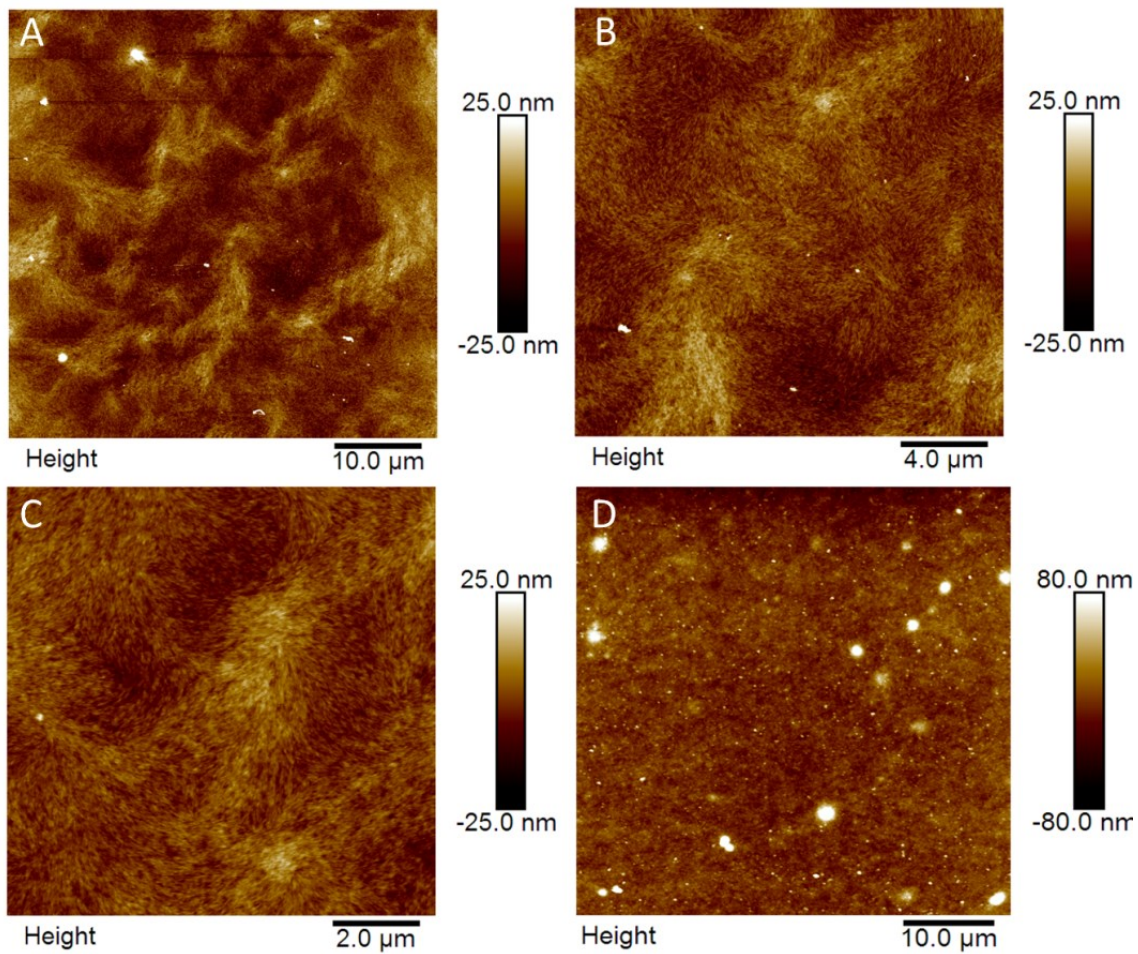


Figure 6.5 AFM Height images of surface of film cast from droplet of 0.05 wt% PEO-1.0wt% CNC mixture (a) (50 μm x 50 μm), (b) (10 μm x 10 μm), (c) (5 μm x 5 μm), and (d) 1.0wt% PEO-1.0wt% CNC mixture (50 μm x 50 μm).

XRD experiments were performed to understand the change in the size of PEO spherulite. The characteristic peaks of CNC particles and PEO chains can be seen in Figure 6.6.

The peak at 18.9° indicates the change in the size of spherulites of PEO chains because only PEO samples had peak at, 18.9° . A decrease in intensity at 18.9° is proportional with the decrease in the size of spherulites in PEO chains; this effect is due to the presence of CNC particles. XRD results are also in accordance with POM results in Figure 5.7 in Chapter 5.

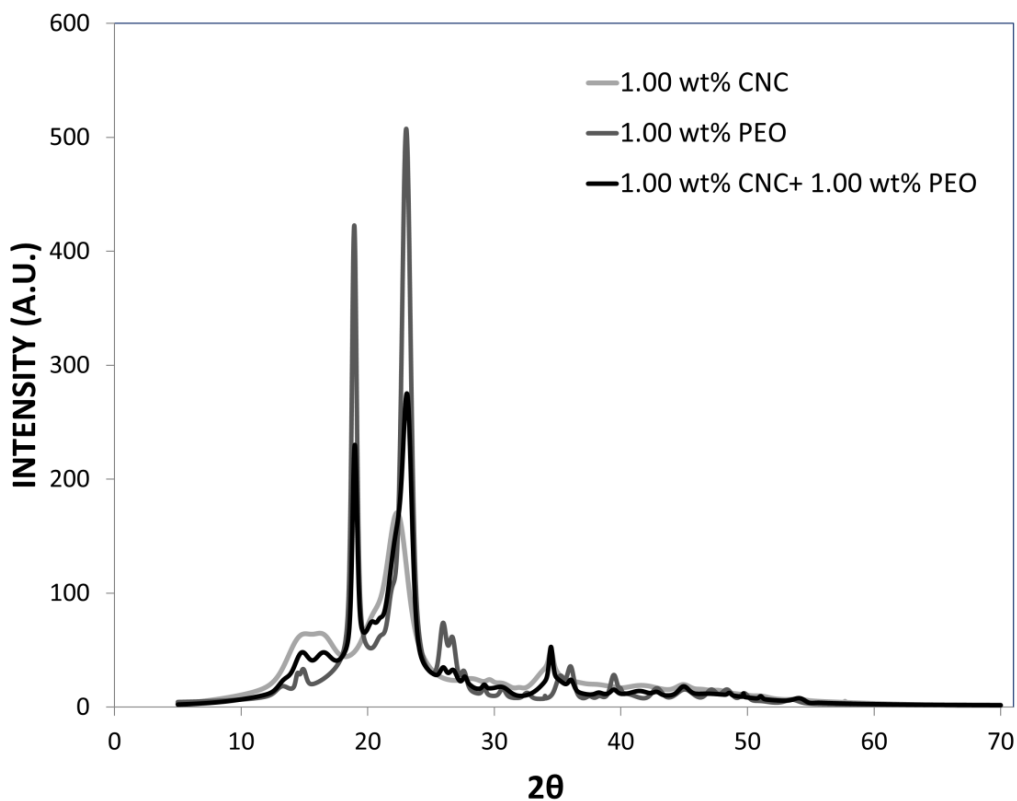


Figure 6.6. X-ray diffractogram of 1.00 wt% CNC, 1.00 wt% PEO and 1.00 wt% CNC+1.00 wt% PEO.

Figure 6.7 consists of 2D height images, 3D height images, and roughness profiles of the film cast from 0.01 wt% CNC suspensions. In Figure 6.7.a CNC particles have a random orientation due to their low concentration. The 3D height image is shown for a better understanding of the surface topography (Figure 6.7.b). According to height profile graphs, the height values fluctuate around 5 nm and fluctuations were distributed uniformly (Figure 6.7.c).

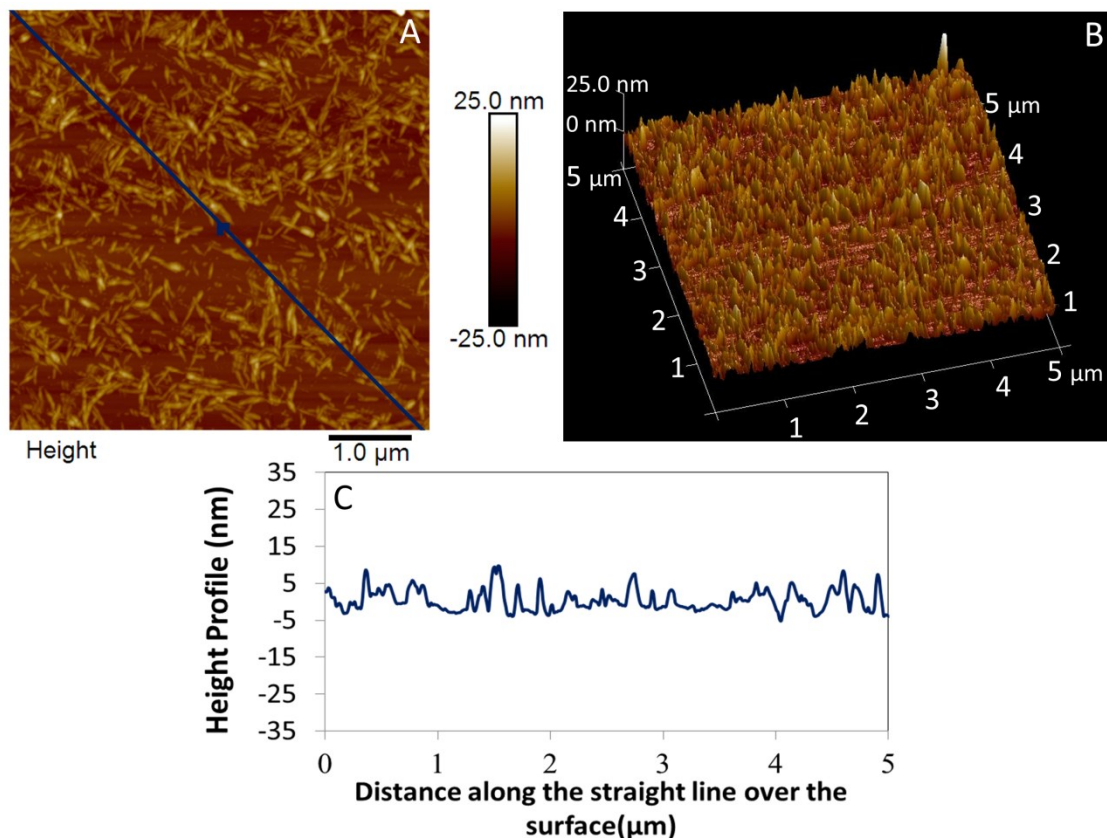


Figure 6.7 AFM results of surface of film cast from droplet of 0.01 wt% CNC suspensions (a) 2D height image ($5\ \mu\text{m} \times 5\ \mu\text{m}$), (b) 3D height image ($5\ \mu\text{m} \times 5\ \mu\text{m}$) obtained by tapping mode, (c) roughness profile along a line chosen in arbitrary direction on the surface and is shown by the diagonal line in (a).

Figure 6.8 consists of 2D height images, 3D height images, and roughness profiles of film cast from 0.01 wt% CNC suspensions in 0.01 wt% CMC solutions. In Figure 6.8.b, two different phases were observed: (1) CNC rich phase and (2) CMC polymer rich phase. Besides, depletion interactions bring the neighboring CNC particles closer to each other. According to height profile graphs, fluctuations values differ changing the height values and in relation to the region studied (Figure 6.8.c).

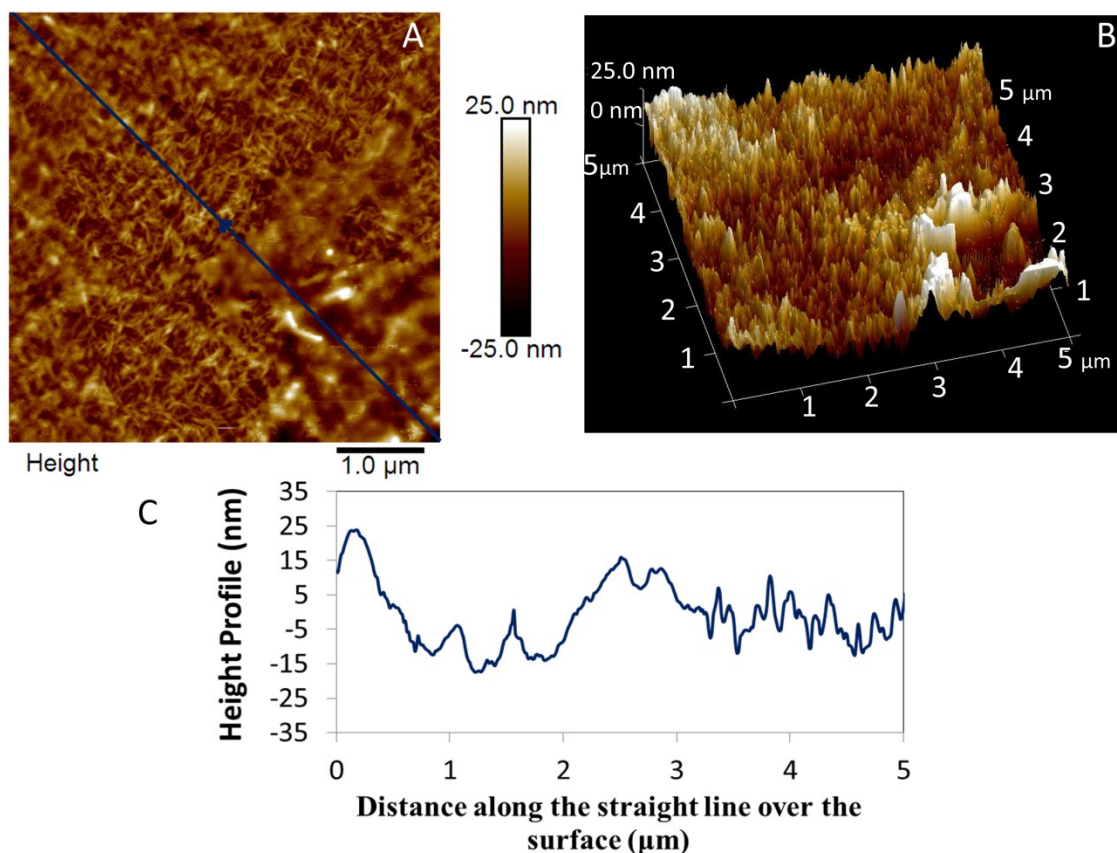


Figure 6.8 AFM results of surface of film cast from droplet of 0.01 wt% CNC- 0.01 wt% CMC mixtures: (a) 2D height image (5 μm x 5 μm), (b) 3D height image (5 μm x 5 μm) obtained by tapping mode, (c) roughness profile along a line chosen in arbitrary direction on the surface and is shown by the diagonal line in (a).

Figure 6.9 consists of 2D height images, 3D height images and roughness profiles of film cast from 0.01 wt% CNC suspensions in 0.01 wt% PEO solutions. In contrast to CNC-CMC samples, the presence of PEO don't generate two separate phase. The degree of ordering of CNC particles in the matrix of PEO is similar to the case of CNC particles without any polymer addition. PEO chains forms a structure similar to isotropic particles. This could also be an evidence of PEO adsorption on CNC surface. Fluctuations around 5 nm represent CNC particles. PEO-adsorbed CNC particles fluctuate in the range to 25-35 nm (Figure 6.9.c)

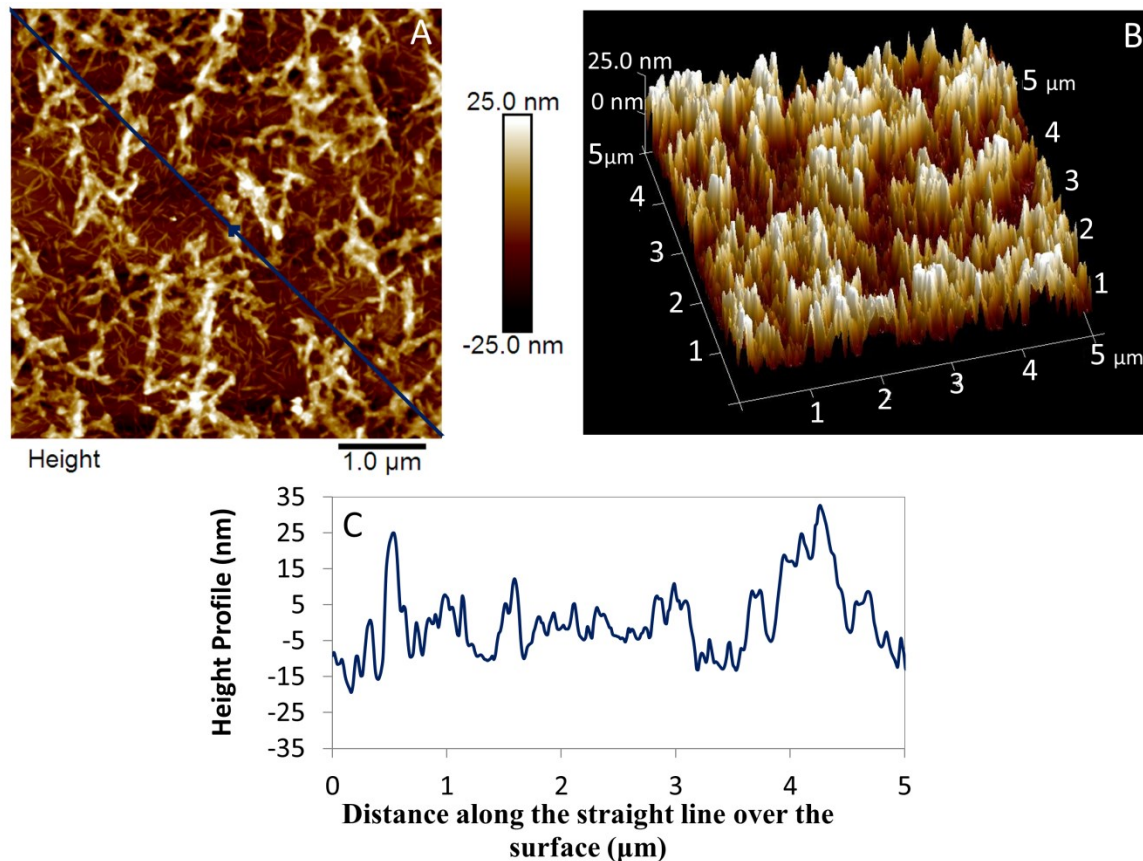


Figure 6.9 AFM results of surface of film cast from droplet of 1.00 wt% CNC- 1.00 wt% PEO solution: (a) 2D height image (5 μm x 5 μm), (b) 3D height image (5 μm x 5 μm) obtained by tapping mode, (c) roughness profile along a line chosen in arbitrary direction on the surface and is shown by the diagonal line in (a).

6.5 Conclusion

Regarding to CNC suspensions with CMC solutions, strong depletion interactions led to an ordered CNC structure. At higher concentrations, these ordered structure resulted in blob structures which were visually observed in AFM images. At dilute concentrations, depletion interactions resulted in two different kinds of media. In the case of CNC suspensions with CMC solutions, the adsorption PEO chains onto CNC surfaces weakened depletion interaction, therefore; the degree of ordering CNC particles is not significant in PEO solution. Moreover, the adsorption of PEO chains on CNC particles was observed visually in AFM images at dilute concentrations. Consequently, different interaction mechanism leads to different ordering behavior of CNC particles.

Chapter 7. Conclusion

Interactions between CNC nanoparticles and polymer chains were determined with the combination of rheological methods, optical measurements, dynamic light scattering techniques and NMR. This study leads to the following conclusions:

- The structure formation in CMC-CNC solutions dramatically thickened the shear viscosity of CNC suspensions at lower shear rates. The presence of CMC chains led to a drastic shear thinning behavior at higher shear rates.
- Formed structures were observed as nematic flocs in dilute CMC-CNC solutions. STEM POM images of concentrated CNC-CMC solutions showed both nematic and chiral-nematic phase. The flocculated structure of CNC particles and formation of non-isotropic flocs in the CMC solution also supported the depletion mechanism.
- An increase in CNC concentration resulted in the entanglement of CMC chains and the formation of CNC blobs from nematic flocs that entrapped water. Therefore, the CMC concentration artificially increased in the bulk state; this increase the shear viscosity, gelation and produce a different response in the Cox-Merz rule.
- Adding PEO polymer in CNC suspensions didn't show any significant thickening behavior in shear viscosities at higher shear rates (Appendix A). PEO solutions in the presence of CNC suspensions show a weak shear thinning behavior at higher shear rates.
- Even though, STEM image of dilute PEO-CNC solution showed randomly dispersed CNC nanoparticles, birefringent structures were observed by means of POM indicating an isotropic-nematic phase transition.
- Regarding to CNC suspension with the PEO solutions, DLS and NMR measurements showed the adsorption of PEO onto CNC surfaces, although non-ionic PEO was supposed to act as a non-adsorbing polymer. The existence of salt in low concentrations could extend the PEO chain and sulfate groups of CNC particles could play a role as cofactors leading to adsorption.
- Depletion interactions were the main reasons for observing a nematic phase below the CNC phase transition concentration (2.70-3.39 vol.%). Both polymers applied osmotic pressure to CNC particles, resulting in two different kinds of depletion interactions.

- In the case of CNC-CMC polymer solutions, depletion flocculation was the reason to the structural change, gelation and increase in viscosity. The presence of sulfate groups of CNC particles and carboxyl groups of CMC chains created the electrostatic repulsion which strengthened depletion interactions.
- In the case of CNC-PEO polymer solutions, the adsorption of PEO onto the CNC surface resulted in a non-zero PEO concentration in depletion layer thickness. After saturation of PEO chains, weak depletion interactions occurred in CNC suspension with PEO. Weak depletion interactions were the results of the adsorption of PEO chains because the presence of PEO chains reduced the applied osmotic pressure.

7.1 Contribution to Knowledge

The nature of CNC polymer interactions and mesoscopic structure of CNC particles in semi dilute state in semi-dilute polymer solutions are not well understood in the literature. Two kinds of interactions may occur between CNC particles and polymer chains: (1) adsorption and (2) depletion. If considering only phase behaviors, understanding weakly interacted colloid polymer mixtures is not easy because both depletion and bridging flocculation lead to phase separation. This study focused on investigating interactions in terms of not only phase behavior but also structure-property relations, particle diffusion, electrophoretic mobility and ^1H NMR solvent relaxation. These techniques were used to explain CNC polymer interactions without any uncertainties. The main achievement of this study was determining the interactions between rod-like CNC particles and flexible anionic and neutral polymer chains.

As an industrial significance, desired macroscopic properties can be obtained by controlling with the presence of polymer solutions, the degree of ordering CNCs can be controlled in mesoscopic level; this determines certain macroscopic properties. Adding CNC particles in polymers enhances the rheological properties such as thickening viscosity at lower shear rates and gel formation. CNC suspensions at low concentrations as a rheology modifier in dilute and semi-dilute polymer concentrations has potential applications in coating formulations, drilling and fracturing fluids, personal care and other industrial and household products. The use of such thickening systems shall bring not only desired performance characteristics by tailoring the thickening behavior but also address the operational concerns such as shear, thermal and bacterial degradation of the formulations. Minimizing the concentrations of water soluble

polymers in any functional fluid while maintaining the thickening rheology by incorporating relatively shear, thermal and bacterially stable CNC can remedy such problems in operations. Besides cellulose nanocrystals are easily dispersible in water and easy to formulate with a minimum mechanical action during preparations of product formulations.

7.2 Future Recommendations

Interactions between unmodified CNC and flexible polymers in aqueous medium were the focus of this study. Recommendations for the future studies on this topic were listed below:

- To enhance understanding of polymer effect on interaction mechanism, interactions between CNC particles and semi-flexible polymers would be also interesting to investigate. Semi-flexible polymers such as Xanthan gum may act on CNC nanoparticles resulting in different interaction mechanism.
- Associating polymers consist of at least one hydrophilic part or block and at least hydrophilic part/block forming associating network and enhancement in viscosity. The presence of CNC and associating polymers in solutions together could also enhance viscosity and viscoelastic properties due to different interaction mechanism.
- Sulfuric acid hydrolysis is used to obtain CNC particles. Depending on the hydrolysis conditions, the morphologies and properties of CNC may vary. The presence of hydroxyl groups on CNC surface allow to functionalization of the nanocrystals. Surface modification effect on interaction mechanism can also be studied to improve understanding of the effect of surface properties of CNC particles.
- TEMPO-mediated oxidation is the other way to obtain CNC. The effect of an oxidation with the TEMPO radical leads to aldehyde and carboxylate groups on CNC surface. This could be interesting work because different functional groups may results in different interaction mechanism and rheological properties
- Interactions between solvent molecules and polymer molecules result in different chain conformations. Radius of gyration of polymer chain is one of the main parameter of depletion interactions. Therefore, aqueous systems even binary solvent systems could be another interesting research to observe solvent effect. However, solvent molecules CNC interaction should also be considered as change in solvent type may also affect dispersion state of CNC in solution.

- According to Onsager theory, phase separation is entropy driven effect. The basis of Lekkerkerker's calculation is chemical potential equation for isotropic-nematic phase transitions of CNC. Therefore, the main parameter of thermodynamics, temperature and its effect could be another promising research to focus in both mesoscopic and macroscopic level.
- AFM and POM results indicate that crystallinity of PEO changes in the presence of CNC. Crystal growth of PEO chains could be investigated in terms of CNC concentration, PEO concentration, temperature change and addition of salt for solid-state application of PEO-CNC solution. For instance, solution casting method could use to form of PEO-CNC films for food packaging, painting or coating applications. Controlling over crystallinity and dispersion state of CNC allow to optimize barrier and mechanical properties of corresponding CNC-PEO films

References

1. Shatkin, J. A.; Wegner, T. H.; Bilek, E.M. Market projections of cellulose nanomaterial enabled products – Part 1: Applications. *Tappi Journal* **2014**, *13*, 9-16.
2. Hunter, R. J. *Foundations of colloid science*, Oxford University Press, New York, 2001 Vol., 2nd ed .
3. Hiemenz, P. C. *Principles of colloid and surface chemistry*; New York, 1986 .
4. Berg, J. C. *An introduction to interfaces & colloids : the bridge to nanoscience*; World Scientific: Singapore, 2010 .
5. Lekkerkerker, H. N. W.; Tuinier, R. *Colloids and the depletion interaction*; Springer: New York, 2011 .
6. Israelachvili, J. N. *Intermolecular and surface forces [electronic resource] / Jacob N. Israelachvili*; MA : Academic Press,; Burlington, 2011 .
7. Howard, G. J.; McConnell, P. Adsorption of polymers at the solution-solid interface. I. Polyethers on silica . *The Journal of Physical Chemistry* **1967**, *71*, 2974-2981.
8. Joanny, J. F.; Leibler, L.; De Gennes, P. G. Effects of polymer solutions on colloid stability. *Journal of Polymer Science: Polymer Physics* **1979**, *17*, 1073-1084.
9. Senff, H.; Richtering, W. Temperature sensitive microgel suspensions: Colloidal phase behaviour and rheology of soft spheres. *J. Chem. Phys.* **1999**, *111*, 1705.
10. Nabzar, L.; Pefferkorn, E.; Varoqui, R. Polyacrylamide-sodium kaolinite interactions: Flocculation behavior of polymer clay suspensions. *J. Colloid Interface Sci.* , *102*, 380-388.
11. Monthieux, M.; Kuznetsov, V. L. Who should be given the credit for the discovery of carbon nanotubes? *Carbon* **2006**, *44*, 1621-1623.

12. Lima, M. M. D.; Borsali, R. Rodlike cellulose microcrystals: Structure, properties, and applications. *Macromolecular Rapid Communications* **2004**, *25*, 771-787.
13. Mewis, J.; Wagner, N. J. *Colloidal suspension rheology*,; Cambridge ; New York : Cambridge University Press, 2012: 2012; .
14. Pamies, R.; Hernandez Cifre, J. G.; del Carmen, L. M.; Garcia de, I. T. Determination of intrinsic viscosities of macromolecules and nanoparticles. Comparison of single-point and dilution procedures. *Colloid & Polymer Science* **2008**, 1223.
15. Wierenga, A. M.; Philipse, A. P. Low-shear viscosity of isotropic dispersions of (Brownian) rods and fibres; a review of theory and experiments. *Colloids and Surfaces a Physicochemical and Engineering Aspects* **1998**, *137*, 355-372.
16. Phung, T. N.; Brady, J. F.; Bossis, G. Stokesian Dynamics simulation of Brownian suspensions. *J. Fluid Mech.* **1996**, *313*, 181-207.
17. Bossis, G.; Brady, J. F. The rheology of Brownian suspensions. *Journal of Chemical Physics* **1989**, *91*, 1866-1873.
18. Jowkarderis, L.; Ven, T. Intrinsic viscosity of aqueous suspensions of cellulose nanofibrils. *Cellulose* **2014**, *21*, 2511-2517.
19. Mansfield, M. L.; Douglas, J. F. Transport properties of rodlike particles. *Macromolecules* **2008**, *41*, 5422-5432.
20. Sherwood, J. D. The primary electroviscous effect in a suspension of rods. *Journal of Fluid Mechanics* **1981**, *111*, 347-366.
21. Boluk, Y.; Lahiji, R., Zhao, L.; McDermott, M. T. Suspension viscosities and shape parameter of cellulose nanocrystals (CNC). *Colloids and Surfaces A: Physicochemical and Engineering Aspects* **2011**, *377*, 297-303.

22. Liu, D.; Chen, X.; Yue, Y.; Chen, M.; Wu, Q. Structure and rheology of nanocrystalline cellulose. *Carbohydr. Polym.* **2011**, *84*, 316-322.
23. Shafiei-Sabet, S.; Hamad, W. Y.; Hatzikiriakos, S. G. Rheology of nanocrystalline cellulose aqueous suspensions. *Langmuir* **2012**, *28*, 17124-17133.
24. Urena-Benavides, E.; Ao, G. Y.; Davis, V. A.; Kitchens, C. L. Rheology and Phase Behavior of Lyotropic Cellulose Nanocrystal Suspensions. *Macromolecules* **2011**, *44*, 8990-8998.
25. Teraoka, I. *Polymer solutions : an introduction to physical properties*; Wiley: New York, 2002.
26. Barth, H. G.; Mays, J. W. *Modern methods of polymer characterization*; New York : J. Wiley, 1991 .
27. Graessley, W. W. *Polymeric Liquids and Networks: Structure and Properties*; 2004; Vol. 1, pp 558.
28. Colby, R. H. Structure and linear viscoelasticity of flexible polymer solutions: comparison of polyelectrolyte and neutral polymer solutions. *Rheologica Acta* **2010**, 425-442.
29. Baumgärtel, M.; Willenbacher, N. The relaxation of concentrated polymer solutions. *Rheologica Acta* **1996**, *35*, 168-185.
30. Clasen, C.; Kulicke, W. -. Determination of viscoelastic and rheo-optical material functions of water-soluble cellulose derivatives. *Progress in Polymer Science* **2001**, *26*, 1839-1919.
31. Daga, V. K.; Wagner, N. J. Linear viscoelastic master curves of neat and laponite-filled poly(ethylene oxide)-water solutions. *Rheologica Acta* **2006**, *45*, 813-824.
32. Masaro, L.; Zhu, X. X. Physical models of diffusion for polymer solutions, gels and solids. *Progress in Polymer Science* **1999**, *24*, 731-775.

33. Kjellander, R.; Florin, E. Water structure and changes in thermal stability of the system poly(ethylene oxide)–water. *Journal of the Chemical Society, Faraday Transactions* **1981**, *77*, 2053-2077.
34. Devanand, K.; Selser, J. Asymptotic behavior and long-range interactions in aqueous solutions of poly(ethylene oxide. *Macromolecules* **1991**, *24*, 5943-5947.
35. Kulicke, W.; Kull, A. H.; Kull, W.; Thielking, H.; Engelhardt, J.; Pannek, J. Characterization of aqueous carboxymethylcellulose solutions in terms of their molecular structure and its influence on rheological behaviour. *Polymer* **1996**, *37*, 2723.
36. Chatterjee, A.; Das, B. Radii of gyration of sodium carboxymethylcellulose in aqueous and mixed solvent media from viscosity measurement. *Carbohydr. Polym.* **2013**, *98*, 1297-1303.
37. Benchabane, A.; Bekkour, K. Rheological properties of carboxymethyl cellulose (CMC) solutions. *Colloid & Polymer Science* **2008**, 1173.
38. Fler, G. J.; Tuinier, R. Analytical phase diagrams for colloids and non-adsorbing polymer. *Adv. Colloid Interface Sci.* **2008**, *143*, 1-47.
39. Fler, G. J.; Stuart, M. A. C.; Scheutjens, J. M. H. M.; Cosgrove, T.; Vincent, B. *Polymers at Interfaces*; Chapman&Hall: Cambridge, 1993; .
40. Gregory, J.; Barany, S. Adsorption and flocculation by polymers and polymer mixtures. *Adv. Colloid Interface Sci.* **2011**, *169*, 1-12.
41. Jingyu, S. Steric Stabilization.
http://muri.lci.kent.edu/References/NIM_Papers/stabilization_of_NP_suspensions/2002_Shi_steric_stabilization.pdf (accessed February, 25, 2015).
42. Gregory, J.; Barany, S. Adsorption and flocculation by polymers and polymer mixtures. *Adv. Colloid Interface Sci.* **2011**, *169*, 1-12.

43. Khalili, Z. An investigation on interaction between nano crystalline cellulose and watersoluble polymers in aqueous solutions, University of Alberta, 2013.
44. Doxastakis, M.; Chen , Y. L.; Guzmán, O.; Pablo, J. J. Polymer-particle mixtures:depletion and packing effect. *Journal of Chemical Physics* **2004**, *120*, 9335-9345.
45. Ramakrishnan, S.; Chen, Y. -.; Schweizer, K. S.; Zukoski, C. F. Elasticity and clustering in concentrated depletion gels. *Physical Review E* **2004**, *70*, 040401-1-040401-4.
46. Klemm, D.; Kramer, F.; Moritz, S.; Lindstrom, T.; Ankerfors, M.; Gray, D.; Dorris, A. Nanocelluloses: A New Family of Nature-Based Materials. *Angewandte Chemie International Edition* **2011**, *50*, 5438-5466.
47. Boluk, Y.; Danumah, C. Analysis of cellulose nanocrystal rod lengths by dynamic light scattering and electron microscopy. *Journal of Nanoparticle Research* **2014**, *16*, 1-7.
48. Doi, M.,; Edwards , S. F. *Theory of Polymer Dynamics*; Oxford Science: Oxford, UK, 1986; .
49. Pennycook, S. J.; Lupini, A. R.; Varela, M.; Borisevich, A.; Peng, Y.; Oxley, M. P.; Van Benthem, K.; Chisholm, M. F. Scanning Transmission Electron Microscopy for Nanostructure Characterization. In ; Zhou, W., Wang, Z., Eds.; Springer New York: 2007; pp 152-191.
50. Malvern Instrument Manual *Zetasizer Nanoseries User Manuals*; Malvern Instruments Ltd: Worcestershire, United Kingdom, 2004; Vol. 2016.
51. Han, C. D. *Rheology and Processing of Polymeric Materials*; Oxford University Press: Oxford, 2007.
52. Lambert, J. B.; Mazzola, E. P. *Nuclear magnetic resonance spectroscopy: an introduction to principles, applications, and experimental methods*; Upper Saddle River, N.J. : Pearson/Prentice Hall,2004 .

53. Cooper, C. L.; Cosgrove, T.; van Duijneveldt, J.; Murray, M.; Prescott, S. W. The use of solvent relaxation NMR to study colloidal suspensions. *Soft Matter* **2013**, *9*, 7211-7228.
54. Blümicha, B.; Casanova, F.; Appelta, S. NMR at low magnetic fields. *Chemical Physics Letters* **2009**, *477*, 231-240.
55. Bowen, W. R.; Hilal, N. *Atomic force microscopy in process engineering: introduction to AFM for improved processes and products*; Oxford ; Burlington, MA : Butterworth-Heinemann, c2009; 1st ed: 2009; .
56. Bellare, J. R.; Davis, H. T.; Miller, W. G.; Scriven, L. E. Polarized Optical Microscopy of Anisotropic Media - Imaging Theory and Simulation. *J. Colloid Interface Sci.* **1990**, *136*, 305-326.
57. Celia, C.; Trapasso, E.; Cosco, D.; Paolino, D.; Fresta, M. Turbiscan Lab (R) Expert analysis of the stability of ethosomes (R) and ultradeformable liposomes containing a bilayer fluidizing agent. *Colloids and Surfaces B-Biointerfaces* **2009**, *72*, 155-160.
58. Klemm, D.; Heublein, B.; Fink, H.; Bohn, A. Cellulose: fascinating biopolymer and sustainable raw material. *Angew. Chem. Int. Ed Engl.* **2005**, *44*, 3358-3393.
59. Xue Min, D.; Jean-Francois, R.; Derek, G. Effect of microcrystallite preparation conditions on the formation of colloid crystals of cellulose. *Cellulose* **1998**, *5*, 19-32.
60. Beck-Candanedo, S.; Roman, M.; Gray, D. G. Effect of reaction conditions on the properties and behavior of wood cellulose nanocrystal suspensions. *Biomacromolecules* **2005**, *6*, 1048-1054.
61. Hamad, W. Y.; Hu, T. Q. Structure-process-yield interrelations in nanocrystalline cellulose extraction. *Canadian Journal of Chemical Engineering* **2010**, *88*, 392-402.
62. Habibi, Y.; Lucia, L. A.; Rojas, O. J. Cellulose Nanocrystals: Chemistry, Self-Assembly, and Applications. *Chem. Rev.* **2010**, *110*, 3479-3500.

63. Siqueira, G.; Bras, J.; Dufresne, A. Cellulosic Bionanocomposites: A Review of Preparation, Properties and Applications. *Polymers* **2010**, *2*, 728-765.
64. Azizi Samir, M., Ahmed Said; Alloin, F.; Dufresne, A. Review of recent research into cellulosic whiskers, their properties and their application in nanocomposite field. *Biomacromolecules* **2005**, *6*, 612-626.
65. Viet, D.; Gray, D. G.; Beck-Candanedo, S. Dispersion of cellulose nanocrystals in polar organic solvents. *Cellulose* **2007**, *14*, 109-113.
66. Revol, J.; Godbout, L.; Dong, X.; Gray, D.; Chanzy, H.; Maret, G. Chiral nematic suspensions of cellulose crystallites; phase separation and magnetic field orientation. *Liquid Crystals* **1994**, *16*, 27-34.
67. Xue Min, D.; Tsunehisa, K.; Jean-Francois, R.; Derek, G. Effects of ionic strength on the isotropic-chiral nematic phase transition of suspensions of cellulose crystallites. *Langmuir* **1996**, *12*, 2076-2082.
68. Edgar, C. D.; Gray, D. G. Influence of dextran on the phase Behavior of suspensions of cellulose nanocrystals. *Macromolecules* **2002**, *35*, 7400-7406.
69. Lu, A.; Boluk, Y.; Khalili, Z.; Hemraz, U. Unique viscoelastic behaviors of colloidal nanocrystalline cellulose aqueous suspensions [electronic resource]. *Cellulose* **2014**, *21*, 1239-1250.
70. Boluk, Y.; Zhao, L. Canada Patent US 20120153214 A1, 2012.
71. Boluk, Y.; Zhao, L. Y.; Incani, V. Dispersions of nanocrystalline cellulose in aqueous polymer solutions: structure formation of colloidal rods. *Langmuir* **2012**, *24*, 6114-6123.
72. Colby, R. H.; Fetters, L. J.; Funk, W. G.; Graessley, W. W. Effects of Concentration and Thermodynamic Interaction on the Viscoelastic Properties of Polymer-Solutions. *Macromolecules* **1991**, *24*, 3873-3882.

73. Liu, W.; Yu, T. L.; Lin, H. Shear thickening behavior of dilute poly(diallyl dimethyl ammonium chloride) aqueous solutions. *Polymer* **2007**, *48*, 4152-4165.
74. Graessley, W. W. Molecular entanglement theory of flow behavior in amorphous polymers. *The Journal of Chemical Physics* **1965**, *43*, 2696-2703.
75. Dogic, Z.; Purdy, K.; Grelet, E.; Adams, M.; Fraden, S. Isotropic-nematic phase transition in suspensions of filamentous virus and the neutral polymer Dextran, *Physical Review E* **2004**, *69*, 051702-1-051702-9.
76. Surve, M.; Pryamitsyn, V.; Ganesan, V. Nanoparticles in Solutions of Adsorbing Polymers: Pair Interactions, Percolation, and Phase Behavior. *Langmuir* **2006**, *22*, 969-981.
77. Zebrowski, J.; Prasad, V.; Zhang, W.; Walker, L. M.; Weitz, D. A. Shake-gels: shear-induced gelation of laponite-PEO mixtures. *Colloids and Surfaces A: Physicochemical and Engineering Aspects* **2003**, *213*, 189-197.
78. Saito, Y.; Hirose, Y.; Otsubo, Y. Shear-induced reversible gelation of nanoparticle suspensions flocculated by poly(ethylene oxide) . *Colloids and Surfaces A: Physicochemical and Engineering Aspects* **2011**, *384*, 40-46.
79. Asakura, S.; Oosawa, F. Interaction between particles suspended in solutions of macromolecules. *Journal of Polymer Science Part A: Polymer Chemistry* **1958**, *33*, 183-192.
80. Snowden, M. J.; Clegg, S. M.; Williams, P. A.; Robb, I. D. Flocculation of silica particles by adsorbing and non-adsorbing polymers. *Journal of the Chemical Society, Faraday Transactions* **1991**, *87*, 2201-2207.
81. Bouldin, M.; Kulicke, W. M.; Kehler, H. Prediction of the non-Newtonian viscosity and shear stability of polymer solutions. *Colloid and Polymer Science* **1988**, *266*, 793-805.

82. Lopez, C. G.; Rogers, S. E.; Colby, R. H.; Graham, P.; Cabral, J. T. Structure and solution properties of sodium carboxymethyl cellulose. *Journal of Polymer Science, Part B: Polymer Physics* **2015**, *53*, 492-501.
83. Scheutjens, J. M. H. M.; Fleer, G. J. Effect of Polymer Adsorption and Depletion on the Interaction between to Parallel Surfaces. *Advances in Colloid and Interface Science* **1982**, *16*, 361-380.
84. Fleer, G. J.; Scheutjens, J. M. H. M.; Cohen Stuart, M. A. Theoretical progress in polymer adsorption, steric stabilization and flocculation. *Colloids and Surfaces* **1988**, *31*, 1-29.
85. Vrij, A. Polymers at Interfaces and the Interactions in Colloidal Dispersions. *Pure & Applied Chemistry* **1976**, *48*, 471-483.
86. Onsager, L. The effects of shape on the interaction of colloidal particles. *Molecular Interaction* **1949**, *51*, 627-659.
87. Lekkerkerker, H. N. W.; Stroobants, A. Phase behaviour of rod-like colloid+flexible polymer mixtures. *Il Nuovo Cimento D* **1994**, *16*, 949-962.
88. Feigin, R. I.; Napper, D. H. Depletion stabilization and depletion flocculation. *J. Colloid Interface Sci.* **1980**, *75*, 525-541.
89. Kamibayashi, M.; Ogura, H.; Otsubo, Y. Shear-thickening flow of nanoparticle suspensions flocculated by polymer bridging. *J. Colloid Interface Sci.* **2008**, *321*, 294-301.
90. Wierenga, A.; Philipse, A. P.; Lekkerkerker, H. N. W.; Boger, D. V. Aqueous dispersions of colloidal boehmite: structure, dynamics, and yield stress of rod gels. *Langmuir* **1998**, *14*, 55-65.
91. Mourad, M. C. D.; Byelov, D. V.; Petukhov, A. V.; De Winter, D. A. M.; Verkleij, A. J.; Lekkerkerker, H. N. W. Sol-gel transitions and liquid crystal phase transitions in concentrated Aqueous suspensions of colloidal gibbsite platelets. *J Phys Chem B* **2009**, *113*, 11604-11613.

92. Buitenhuis, J.; Donselaar, L. N.; Buining, P. A.; Stroobants, A.; Lekkerkerker, H. N. W. Phase-separation of mixtures of colloidal boehmite rods and flexible polymer. *Journal of colloid and interface science* **1995**, *175*, 46-56.
93. Bercea, M.; Navard, P. Shear Dynamics of Aqueous Suspensions of Cellulose Whiskers. *Macromolecules* **2000**, *33*, 6011-6016.
94. Araki, J.; Wada, M.; Kuga, S.; Okano, T. Influence of surface charge on viscosity behavior of cellulose microcrystal suspension. *Journal of Wood Science (Japan)* **1999**, 258.
95. Srinivasarao, M. Rheology and Rheo-Optics of Polymer Liquid-Crystals. *International Journal of Modern Physics B* **1995**, *9*, 2515-2572.
96. Liu, D.; Chen, X.; Yue, Y.; Chen, M.; Wu, Q. Structure and rheology of nanocrystalline cellulose. *Carbohydr. Polym.* **2011**, *84*, 316–322.
97. Hu, Z.; Cranston, E. D.; Ng, R.; Pelton, R. Tuning cellulose nanocrystal gelation with polysaccharides and surfactants. *Langmuir* **2014**, *30*, 2684-2692.
98. Oguzlu, H.; Danumah, C.; Boluk, Y. The Role of Dilute and Semi-Dilute Cellulose Nanocrystal Suspensions on the Rheology of Carboxymethyl Cellulose Solutions. *The Canadian Journal of Chemical Engineering* **2016**, *94*, 1841-1847.
99. Thuresson, K.; Lindman, B.; Bo, N. Effect of hydrophobic modification of a nonionic cellulose derivative on the interaction with surfactants rheology. *The Journal of Physical Chemistry* **1997**, *101*, 6450-6459.
100. Vadodaria, S.; English, R. Aqueous solutions of HEC and hmHEC: effects of molecular mass versus hydrophobic associations on hydrodynamic and thermodynamic parameters. *Cellulose* **2016**, *23*, 1107-1121.
101. Tirtaatmadja, V.; Tam, K. C.; Jenkins, R. D. Effect of a nonionic surfactant on the flow dynamics of a model HASE associative polymer. *AIChE J.* **1998**, *44*, 2756-2765.

102. Tirtaatmadja, V.; Tam, K. C.; Jenkins, R. D. Effects of Temperature on the Flow Dynamics of a Model HASE Associative Polymer in Nonionic Surfactant Solutions. *Langmuir* **1999**, *15*, 7537.
103. Benchabane, A.; Karim, B. Rheological properties of carboxymethyl cellulose (CMC) solutions. *Colloid and Polymer Science* **2008**, *286*, 1173-1180.
104. Liu, W. -.; Yu, T. L.; Lin, H. -. Shear thickening behavior of dilute poly(diallyl dimethyl ammonium chloride) aqueous solutions. *Polymer* **2007**, *48*, 4152-4165.
105. Kokini, J. L.; Mills, P. L. Comparison of steady shear and dynamic viscoelastic properties of guar and karaya gums. *J. Food Sci.* **1984**, *49*, 1-4.
106. Rochefort, W. E.; Middleman, S. Rheology of Xanthan Gum: Salt, Temperature, and Strain Effects in Oscillatory and Steady Shear Experiments. *J. Rheol.* **1987**, *31*, 337-369.
107. Urakami, N.; Imai, M. Dependence on sphere size of the phase behavior of mixtures of rods and spheres. *J. Chem. Phys.* **2003**, *119*, 2463-2470.
108. Dufresne, A. Research: Nanocellulose: a new ageless bionanomaterial. *Materials Today* **2013**, *16*, 220-227.
109. Zaman, A. A.; Delorme, N. Effect of polymer bridging on rheological properties of dispersions of charged silica particles in the presence of low-molecular-weight physically adsorbed poly(ethylene oxide). *Rheologica Acta* **2002**, *41*, 408-417.
110. Zhou, C. J.; Chu, R.; Wu, R.; Wu, Q. L. Electrospun Polyethylene Oxide/Cellulose Nanocrystal Composite Nanofibrous Mats with Homogeneous and Heterogeneous Microstructures. *Biomacromolecules* **2011**, *12*, 2617-2625.
111. van de Ven, T. Association-induced polymer bridging by poly(ethylene oxide)-cofactor flocculation systems. *Adv. Colloid Interface Sci.* **2005**, *114*, 147-157.

112. Otsubo, Y. Effect of Surfactant Adsorption on the Polymer Bridging and Rheological Properties of Suspensions. *Langmuir* **1994**, *10*, 1018-1022.
113. Graessley, W. W. *Polymeric Liquids and Networks: Dynamics and Rheology*; 2004; Vol. 2, pp 801.
114. Lagerwall, J. P. F.; Schütz, C; Salajkova, M.; Noh, J.; Park, J. H.; Scalia, G.; Bergström, L. Cellulose nanocrystal-based materials: from liquid crystal self-assembly and glass formation to multifunctional thin films. *NPG Asia materials* **2014**, *6*, 1-12.
115. Winter, H. H.; Chambon, F. Analysis of Linear Viscoelasticity of a Crosslinking Polymer at the Gel Point. *J. Rheol.* **1986**, *30*, 367-382.
116. Akira, K.; Sei, H. Ordered structure in weakly flocculated monodisperse latex. *Journal of Colloid and Interface Science* **1976**, *55*, 487-498.
117. Asakura, S.; Oosawa, F. On interaction between two bodies immersed in a solution of macromolecule. *The Journal of Chemical Physics* **1954**, *22*, 1255-1256.
118. Charles L. Sieglaff Phase Separation in Mixed Polymer Solutions. *Journal of Polymer Science* **1959**, *12*, 319-326.
119. Lu, A.; Song, Y.; Boluk, Y. Electrolyte effect on gelation behavior of oppositely charged nanocrystalline cellulose and polyelectrolyte. *Carbohydr. Polym.* **2014**, *114*, 57-64.
120. Lu, A.; Wang, Y.; Boluk, Y. Investigation of the scaling law on gelation of oppositely charged nanocrystalline cellulose and polyelectrolyte. *Carbohydr. Polym.* **2014**, *105*, 214-221.
121. Zaman, A. A.; Bjelopavlic, M.; Moudgil, B. M. Effect of adsorbed polyethylene oxide on the rheology of colloidal silica suspensions. *J. Colloid Interface Sci.* **2000**, *226*, 290-298.

122. Laurati, M.; Petekidis, G.; Koumakis, N.; Cardinaux, F.; Schofield, A. B.; Brader, J. M.; Fuchs, M.; Egelhaaf, S. U. Structure, dynamics, and rheology of colloid-polymer mixtures: From liquids to gels. *J. Chem. Phys.* **2009**, *130*, 134907.
123. Hilhorst, J.; Meester, V.; Groeneveld, E.; Dhont, J. K. G.; Lekkerkerker, H. N. W. Structure and rheology of mixed suspensions of montmorillonite and silica nanoparticles. *J Phys Chem B* **2014**, *118*, 11816-11825.
124. Cosgrove, T.; Obey, T. M.; Taylor, M. Solvent relaxation NMR: bound fraction determination for sodium poly(styrene sulphonate) at the solid/solution interface. *Colloids and Surfaces* **1992**, *64*, 311-316.
125. Schonhoff, M.; Larsson, A.; Welzel, P. B.; Kuckling, D. Thermoreversible Polymers Adsorbed to Colloidal: A H NMR and DSC Study of the Phase Transition in Confined Geometry. *Journal of Physical Chemistry* **2002**, *106*, 7800-7808.
126. Buining, P. A.; Philipse, A. P.; Lekkerkerker, H. N. W. Phase behavior of aqueous dispersions of colloidal boehmite rods. *Langmuir* **1994**, *10*, 2106-2114.
127. Davis, V. A.; Parra-Vasquez, A.; Green, M. J.; Rai, P. K.; Behabtu, N.; Prieto, V.; Booker, R. D.; Schmidt, J.; Kesselman, E.; Zhou, W.; Fan, H.; Adams, W. W.; Hauge, R. H.; Fischer, J. E.; Cohen, Y.; Talmon, Y.; Smalley, R. E.; Pasquali, M. True solutions of single-walled carbon nanotubes for assembly into macroscopic materials. *Nature Nanotechnology* **2009**, *4*, 830-834.
128. Beck-Candanedo, S.; Gray, D. G. Induced phase separation in low-ionic-strength cellulose nanocrystal suspensions containing high-molecular-weight blue dextrans. *Langmuir* **2006**, *22*, 8690-8695.
129. Beck-Candanedo, S.; Bouchard, J.; Berry, R. Dispersibility in water of dried nanocrystalline cellulose. *Biomacromolecules* **2012**, *13*, 1486-1494.

130. Stroobants, A.; Lekkerkerker, H. N. W.; Odijk, T. Effect of electrostatic interaction on the liquid crystal phase transition in solutions of rodlike polyelectrolytes. *Macromolecules* **1986**, *19*, 2232-2238.
131. Strawhecker, K. E.; Manias, E. Crystallization behavior of poly(ethylene oxide) in the presence of Na plus montmorillonite fillers. *Chemistry of Materials* **2003**, *15*, 844-849.
132. Liimatainen, H.; Haavisto, S.; Haapala, A.; Niinimäki, J. Influence of Adsorbed and Dissolved Carboxymethyl Cellulose on Fibre Suspension Dispersing, Dewaterability, and Fines Retention. *BioResources* **2009**, *4*, 321-340.
133. Walz, J. Y.; Sharma, A. Effect of Long Range Interactions on the Depletion Force between Colloidal Particles. *J. Colloid Interface Sci.* **1994**, *168*, 485.
134. Tuinier, R.; Fan, T.; Taniguchi, T. Depletion and the dynamics in colloid-polymer mixtures. *Current Opinion in Colloid & Interface Science* **2015**, 66.
135. Burns, J. L.; Yan, Y. D.; Jameson, G. J.; Biggs, S. The effect of molecular weight of nonadsorbing polymer on the structure of depletion-induced flocs. *J. Colloid Interface Sci.* **2002**, *247*, 24-32.
136. Hemraz, U. D.; Lu, A.; Sunasee, R.; Boluk, Y. Structure of poly(N-isopropylacrylamide) brushes and steric stability of their grafted cellulose nanocrystal dispersions. *J. Colloid Interface Sci.* **2014**, *430*, 157-165.
137. Beek, G. P.; Cohen Stuart, M. A.; Cosgrove, T. Polymer adsorption and desorption studies via ¹H NMR relaxation of solvent. *Langmuir* **1991**, *7*, 327-334.
138. Grzybowski, B.; Wilmer, C.; Kim, J.; Browne, K.; Bishop, K. M. Self-assembly: from crystals to cells. *Soft Matter* **2009**, *5*, 1110-1128.

Appendix A. Supplementary for NMR Results in Chapter 4

This section is a supplementary document for Chapter 5. Table A.1 shows spin-lattice relaxation times of samples. Relation between spin-lattice and spin-spin relaxation times was discussed in Chapter 5.

Table A.1. Spin-lattice relaxation times of samples with respect to molecular weight, CNC concentration and salt concentration.

Polymer Type	Mw (kDa)	Polymer Conc. (wt%)	CNC Conc. (wt%)	NaCl (ppm)	T₁ (s)	
-	-	0	0	0	18.23	
-	-	-	1	0	8.66	
PEO	600	1	0	0	9.05	
CMC	700	1	0	0	11.42	
CMC	90	1	1	0	21.80	
CMC	250	1	1	0	19.21	
CMC	700	1	1	0	9.05	
CMC	700	1	1	200	10.90	

Polymer Type	Mw (kDa)	Polymer Conc. (wt%)	CNC Conc. (wt%)	NaCl (ppm)	T_{1,1} (s)	T_{1,2} (s)
PEO	600	0.1	1	0	16.75	0.71
PEO	600	0.1	0.5	0	16.23	0.70
PEO	600	0.1	0.05	0	19.20	0.68
PEO	600	0.1	0.01	0	17.95	0.68